Université du Québec

Institut National de la Recherche Scientifique

Énergie Matériaux Télécommunications

Doctorate of Philosophy

In

STUDY ON THE MICROWAVE RECTENNAS FOR WIRELESS POWER TRANSFER AND ENERGY HARVESTING

Rached Agwil

Jury d'évaluation

Président du jury : Tarek Djerafi, professeur INRS-ÉMT

Examinateurs externes :

Mihai Sima, professeur, Université Victoria, British Columbia

Halim Boutayeb, professeur, Université du Québec en Outaouais

Directeur de recherche : Serioja Tatu, professeur INRS-ÉMT

Acknowledgments

The thesis results could not have been possible without the support of my supervisor. I would like to express my appreciation to Professor Serioja O. Tatu for his expert supervision on this task and for his valuable input on this academic thesis and writing research papers.

I would also like to express my gratitude to INRS Montreal Professors Tayeb Denidni, and Tarek Djerafi, who advised me to discover researchers. Also, I would like to express my sincere gratitude to Professor Mihai Sima, Victoria University and, professor Halim Boutayeb, Québec en Outaouais University for their insightful comments and suggestions.

Also, a considerable appreciation for technicians at Polytechnique Montreal who facilitated the fabrication of the prototype circuits. I would like to acknowledge printed technology expert Traian Antonescu, and technical supervisor Jules Gauthier at Polytechnique Montreal. I would like to thank my classmates in the antenna and radio frequency department for their useful discussions. I am incredibly grateful to INRS Montreal management for helping me during a challenging time.

I would also like to express my thanks to my father, Omar, and my mother, Masouda, for having continuously supported me to pursue this degree. Many thanks to all my family for pushing me positively. I am deeply grateful to the Ministry of Education in Libya for providing me the scholarship.

Résumé

Cette thèse propose une nouvelle conception des circuits dans les fréquences micro-ondes comme solution alternative au transfert de puissance sans fil et à la récupération de l'énergie radiofréquence. En raison de l'utilisation limitée des batteries et des fils dans certaines circonstances, l'auto-alimentation peut être bénéfique pour les dispositifs électroniques sans fil. Le problème consiste à trouver un moyen de charger des dispositifs à faible consommation d'énergie en utilisant les systèmes de transmission sans fil existants. Ce travail met en évidence des conceptions de circuits qui intègrent des composants passifs et actifs pour le transfert d'énergie sans fil. Les fonctions principales de ces circuits sont de collecter l'énergie de rayonnement d'origine ambiante et de recycler l'énergie récupérée. Les circuits, appelés rectennas qui sont des Antennes redresseuses, sont construits avec de composants non linéaires passifs, d'antennes intégrées et de redresseurs de radiofréquence.

Les circuits passifs se composent d'une antenne micro-ruban et de l'un des composants suivants : un coupleur Wilkinson, une jonction en T et un coupleur hybride à 90º ou 180º utilisé comme combinateur de puissance. Les principaux avantages des circuits passifs sont l'isolation de l'adaptation et les faibles pertes. Ils peuvent être utilisés pour combiner la puissance reçue des antennes afin d'alimenter le circuit redresseur. Les circuits non linéaires constituent une autre partie, composée d'une ou plusieurs diodes (deux pour le doublement de la tension, et quatre pour le pont de diodes) qui sont intégrées à l'étage de charge.

L'objectif de ces circuits est double : (i) recevoir et combiner les signaux d'entrée de radiofréquence, et (ii) rectifier avec une plus grande efficacité et convertir les signaux de radiofréquence en courant continu ou alimenter les dispositifs électroniques sans fil.

Les principaux objectifs de ce travail sont de développer des circuits récepteurs efficaces qui utilisent l'énergie radiofréquence existante et augmentent la puissance de sortie. Comme les systèmes de dispositifs sans fil sous la bande 6 GHz sont utilisés pour l'Internet des objets et l'identification par radiofréquence, les conceptions d'antennes patch et de coupleurs sont modifiées pour améliorer l'efficacité et minimiser les pertes de retour.

Deux techniques de simulation sont employées dans cette étude : l'optimisation et le réglage. Comme ces deux stratégies sont essentielles pour obtenir les performances requises, le logiciel Advanced Design System de Keysight (Agilent) Technologies est utilisé à cet effet. Tous les prototypes proposés sont conçus, simulés, fabriqués et validés par des mesures sur des bancs d'essai. De plus, des circuits redresseurs de radiofréquence en courant continu ont été mis en œuvre pour l'efficacité de la conversion de puissance et la tension de sortie appropriée aux applications ciblées, tandis que des diodes Schottky sont utilisées pour les circuits redresseurs pleine onde avec des doubleurs de tension pour obtenir la tension de sortie continue requise.

En outre, un réseau d'adaptation de type L est utilisé pour les redresseurs mono-bande et multi-bande afin de maximiser la tension de sortie CC. Des transformateurs d'impédance sont également utilisées comme technique d'adaptation pour augmenter l'efficacité du rectenna. Les prototypes sont fabriqués à Polytechnique Montréal, Circuits Imprimes De La Capitale, et Cancino Technologies, tandis que les mesures sont effectuées au Laboratoire RF de l'INRS-EMT Montréal.

Les principaux avantages du système proposé pour les appareils auto-alimentés sont l'élimination des fils et des piles, et la réduction des coûts. De plus, le système peut être pratique dans les applications industrielles, scientifiques et médicales (ISM).

Abstract

This thesis proposes a novel microwave design and the proposed solution is a power transfer/harvesting. Due to the limited use of batteries and wires in some circumstances, self-powering is beneficial for wireless electronic devices. The problem involves finding a way to charge low-power consumption devices using existing telecommunication wireless transmitting systems. This work proposes circuit designs that integrate passive and active components for wireless power transfer. The primary functions of these circuits are to collect ambient-sourced radiation energy and to recycle energy scavenging. The circuits, called rectennas, are built with passive non-linear components, integrated antennas, and radio frequency rectifiers.

Passive circuits consist of a microstrip antenna and one of the following components: a Wilkinson coupler, a T-junction, and either a 90º or a 180º hybrid coupler used as a power combiner. The main advantages of passive circuits are matching isolation and low losses. They can be used for combining received power from antennas to feed the rectifier circuit. Non-linear circuits are another part, consisting of one or more diodes (two for double voltage, and four for Diode Bridge) that are integrated with the load stage.

The purpose of the circuits is twofold: (i) to receive and combine radio frequency input signals, and (ii) to rectify with higher efficiency and convert radio frequency signals to direct current or power electronic wireless devices.

The main objectives of this work are to develop efficient receiver circuits that employ existing radiofrequency energy and increase output power. As wireless device systems under 6 GHz band are used for the Internet of Things and radiofrequency identification, patch antenna and coupler designs are being modified to improve efficiency and minimize return losses.

The Advanced Design System software of Keysight (Agilent) Technologies is used for this purpose. All of the proposed prototypes are designed, simulated, fabricated, and validated by measurements on test benches. Also, radiofrequency to direct current rectifier circuits have been implemented for power conversion efficiency and output voltage appropriated for targeted applications, while Schottky diodes are used for full-wave rectifier circuits with voltage doublers to obtain the required DC output voltage.

Additionally, an L-type matching network is used to maximize DC output voltage. Also, impedance transformers are used as a matching technique to boost the rectenna efficiency. The prototypes are fabricated at Polytechnique Montréal, Circuits Imprimes De La Capitale, and Cancino Technologies, and the measurements are done at INRS-EMT Montreal RF Laboratory.

The main benefits of the proposed system for self-powering devices are getting rid of wires and batteries, and reducing costs. Furthermore, the system can be practical in industrial, scientific, and medical (ISM) applications.

Table of Contents

List of Tables

List of Figures

List of Acronyms and abbreviations	
AC	Alternative Current
ADS	Advanced Design System software
BTSs	Base Transceiver Stations
C	Capacitor
cm	Centimeter
d	Distance
DC	Direct Current
dB	Decibel
dBm	decibel-milliwatts
EH	Energy Harvesting
EIRP	Effective Isotropic Radiated Power
EL	Electrical Length of the Line
EM	Electromagnetic
η	Efficiency
f	Frequency
FCC	Federal Communications Commission
G_{rx}	Gain of the receiver antenna
G_{tx}	Gain of the transmitter antenna
h	Substrate Thickness
Hz	Hertz
I_load	Current load
IoTs	Internet of Things
ISM	Industrial, Scientific and Medical
IMN	Impedance Matching Network
KΩ	Kilo ohm
L	Physical Length
LED	Light-Emitting Diode
LOS	Line-of-Sight
m	meter
MHz	Megahertz
mW	milliwatts
nH	nano Henry
PCB	Printed Circuit Board
PCE	Power conversion efficiency
pF	Pico Farad
PH	Power Harvesting
P_{in}	Input Power
P_{rx}	Power Received
Psec	Peer second
P_{tx}	Power Transmitter
R	Resistance
RF	Radio Frequency
RF-EHWC	Radio Frequency Energy Harvesting Wireless Communication
R_L	Load Resistance
R_x	Receiver
ε_r	Relative Permittivity
SHARP	Stationary High Altitude Relay Platform
SMA	Subminiature Assembly Connector

T	**Period**
TL	**Transmission Line**
V	**Volt**
V_{in}	**Input Voltage**
V_{out}	**Output Voltage**
W	**Width**
WLAN	**Wireless Local Area Network**
WPT	**Wireless power transfer**
Z_0	**Characteristic Impedance**
ε_{eff}	**Effective dielectric constant**
ΔL	**Correction factor**
λ	**Wavelength**
μA	**Micro ampere**
μF	**Micro Farad**
μW	**Microwatt**

Chapitre F - Introduction et analyse documentaire

F.1 Introduction

F.1.1 Contexte

Les progrès des appareils de télécommunication et l'avènement de l'Internet des objets (IoT) nécessitent une énergie interne ou externe permanente pour assurer leur longévité [1-8]. De nombreux appareils électroniques sont désormais chargés à l'aide d'approches sans fil. Cela est considéré comme pratique par les utilisateurs, car l'auto-alimentation évite de changer périodiquement les piles et réduit également les fils disgracieux et limitant la distance. Dans le même temps, de nombreuses radiofréquences (RF) sont générées par diverses sources [1-8].

Le concept de récolte d'énergie (EH) existe depuis des décennies. Un autre concept, le transfert d'énergie sans fil (WPT), est le transfert d'énergie électrique sans connexion filaire. Avec l'avènement de nouvelles applications et l'augmentation de la puissance de certaines sources RF, la récolte d'énergie à l'aide du transfert d'énergie sans fil peut constituer une nouvelle solution pour alimenter certains appareils électroniques [1-8].

L'EH collecte des signaux à partir de sources disponibles telles que la lumière ambiante, les vibrations/mouvements, l'énergie thermique et les RF utilisées pour alimenter des dispositifs.

La figure F.1 montre le processus des différentes sources d'énergie qui peuvent être utilisées pour la récupération d'énergie. La RF est disponible de jour comme de nuit, à l'intérieur comme à l'extérieur, et son exploitation n'est pas coûteuse. Par conséquent, la transmission RF est permanente dans tout l'environnement, ce qui permet de recueillir des signaux pour l'auto-alimentation des dispositifs. En fait, dans certaines conditions, elles pourraient alimenter de nombreux dispositifs, comme les capteurs, Wi-Max, les réseaux locaux sans fil (WLAN) et Wi-Fi, éliminant ainsi efficacement les liaisons filaires et les batteries.

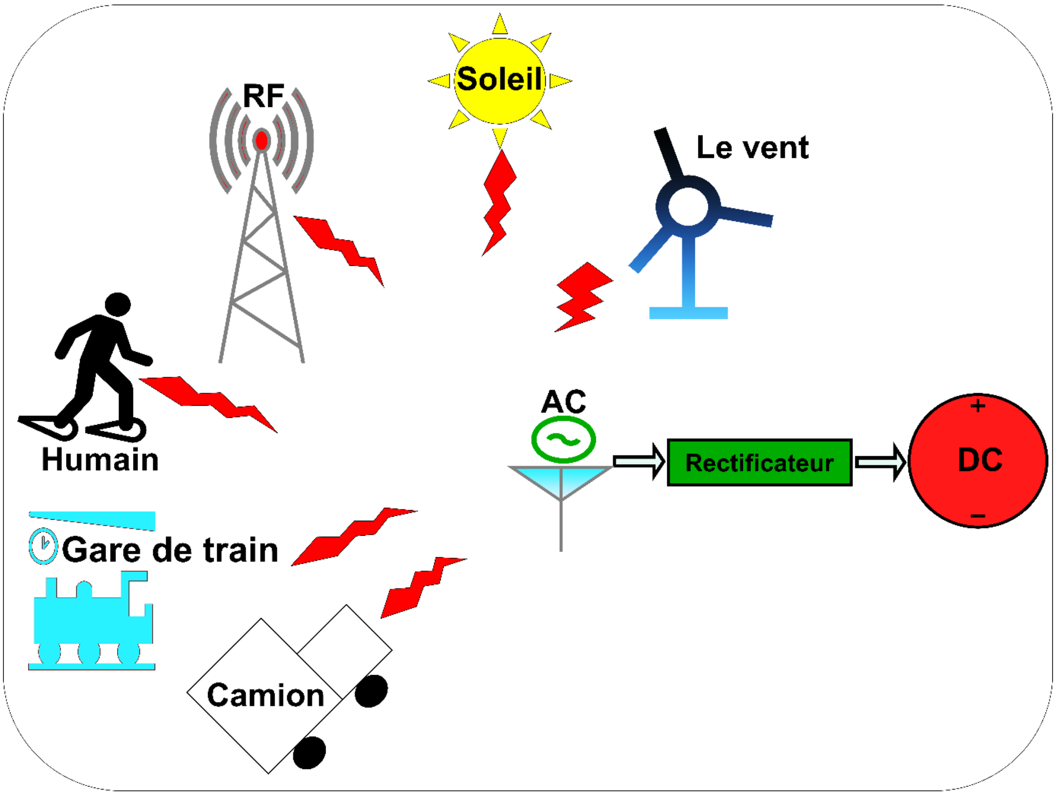

Figure F.1. Diverses sources d'énergie disponibles pour la récupération de l'énergie.

L'utilisation des bandes RF et micro-ondes sont standardisées, certaines bandes attirant davantage l'attention dans les domaines industriel, scientifique et médical (ISM). Le présent travail se concentre sur les fréquences micro-ondes des bandes L, S et C en raison de leur application dans le processus RF-DC pour le WPT. En outre, le test en laboratoire des fréquences ISM ne nécessite pas de licence de la

Fédéral Communications Commission (FCC) ou Industries Canada. En effet, par rapport aux systèmes de diffusion TV ou FM conventionnels, des circuits de plus petite taille sont utilisés en raison des plus courtes longueurs d'onde. Les stations émettrices-réceptrices de base (BTS) de radiofréquence sont de plus en plus courantes dans les environnements urbains et suburbains, car elles sont polyvalentes pour transmettre des informations. Plus précisément, elles ont une puissance isotrope rayonnée (PIRE) d'environ 100 W (50 dBm) [9-10]. Dans le même temps, les récepteurs de dispositifs électroniques sont également nombreux. Ces appareils récepteurs ont incité de nombreux chercheurs à concevoir des circuits de récolte d'énergie pour éviter l'utilisation de batteries.

D'après les recherches de nombreux chercheurs [1-10], le développement de solutions écologiques est l'un des problèmes les plus fondamentaux des systèmes de communication sans fil à faible puissance. La puissance d'entrée RF provenant de l'énergie RF ambiante offre une faible densité de puissance.

En fonction des défis mentionnés ci-dessus, cette recherche vise à développer et étudier un récepteur de circuit pour WPT et EH, comme le montre le schéma bloc de la figure F.2. Le récepteur proposé peut fonctionner à des fréquences ciblées et rectifier la RF en une sortie CC appropriée pour l'application de capteurs autoalimentés sur 5G.

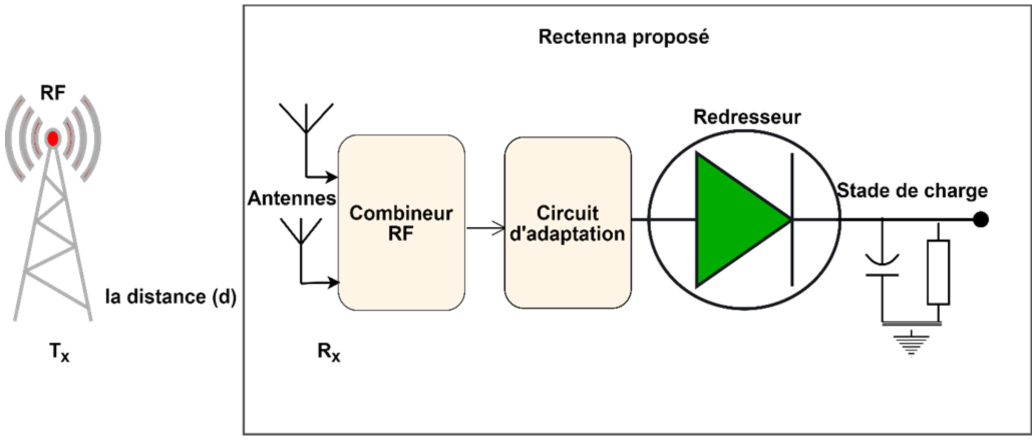

Figure F.2. RF-WPT-EH de l'architecture du système.

F.1.2 Motivations

- Aujourd'hui, les sources RF sont disponibles presque partout et constituent un moyen relativement peu coûteux de fournir de l'énergie aux dispositifs de télécommunication qui nécessitent une source d'énergie durable. L'intention de ce travail est de concevoir un circuit performant permettant de collecter de l'énergie pour charger des dispositifs et d'analyser les limites physiques de son utilisation dans un environnement RF. De plus, comme la plupart des appareils électroniques nécessitent une alimentation continue, nos motivations se limitent à quelques points d'appui, comme le montre la figure F.3 ;

- L'omniprésence des stations de base émettrices-réceptrices (TBS) et des stations cellulaires, pour l'émission RF, fournit une source d'information et d'énergie toute prête.

- La plupart des câbles et des batteries seront finalement envoyés dans des décharges, entraînant la pollution de la terre et de la nappe phréatique. Les signaux RF pourront être une solution alternative pour la technologie WPH.

- Les câbles et les batteries doivent être entretenus, remplacés et recyclés.

- Certains endroits sont difficiles d'accès pour remplacer le fournisseur d'énergie des capteurs et des appareils.

De plus, certains problèmes sont apparus en relation avec les systèmes de dispositifs sans fil, tels que la puissance de sortie CC, la bande passante, l'efficacité, la sensibilité et l'angle de réception. Ces problèmes entraînent des résultats non satisfaisants dans le circuit redresseur. L'objectif de cette thèse est de développer des récepteurs de circuit très efficaces en exploitant la technique de récupération de l'énergie RF de la BTS.

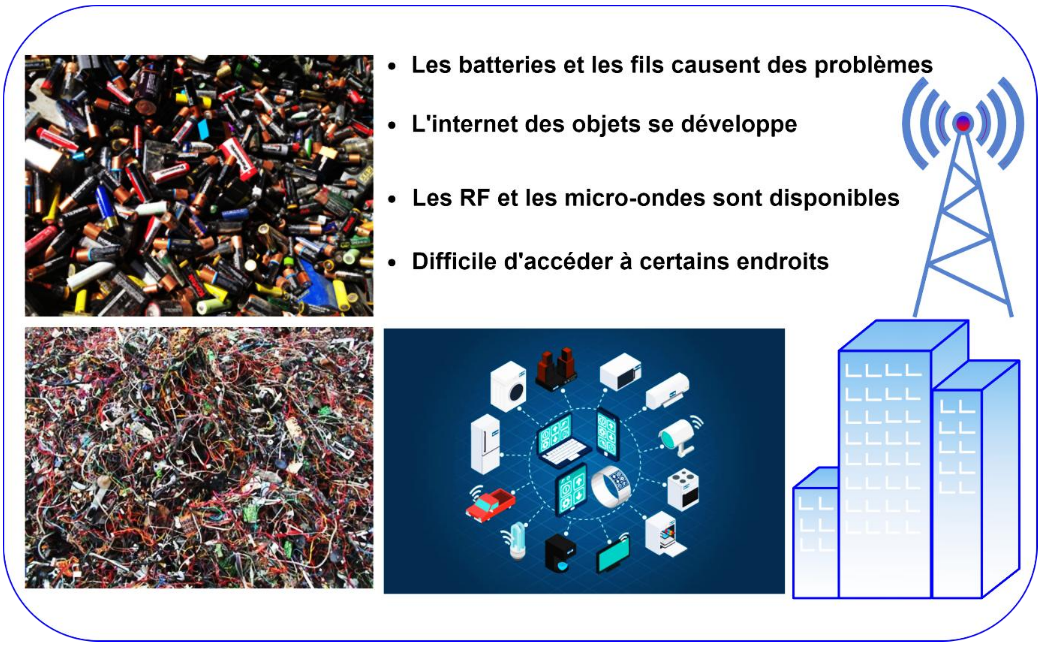

Figure F.3. Photos des facteurs favorisant les techniques RF - WPT- EH.

F.1.3 Questions de recherche

Quelques questions utiles doivent être posées avant de fixer des objectifs pour réaliser un système WPT approprié.

- Quelle source doit être transférée en fonction du temps et du lieu ?

- Quelle est l'application visée et ses exigences ?

- Quelle est la fréquence de fonctionnement pour laquelle les niveaux de puissance RF d'entrée et de puissance CC de sortie sont suffisants ?

- Quels sont les composants et la topologie qui augmentent la sensibilité et la puissance CC par rapport au niveau de puissance faible d'entrée ?

- Quel est l'effet de l'utilisation de plus d'une source ?

- Existe-t-il une application pratique qui en a besoin ?

- Où pouvons-nous utiliser un système WPT ?

- Quelle est la valeur pratique et ajoutée de ce système de recherche pour le domaine RF ?

Les réponses à ces questions de recherche permettront d'étayer la mise en œuvre du système RF-WPT, et pourront également mettre en évidence certains compromis raisonnables. La figure F.4 illustre les piliers nécessaires à la construction du système WPT.

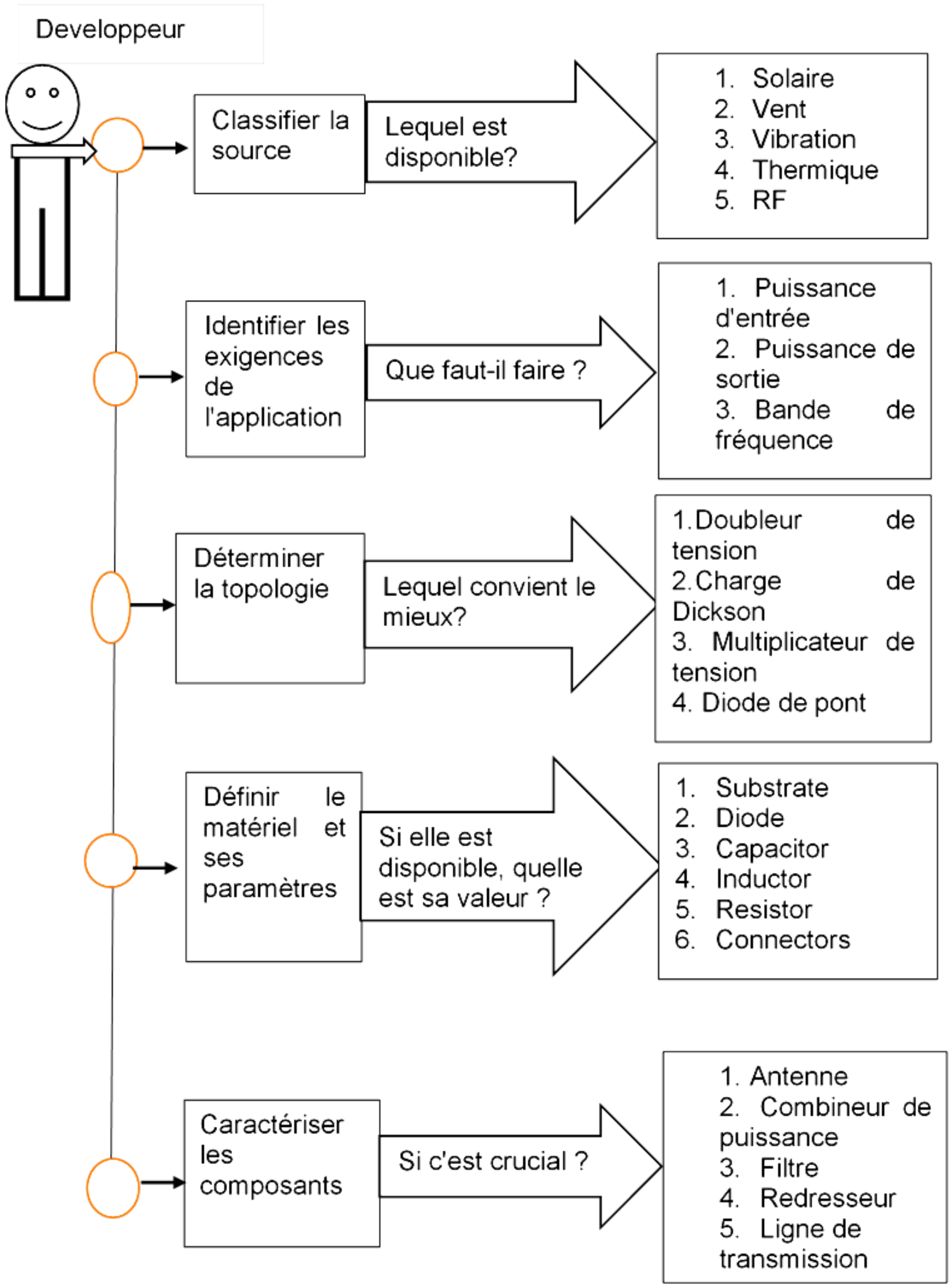

Figure F.4. Diagramme d'activité pour la mise en œuvre d'un système RF-WPT-EH.

F.1.4 Objectifs

L'objectif général est de concevoir des systèmes prototypes pour le transfert d'énergie sans fil et la récolte d'énergie dans l'environnement sous 6 GHz. Ces systèmes seront utiles dans les applications industrielles, scientifiques et médicales (ISM).

Les objectifs spécifiques sont de déterminer la source d'énergie, les composants, les matériaux et la conception, en réalisant les compromis avec certaines restrictions.

- Identifier, concevoir et fabriquer le système de rectenna pour traiter une faible puissance RF pour le WPT avec une grande efficacité.
- Récupérer suffisamment de courant continu et augmenter l'angle de réception pour les applications requises.
- Analyser les facteurs qui affectent l'amélioration de la sensibilité, de la large bande et de l'efficacité.

F.1.5 Aperçu de la thèse

Cette thèse a mis en évidence l'étude de RF-WPT pour être prospective dans les systèmes de télécommunication. Elle s'est également concentrée sur les considérations de la puissance de sortie DC à utiliser dans les applications IoT ou RFID sur 5G. Le WPT est une colonne vertébrale car tous les dispositifs électroniques en deviennent dépendants. Les résultats de la recherche, avec une efficacité élevée et une sensation de faible niveau de puissance RF provenant des signaux BTS et cellulaires ambiants, pourraient être utilisés dans des environnements industriels, scientifiques, médicaux, etc. Le produit final comprendra un circuit récepteur de petite taille, idéal pour une utilisation dans des systèmes de dispositifs sans fil.

F.1.6 Portée de la recherche

Les signaux RF et micro-ondes sont actuellement transmis dans les zones urbaines et suburbaines dans des applications telles que le communications sans-fil, incluant les réseaux cellulaires, l'identification par radiofréquence (RFID) et l'Internet des objets (IoT). Ces applications consomment des quantités d'énergie relativement faibles (c'est-à-dire entre des microwatts et des milliwatts). La présente thèse propose plusieurs prototypes permettant d'obtenir une plus grande largeur de bande, une plus grande efficacité et une plus grande compacité pour combler ce manque de recherche. Le WPT en particulier se concentre sur les exigences spécifiques des développements ISM, comme illustré dans le tableau F.1.

Tableau F.1. Piliers du RF-WPT-EH.

RF-WPT EH piliers	Exigences de mise en œuvre	Raisons de la sélection
Source d'énergie	RF	Disponibilité et gratuité
Fréquence de fonctionnement	Bandes L, C	Atténuation moins affectée, pas besoin de licence FCC, couvert ISM, et longueur d'onde courte par rapport aux services de diffusion
Applications appliquées	IoTs, RFID, 5G	Plus de capacité, beaucoup d'appareils, et moins de consommation d'énergie
Composants	Antennes, Combinateurs/coupleurs de puissance	Composants cruciaux, peuvent récolter de l'énergie faciles (intégrés, fabriqués), bon marché
Matériau éléments substrat	RO3010, RO4350	Disponibilité, bon marché, large gamme de fréquences et faible perte
Composants des éléments matériels	L-lumped	Simple à installer et très efficace
Matériaux composants actifs	Diodes telles que HSMS-286K, SMS-7630-006LF	Haute sensibilité, et peut fonctionner sur les bandes L, S, C
Outils	Logiciel Advanced Design System (ADS)	Circuits de conception intégrée, et conception de dispositifs RF

F.1.7 Contributions novatrices

A. La principale contribution de cette thèse est l'analyse de l'extraction de l'énergie des RF et des micro-ondes pour le WPT et l'EH. De nos jours, la technologie évolue vers le WPT, par exemple, nous avons besoin de charger des appareils sans fil à partir de sources RF. De même, certains appareils nécessitent un changement de batterie pour être rechargés, par conséquent, la charge de ces appareils sans fil peut apporter un confort.

B. Les nouvelles contributions présentées dans cette recherche peuvent être résumées comme suit :

(I) Un circuit rectenna utilisant un coupleur hybride 90° avec un transformateur et un composant de redressement différentiel pleine onde est proposé. Le circuit rectenna intègre essentiellement une antenne patch unique avec un coupleur 90^{O} pour faciliter la connexion entre l'antenne et le circuit redresseur différentiel. L'isolation entre les deux antennes est renforcée par le transformateur λ/4 et le coupleur hybride 90°.

(II) Un coupleur hybride redresseur 180° pour un composant redresseur différentiel pleine onde est présenté. Il est utilisé pour traiter l'analyse et la conception. Le circuit proposé est capable de convertir le courant alternatif en courant continu.

(III) Un circuit redresseur simple à couplage en T est également proposé. Ce circuit combine essentiellement les signaux RF et produit une tension de sortie qui est le double des signaux combinés.

(IV) Un circuit coupleur Wilkinson à antenne rectangulaire est présenté. Ce circuit intègre une antenne patch avec un redresseur Wilkinson pour minimiser les pertes, améliorer l'isolation et augmenter la large bande.

V) Un circuit redresseur à double jonction en T est également proposé. Ce circuit consiste en un combinateur de puissance à deux couches pour augmenter la sortie, ce qui est essentiellement réalisé en intégrant le redresseur différentiel au combinateur de puissance. Ainsi, deux sous-redresseurs correspondants en combinaison parallèle sont efficaces pour améliorer l'efficacité et permettre la puissance de la sortie CC.

Le haut débit fonctionne dans les bandes S, L et C pour couvrir les applications 3G, 4G et 5G. Il obtient un rendement élevé de 75% à faible puissance d'entrée, et une résistance de charge élevée de 5 KΩ, atteignant -30 dBm dans les paramètres de sensibilité.

Comme mentionné, la contribution de l'origine d'un combinateur de puissance RF pleine onde ou à deux couches est l'amélioration de la sortie et de l'efficacité. Ceci est essentiellement accompli en utilisant l'alimentation.

F.2 Implémentation des prototypes

F.2.1 Prototype 1 - Prototype d'antenne rectangulaire intégrée utilisant des antennes patch et un coupleur hybride de 90°

F.2.1.1 Fabrication

Le prototype compact fabriqué est présenté à la figure F.2.1. Il comprend des antennes patch doubles connectées au coupleur hybride 90º qui sont intégrées au réseau d'adaptation et à l'étage redresseur. La ligne λ/4 supplémentaire entre l'antenne et l'entrée supérieure du coupleur hybride 90º est nécessaire pour obtenir des signaux déphasés à l'entrée du pont, comme expliqué précédemment au début du paragraphe 2.6. Les dimensions du circuit imprimé sont de 5,5 cm × 5,5 cm.

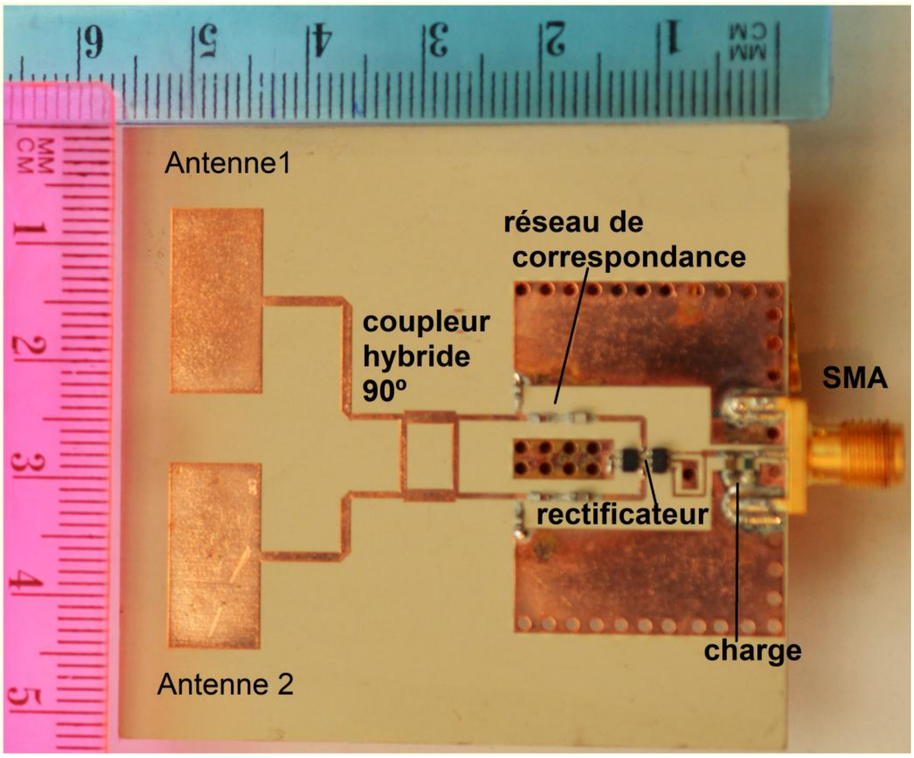

Figure F.2.1. Photo du circuit de fabrication du coupleur hybride 90º intégré au réseau d'adaptation et à l'étage redresseur.

F.2.1.2 Mesures

Le montage de mesure est présenté à la figure F.2.2. Il utilise un générateur de signaux modèle DS SG6000LDQ connecté à une antenne présentée. Du côté réception, le signal de sortie CC du dispositif testé (DUT) est mesuré à l'aide d'un multimètre numérique Agilent 34401A.

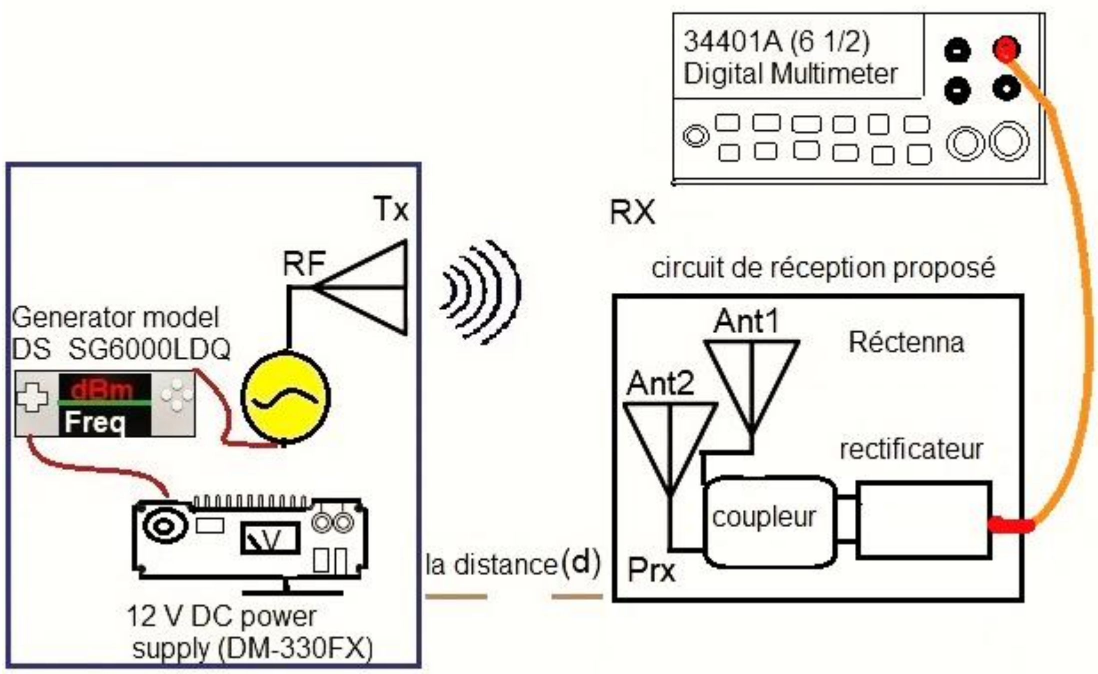

Figure F.2.2. Schéma de l'installation de mesure.

L'antenne d'émission est utilisée comme référence pour transmettre le signal au circuit de réception. La puissance du signal RF est de 7 dBm, le gain de l'antenne d'émission est de 6 dBi, le gain du récepteur est de 6 dB, et la distance est de 0,55 m. La puissance de sortie du récepteur est de -25,5 dBm, et la largeur de bande est de 5380 MHz à 5450 MHz.

La dimension de l'antenne de l'émetteur est choisie pour déterminer le champ lointain à l'aide de l'équation, où D = 0,12 m et λ = 0,56 m. La distance (d) entre les antennes de l'émetteur et du récepteur est choisie pour être au début du champ lointain. Les paramètres sont utilisés pour calculer la puissance d'estimation du récepteur (Prx) dans (F.2.1), l'émetteur de puissance (Ptx), l'émetteur de gain (Gtx) et le récepteur de gain (Grx).

Far field (d) ≥ $\frac{2 \cdot D^2}{\lambda} = 0.56\, m$.

Quand d = 0,56 m, et la fréquence = 5,8 GHz.

$$Prx = Ptx + Gtx + Grx + 20 \cdot log10 \cdot (\frac{\lambda}{4\pi d}) \qquad \text{(F.2.1)}$$

= 7 + 6 + 6 + (- 42.7) = - 23.7 dBm.

La mesure a été effectuée sur un redresseur à pont complet avec deux antennes de réception pour la charge RF sans fil d'un appareil électronique. De plus, la topologie du redresseur est une structure simple et compacte. Ce circuit imprimé peut être facilement intégré dans le rayonnement électromagnétique ambiant pour les applications WPT.

La FCC [55], [56] a déclaré que la plupart des émetteurs-récepteurs de base cellulaires dans les zones urbaines et suburbaines transmettent des signaux aux dispositifs électroniques sans fil à une puissance rayonnée suffisante égale ou inférieure à 100 W (50 dBm) par canal.

F.2.1.3 Conclusion

Ce circuit redresseur montre la mise en œuvre d'une antenne pour le transfert de puissance sans fil et la récolte d'énergie par la méthode RF-DC. En raison de la disponibilité de la RF, l'énergie récoltée est appropriée pour alimenter des capteurs sans fil. Le coupleur hybride à 90° est l'épine dorsale du récepteur proposé et est mis en œuvre ici avec deux antennes micro-ruban, un pont redresseur pleine onde et un réseau d'adaptation. Ce circuit proposé couvre 5,8 GHz (WLAN) et offre une alimentation pour les capteurs 4G et 5G dans certaines conditions. Les avantages du circuit conçu sont la petite taille, la légèreté et la facilité d'installation. Les travaux futurs se concentreront sur l'amélioration de la puissance du détecteur.

F.2.2 Prototype 2 - Prototype de redresseur intégré utilisant un coupleur hybride à 180 degrés

F.2.2.1 Fabrication

Le prototype a été fabriqué, et des photos sont présentées à la figure F.2.3. Sa taille physique est de (6 cm × 8 cm). Il comprend le coupleur hybride à 180º, les éléments localisés, le HSMS286K pour le pont redresseur à diodes, et la charge.

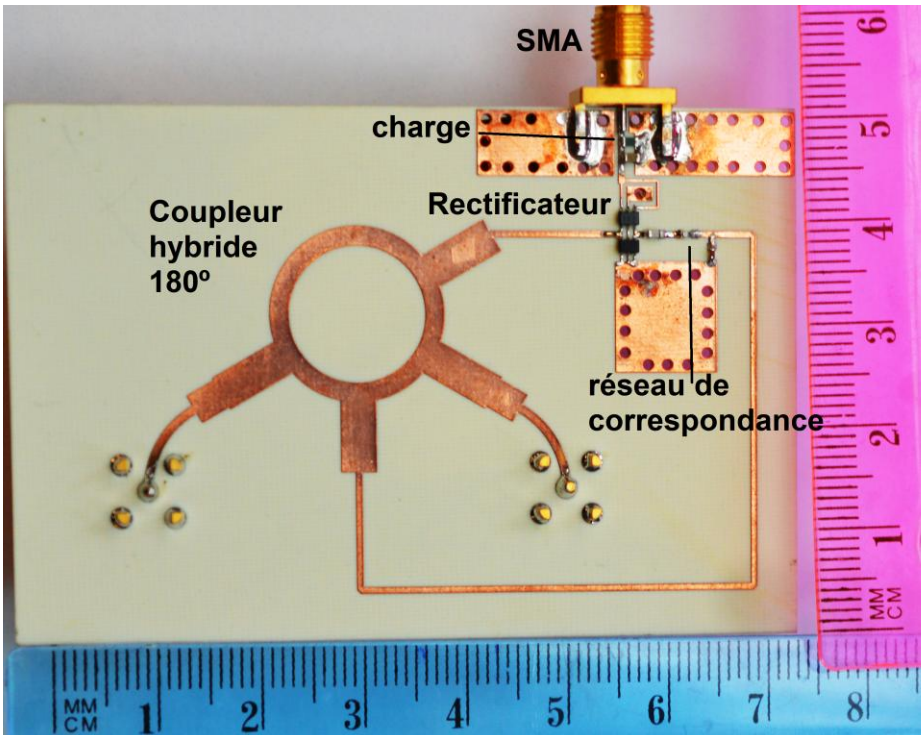

Figure F.2.3. Photo du prototype: Coupleur hybride 180º intégré avec réseau d'adaptation et étage redresseur.

F.2.2.2 Mesure

Le montage de mesure est présenté à la figure F.2.2. Il utilise un générateur de signaux modèle DS SG6000LDQ connecté à une antenne, qui est représentée sur du côté de l'émetteur. Du côté de la réception, deux antennes sont connectées aux entrées du coupleur hybride à 180º. Le signal de sortie du dispositif testé (DUT) est mesuré à l'aide d'un multimètre numérique Agilent 34401A.

Les paramètres de l'émetteur sont le niveau de puissance d'entrée Ptx (5 dBm), les gains Gtx (6 dB), et la distance (d = 0,5 m). La puissance au niveau du récepteur (Prx) est mesurée sur toute la largeur de bande. Le résultat de la mesure de crête pour le récepteur est de -10 dBm dans la largeur de bande (1540-1630 MHz), -5 dBm dans la largeur de bande (1830-2200 MHz), -18 dBm dans la largeur de bande (3000-3030 MHz), et -24 dBm dans la largeur de bande (5330-5370 MHz).

L'équation de Friis [52] (F.2.2) est appliquée pour calculer le Prx lorsque d = 0,50 m et la fréquence = 5,8 GHz.

$$Prx = Ptx + Gtx + Grx + 20 \cdot log10 \cdot (\frac{\lambda}{4 \cdot \pi \cdot d}) \qquad \text{(F.2.2)}$$

$$= 5 + 6 + 8 + (-35.7) = -16.7 \text{ dBm.}$$

La source RF peut capter l'énergie ambiante, qui est utilisée dans les applications WPT et PH. Cependant, elle est basée sur la puissance de l'émetteur, et la distance entre l'émetteur et le circuit récepteur. Le circuit récepteur fournit une puissance de sortie de -10 dBm en courant continu pour une puissance d'entrée de 0 dBm (1 mW) à une distance de 1 m entre T_x et R_x. La conception montre une efficacité de 50% à 0 dBm, prouvant la capacité de la récolte de l'énergie RF ambiante pour stimuler l'application à l'IoT.

F.2.2.3 Conclusion

Cette contribution, coupleur hybride 180º, RF vers DC peut être améliorée pour l'alimentation en inversant l'étage redresseur. Le rendement obtenu est de 50% à une puissance d'entrée à deux bornes de 0 dBm pour une charge de résistance de RL = 5 KΩ. La conversion DC de sortie dépend de la collecte d'encore plus d'énergie RF. A travers le redresseur, des composants supplémentaires seront envisagés, comme un multiplicateur de tension pour augmenter l'efficacité du recensa.

F.2.3 Prototype 3 - Redresseur intégré en bande C utilisant un combinateur de puissance à jonction en T

F.2.3.1 Fabrication

Le système proposé, qui comprend un coupleur combineur de puissance à jonction en T, un réseau d'adaptation de type L, un doubleur de tension et une résistance de charge, a été fabriqué, comme le montre la figure F.2.4. Le système proposé a une taille physique de 4 cm x 3 cm.

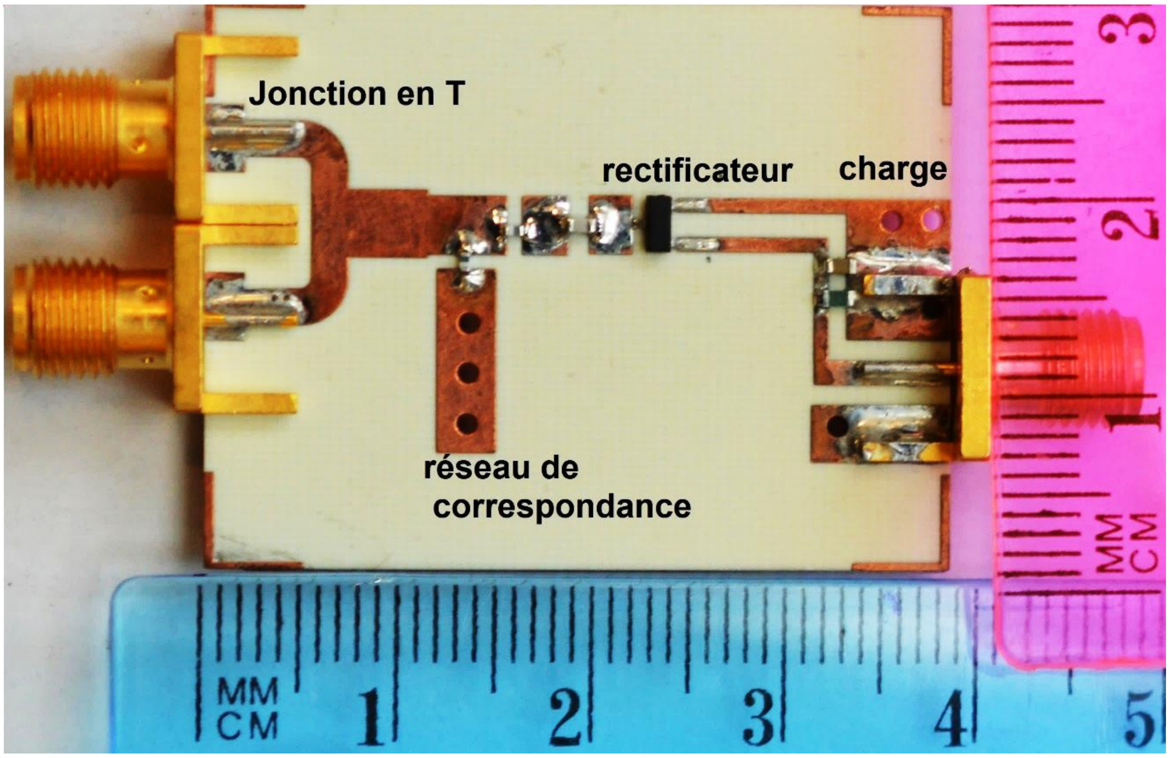

Figure F.2.4. Photo du prototype fabriqué du système proposé.

F.2.3.2 Mesure

Comme le montre déjà la figure F.2.2, le montage de mesure comprend un générateur de signaux modèle DS SG6000LDQ connecté à une antenne d'émission. De même, deux antennes de réception sont fixées aux bornes d'entrée. La photo de l'antenne utilisée pendant nos mesures est présentée. Le tableau F.2.1 montre les régions de champ lointain calculées pour les fréquences et les longueurs d'onde correspondantes. Le signal de sortie du dispositif testé (DUT) a été mesuré à l'aide d'un multimètre numérique Agilent 34401A.

Tableau F.2.1. Calculez les longueurs d'onde (λ) pour les trois fréquences (f) avec le champ lointain (d).

f (GHz)	2	5	7.5
λ (m)	0.15	0.06	0.04
Far-field d (m) $\geqq \frac{2\,D^2}{\lambda}$	0.19	0.48	0.72

Trois régions de champ lointain de 0,19 m, 0,48 m et 0,72 m pour λ = 0,15, 0,06 et 0,04 m, respectivement, sont obtenues tout en maintenant une distance d = 1 m. L'équation de Friis (F.2.3) est appliquée pour calculer l'estimation de la puissance reçue.

$$Prx = Ptx + Gtx + Grx + 20 \cdot log10 \cdot \left(\frac{\lambda}{4 \cdot \pi \cdot d}\right) \qquad \text{(F.2.3)}$$

= 0 + 5 + 8 + (−38.46) = -25.46 dBm,

= 0 + 5 + 8 + (−46.45) = -33.45 dBm,

= 0 + 5 + 8 + (−49.94) = -36.94 dBm.

Pendant les mesures, la puissance d'entrée de l'émetteur était fixée à Pin = 0 dBm et la distance d = 1 m. Les puissances de sortie obtenues étaient de -17 dBm pour une largeur de bande de (1650-2000 MHz), - 20 dBm pour une largeur de bande de (3000-3400 MHz), - 24 dBm pour une largeur de bande de (2050-2500 MHz), et -24 dBm pour une largeur de bande de (6550- 6950 MHz).

Les résultats des mesures, qui ont été vérifiés par l'équation de Friis (F.2.4), sont donnés ci-dessous ; un bon accord a été trouvé entre les données mesurées et calculées.

$$Prx = Ptx + Gtx + Grx + 20 \cdot log10 \cdot \left(\frac{\lambda}{4 \cdot \pi \cdot d}\right) \quad \text{(F.2.4)}$$

Quand d = 250 m, et λ identifiés dans le tableau 4.2 ci-dessus.

= 47 + 15 + 8 + (-86.42) = - 16.42 dBm.

= 47 + 15 + 8 + (-94.37) = - 24.37 dBm.

= 47 + 15 + 8 + (-97.89) = - 27.89 dBm.

Ces résultats peuvent être appliqués aux dispositifs électroniques industriels, scientifiques et médicaux. Lorsque la puissance d'entrée est de 0 dBm, la tension de sortie peut atteindre environ 2 V, ce qui est une valeur pratique pour l'alimentation des capteurs. Par conséquent, le circuit peut être très utile pour le transfert de puissance sans fil. Ces résultats peuvent être appliqués à des dispositifs électroniques industriels, scientifiques et médicaux. Lorsque la puissance d'entrée est de 0 dBm, la tension de sortie peut atteindre environ 2 V, ce qui est une valeur pratique pour l'alimentation des capteurs. Par conséquent, le circuit peut être très utile pour le transfert de puissance sans fil.

F.2.3.3 Conclusion

Ce circuit de réception utilise un coupleur combinateur de puissance à jonction en T pour un doubleur de tension RF à double entrée via un réseau d'adaptation de type L. Ces composants sont intégrés dans un circuit simple et de petite taille. Ces composants sont intégrés dans un circuit simple et de petite taille. La tension continue de sortie est maximisée à l'étage de charge. En commençant par -30 dBm, l'efficacité augmente avec la puissance d'entrée de quelques pour cent à environ 43 % à un niveau de puissance d'entrée de 0 dBm à partir de deux bornes, et une résistance de charge de 5 kΩ. Les résultats mesurés donnent confiance aux capteurs de puissance et pourraient être dans ce chapitre appliqués à la 3, 4, et 5G des systèmes de communication sans fil. L'idée présentée peut être appliquée dans une gamme plus large d'applications.

Les travaux futurs permettront d'améliorer une double RF avec un détecteur de puissance multiple pour augmenter le balayage de puissance.

F.2.4 Prototype 4 - Prototype de redresseur intégré utilisant un combinateur de puissance Wilkinson

F.2.4.1 Fabrication

Le circuit est fabriqué avec le combinateur de puissance Wilkinson avec un réseau d'adaptation en L et un redresseur doubleur de tension sur le même substrat. La figure F.2.5. illustre la photo du circuit (7,5 x 7,5 cm) qui ressemble à un circuit imprimé (PCB). De plus, les articles sont facilement disponibles et peu coûteux, et la société Rogers fournit le substrat.

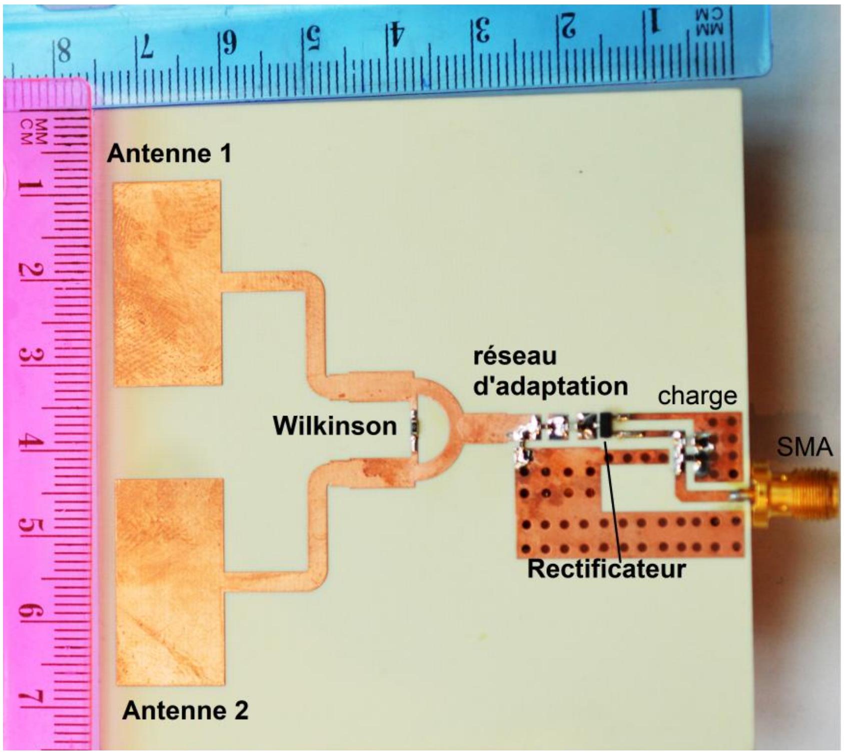

Figure F.2.5. Photo des redresseurs du circuit de fabrication.

F.2.4.2 Mesure

Le montage de mesure est présenté à la figure F.2.2. Le résultat de la puissance de sortie est présenté dans le tableau 5.3. Une puissance d'émission = 7 dBm est configuré à la sortie du générateur de micro-ondes. Les résultats liés à la simulation, à l'équation de Friis et au processus de mesure concordent approximativement.

L'équation de Friis (F.2.5) est utilisée pour estimer la puissance du récepteur (Prx) à l'entrée du circuit du détecteur. La configuration représentative du champ proche et du champ lointain de la classification WPT est basée sur le tableau F.2.2.

En appliquant les valeurs de la puissance de l'émetteur (Ptx) de 7 dBm, du gain de l'antenne de l'émetteur (Gtx = 7 dBi), du gain de l'antenne du récepteur (Grx = 8 dBi), pour une distance entre l'émetteur et le récepteur de 50 cm, on obtient une puissance reçue de -19,70 dBm à la fréquence de 5,8 GHz.

$$Prx = Ptx + Gtx + Grx + 20 \cdot log10 \cdot \left(\frac{\lambda}{4 \cdot \pi \cdot d}\right) = -19.7 \text{ dBm}. \quad \text{(F.2.5)}$$

L'équation (F.2.6) est utilisée pour trouver une estimation de l'affaiblissement du trajet en espace libre à la fréquence de 5,8 GHz, Gtx=7 dB, Grx=8 dB, et d=0,50 mètre :

$$Path\ loss = Gtx + Grx + 20\ log10\ \left(\frac{\lambda}{4 \cdot \pi \cdot d}\right) = -26.7 \text{ dBm}. \quad \text{(F.2.6)}$$

Tableau F.2.2. Les résultats mesurés du redresseur de puissance DC à sortie Wilkinson.

D (cm) / (MHz)	100	75	50	25
	Puissance de sortie (dBm) à un niveau de puissance d'entrée de 7 dBm			
1760 to 1930	-32	-26	-22	-18
3020 to 3160	-34	-19	-17	-15
5320 to 5700	-35	-27	-21	-17
6000 to 6060	-36	-34	-24	-19

F.2.4.3 Conclusion

Ce travail présente un prototype implémenté avec un combineur Wilkinson qui est conçu pour collecter plus d'énergie, à partir de deux antennes patch intégrées. En outre, il fournit une tension RF deux fois plus élevée à la sortie combinée grâce à la topologie du doubleur de tension. Il augmente la tension continue, l'efficacité et la sensibilité en employant un redresseur à pleine onde. Le rendement du circuit redresseur est de 51,86 % à 0 dBm pour RL = 5 KΩ, et la sensibilité de 2,7 % à une puissance d'entrée de -25 dBm à deux bornes.

En mesure, une puissance d'entrée de 7 dBm fournit la puissance de sortie avec une fréquence à large bande. La puissance de sortie est indiquée dans le tableau 5.3. En conséquence, le circuit de récolte de puissance pourrait être utilisé pour la 3G et aussi la 5G qui a été lancée en 2020 sur les fréquences des bandes L et C. Par conséquent, la récolte de tension du circuit proposé.

Les travaux futurs seront étendus pour combiner la RF dans le rectenna afin d'accumuler plus de RF. Ils pourraient également se concentrer sur certains aspects qui contribuent à améliorer le résultat.

F.2.5 Prototype 5 - Redresseur intégré utilisant un coupleur combinateur de puissance à double jonction en T

F.2.5.1 Fabrication

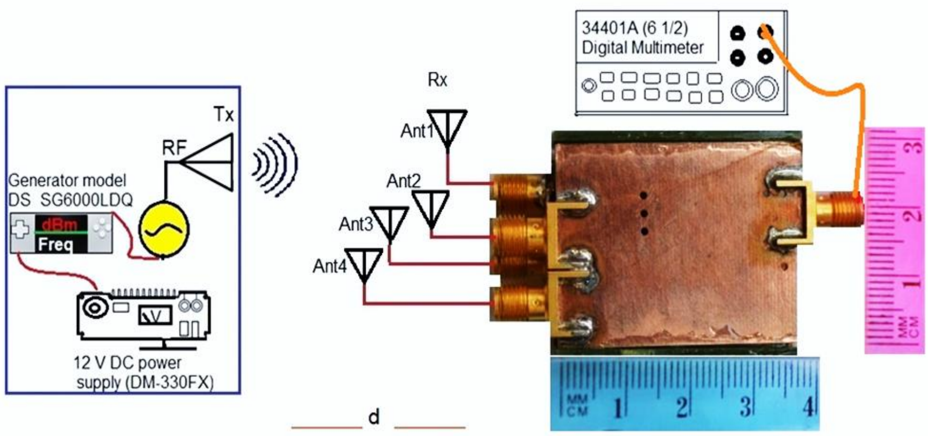

Figure F.2.6. Photo du circuit fabriqué (coupleur combinateur de puissance à double jonction en T rectifier).

Le circuit proposé, un coupleur combinateur de puissance à double jonction en T avec redresseur doubleur de tension parallèle, est illustré à la figure F.2.6. La photo du prototype fabriqué a des dimensions de 4 cm x 3 cm x 1 cm, plus la taille du SMA en longueur.

F.2.5.2 Mesure

La figure F.2.6. montre la configuration mesurée. Il est évident qu'une antenne d'émission est connectée au générateur et que quatre antennes de réception sont connectées à notre prototype fabriqué. Le multimètre numérique est connecté à la sortie du prototype pour mesurer la puissance disponible à la sortie.

Les équations (F.2.7) et (F.2.8) sont utilisées pour calculer la distance de champ lointain (d) à 2 et 6 GHz.

$$d \geqq \frac{2\,D^2}{\lambda} = \frac{2 \cdot 12^2}{15} = 19.2 \text{ cm} \qquad \text{(F.2.7)}$$

Pour un champ lointain de 6 GHz :

$$d \geqq \frac{2\,D^2}{\lambda} = \frac{2 \cdot 12^2}{5} = 57.6\ cm \qquad \text{(F.2.8)}$$

L'équation de Friis (F.2.9) estime la puissance reçue.

$$Prx = Ptx + Gtx + Grx + 20 \cdot log10 \cdot \left(\frac{\lambda}{4 \cdot \pi \cdot d}\right) \qquad \text{(F.2.9)}$$

Pour la fréquence = 2 GHz (λ = 15 cm), et en substituant Ptx, Gtx, et Grx, on a,

= −5 + 6 + 12 + (−38.46) = −25.46 dBm.

Pour la fréquence = 6 GHz (λ = 5 cm),

$= -5 + 6 + 12 + (-48) = -35$ dBm.

Lors des mesures effectuées en intérieur dans le laboratoire, la puissance de l'émetteur était réglée à Ptx = - 5 dBm et la distance entre l'émetteur et le prototype était de 1 m. La puissance de sortie mesurée était de - 20 dBm à (1650-1950 MHz), -14 dBm à (2000-2050 MHz) et -20 dBm à (6550- 7000 MHz).

L'équation de Friis dans (F.2.10) - (F.2.11) est appliquée pour trouver la puissance de sortie du circuit récepteur fabriqué, dans le cas d'une puissance transmise de 100 W (50 dBm). Dans ce cas, nous prenons λ = 0,15 m et nous avons utilisé une distance d = 500 m :

$P_{rx} = 50 + 15 + 6 + (-92.4) = -21.4$ dBm. (F.2.10)

Si la distance d est réduite à 250 m avec le même λ = 0,15 m, la puissance reçue est de $P_{rx} = 50 + 15 + 6 + (-86.4) = -15.4$ dBm. (F.2.11)

F.2.5.3 Conclusion

Dans ce travail, deux redresseurs à jonction en T ont été combinés pour améliorer les performances du redresseur à jonction en T individuel. Il a combiné quatre signaux RF pour alimenter l'étage du redresseur. Le redresseur a été vérifié pour couvrir la plupart des bandes de fréquences ISM, en particulier pour le WPT. Le rendement atteint est de 75 % à un niveau de puissance d'entrée de 0 dBm provenant de quatre générateurs, avec une faible perte de puissance de sortie en courant continu, ce qui est essentiel pour l'auto-alimentation des dispositifs électroniques sans fil.

En outre, l'efficacité de la conception en fait un candidat potentiel pour faciliter l'auto-alimentation dans les systèmes de communication. En outre, le circuit offre une protection des composants contre les impacts environnementaux, et il est peu coûteux, léger et de petite taille. Les travaux futurs se concentreront sur l'amélioration des combinaisons multi rectificateurs afin d'augmenter l'efficacité et la puissance de sortie.

F.3 - Conclusion et travaux futurs

Cinq prototypes ont été proposés dans cette thèse, tous basés sur la combinaison et le redressement de signaux RF à l'aide d'un doubleur de tension ou d'une diode en pont. Plusieurs coupleurs, allant des coupleurs à large bande aux simples jonctions en T, ont été utilisés comme éléments de combinaison. Les résultats des simulations et des mesures ont confirmé à la fois le rendement énergétique et la tension de sortie continue des circuits proposés.

F.3.1 Conclusions

Les conclusions de ce travail de doctorat sont résumées ci-dessous.

Les technologies WPT et PH peuvent être utiles lorsqu'une station de base émet de l'énergie dans des conditions spécifiques :

Ces technologies fonctionnent mieux à courte distance pour alimenter des capteurs, WLAN, RFID et Wi-Fi.

L'utilisation des dispositifs proposés dépend du niveau de puissance Tx et de la distance, comme nous le verrons plus loin.

La technologie WPT peut être utilisée pour alimenter des implants à quelques mètres ou d'autres applications ISM.

Toutes les expériences et les prototypes de fabrication révèlent cette limitation :

EH est limitée à la portée autour d'une station de base.

Les cinq prototypes utilisent différents combinateurs de puissance (coupleur hybride 90^{O}, coupleur hybride 180^{O}, jonction en T, Wilkinson), des antennes patch intégrées ou des antennes omnidirectionnelles externes.

Différentes techniques de redressement sont appliquées (doubleur de tension, diode en pont) pour augmenter la tension continue de sortie.

Comme prévu, l'efficacité est meilleure lorsque l'entrée RF est augmentée. Par exemple, comme nous l'avons vu au chapitre 6, le rendement peut atteindre 75 %.

F.3.2 Travaux futurs

La puissance de la source radiofréquence est étroitement contrôlée par des restrictions gouvernementales et de sécurité. Cependant, le WPT et le PH efficaces dépendent de la puissance Tx et de la distance, comme nous l'avons vu précédemment. Par conséquent, les restrictions gouvernementales peuvent empêcher l'adoption commerciale d'une partie de cette technologie émergente.

Les applications IoT sont de grands utilisateurs potentiels des technologies WPT et PH. Lors du développement d'une technologie pour l'IdO, certains aspects doivent être pris en compte, tels que le gain et les dimensions de l'antenne, la tension de sortie CC requise et l'efficacité opérationnelle des dispositifs IdO lors de l'utilisation de la PH et du WPT. Les principales considérations sont énumérées ci-dessous.

Les réseaux d'antennes ont des limites d'utilisation concernant la puissance d'entrée, le couplage mutuel et la taille, mais ils peuvent être utilisés pour augmenter le gain. Bien que la taille et le couplage mutuel soient généralement considérés comme des défis pour les réseaux d'antennes, ils peuvent également être considérés comme des avantages. Par exemple, la taille peut être améliorée en ce qui concerne la permittivité et la longueur d'onde, et le couplage mutuel peut être réduit grâce à des techniques telles que l'isolation et l'orientation des éléments d'antenne.

De nouvelles topologies de multiplicateurs à diodes pourraient être étudiées plus avant afin d'augmenter la tension continue de sortie aux niveaux requis pour des dispositifs spécifiques. Les diodes conçues pour les faibles niveaux de puissance sont recommandées. Elles sont sensibles et ont un faible seuil, ce qui les rend pratiques pour les PH dans les environnements à faible densité RF.

Les systèmes des villes intelligentes évoluent en permanence, et la technologie PH et WPT peut faire partie de cette évolution. De nombreux dispositifs IoT ont besoin d'être auto-alimentés. Certains dispositifs peuvent intégrer des réseaux d'antennes, en particulier à des fréquences micro-ondes plus élevées, mais l'augmentation de l'atténuation en espace libre doit également être prise en compte.

En conclusion, les conceptions actuelles et futures de WPT et de PH constituent un défi, et l'utilisation de ces dispositifs doit être correctement justifiée. Il n'est pas possible de se contenter d'augmenter la puissance T_x afin d'avoir suffisamment d'énergie pour alimenter un dispositif sans fil. Cette approche peut être acceptable pendant une courte période et/ou pour des applications spécifiques. Cependant, en ce qui concerne la sécurité, ce n'est pas une source viable d'énergie verte, comme certains chercheurs le prétendent dans leurs articles.

Le travail de cette thèse prouve que malgré les résultats obtenus dans la conception et le prototypage, les concepts WPT et PH montrent encore des limites claires pour les applications commerciales.

Chapter 1 – Introduction and Literature Review

1.1 Introduction

1.1.1 Background

Advances in telecommunication devices and the advent of the Internet of Things (IoT) require permanent internal or external energy to increase longevity [1-8]. Many electronic devices are now being charged using wireless approaches. This is considered convenient by users, as self-powering avoids changing batteries periodically and also reduces unsightly and distance-limiting wires. At the same time, there is plenty of radio frequency (RF) being generated from various sources [1-8].

The concept of energy harvesting (EH) has existed for decades. Another concept of wireless power transfer (WPT) is the transfer of current energy without wire connections. With the advent of new applications and increased power from some RF sources, EH using WPT can provide a novel solution for powering some electronic devices [1-8].

EH collects signals from available sources such as ambient light, vibration/motion, thermal energy, and RF used for powering devices.

Figure 1.1 shows the process of various energy sources that can be used in power harvesting. RF is available both day and night, indoor/outdoor, and is not costly to harvest. Therefore, RF transmission is permanent throughout the environment, enabling signals to be gathered for self-powering the devices. In fact, in certain cases, RF could power numerous devices, such as sensors, Wi-Max, wireless local area network (WLAN), and Wi-Fi, effectively eliminating wire links and batteries.

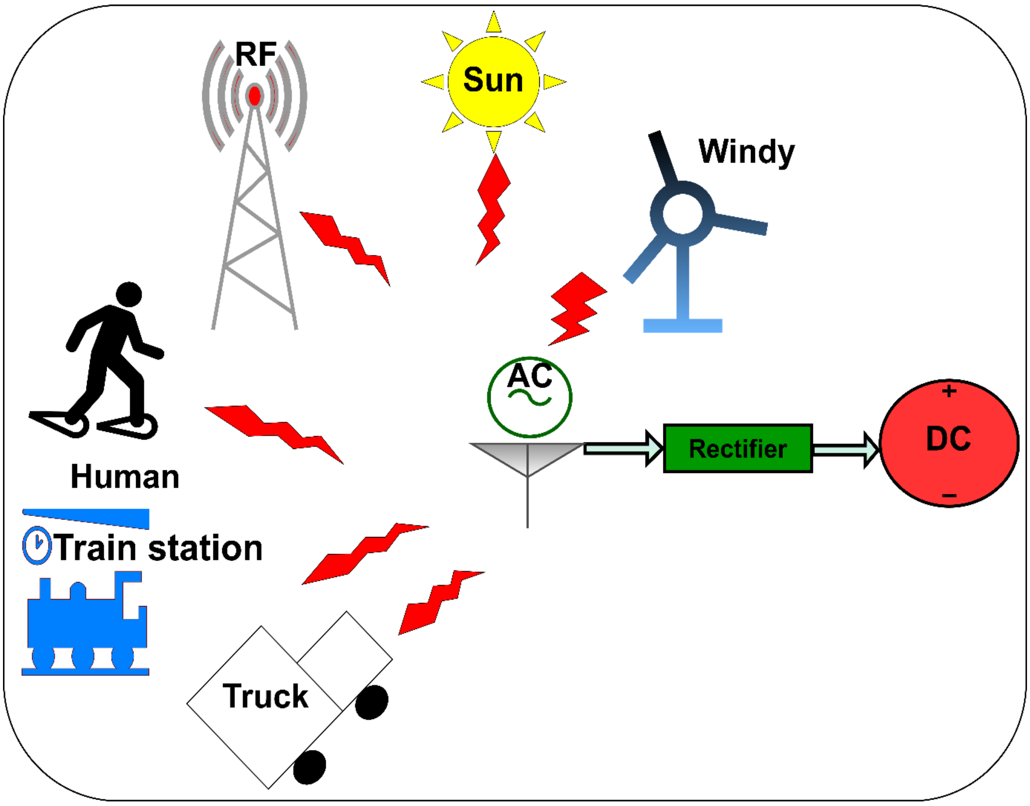

Figure 1.1. The process various energy sources are available for EH.

RF and microwave band designations are standardized, with some bands attracting more attention in industrial, scientific, and medical (ISM) fields. The present work focuses on the L (1-2 GHz), S (2-4 GHz), and C (4-8 GHz) band microwave frequencies. L-Band is used to satellite, and wireless connections like GSM mobile phones. C band uses for applications satellite, large ships that traverse the oceans, public telephone networks, terrestrial microwave links, and data back-hauls. S band standards use the 2.4 GHz, widely used computer networks, and public Internet access for mobile devices. Moreover, the ISM frequency laboratory test does not require a license from the Federal Communications Commission (FCC) or Industry Canada. This is because, compared to conventional TV or FM broadcasting systems, smaller-sized circuits are used due to shorter wavelengths. Radiofrequency base transceiver stations (BTSs) are becoming more and more commonplace in urban and suburban environments, as they are versatile for transmitting information. Specifically, they have an isotropic radiated power (EIRP) of about 100 W (50 dBm) [9-10]. At the same time, electronic device receivers are also plentiful. These recipient apparatuses have attracted many researchers to design power harvesting circuits to avoid the use of batteries.

Based on the investigations of numerous researchers [1-10], developing green-compliant solutions is one of the most fundamental problems for low-power wireless communication systems. The RF input power from ambient RF energy provides low power density.

According to the challenges mentioned above, this research aims to develop and study a circuit receiver for WPT and EH, as seen in the block diagram of Figure 1.2. The proposed receiver can operate at targeted frequencies and rectify RF to appropriate DC output for self-powering sensors application over 5G.

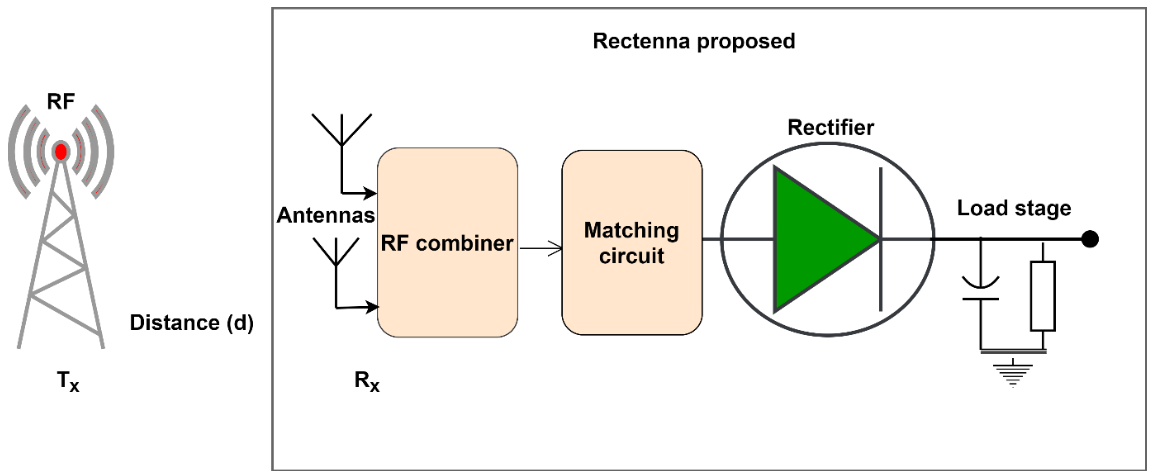

Figure 1.2. RF-WPT-EH of system architecture.

1.1.2 Motivations

- Today, RF sources are available nearly everywhere and are a relatively inexpensive way to provide power for telecommunication devices that require a sustainable power source. The intention of this work is to design a performant circuit to collect energy to charge devices and to analyze the physical limits of its use in an RF environment. Moreover, as most electronic devices require continuous feeding, our motivations are confined in some supporting points, as shown in Figure 1.3.

- The ubiquity of Transceiver Base Stations (TBSs) and cellular stations, for RF emission, provides a ready source of information and energy.

- Most cables and batteries will ultimately be sent to landfills, leading to the pollution of the earth and water table. RF signals could be an alternative solution for WPH technology.

- Wires and batteries need to be maintained, replaced, and recycled.

- Some places are difficult to access when replacing the power supplier of sensors and devices.

Moreover, some problems have emerged in relation to wireless device systems, such as DC output power, bandwidth, efficiency, sensitivity, and reception angle. These issues cause non-satisfactory outcomes due to the rectifier stage. The focus of this thesis is to develop highly efficient circuit receivers by exploiting the BTS RF energy scavenging technique.

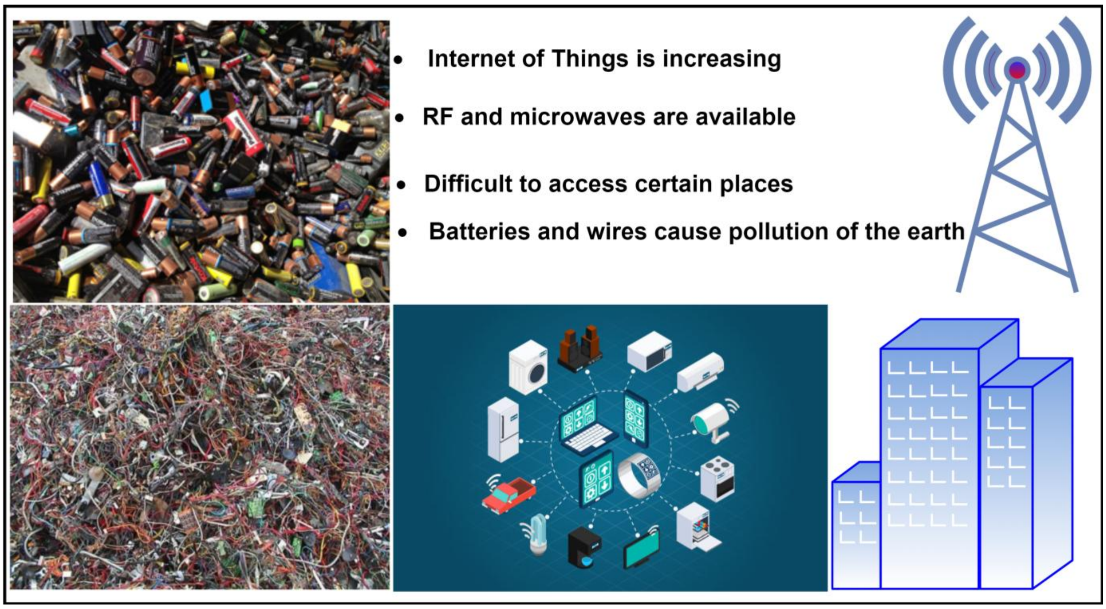

Figure 1.3. Photos of factors to encourage RF – WPT- EH techniques.

1.1.3 Research Questions

Some helpful questions have to be asked before setting objectives to achieve a suitable WPT system.

- Which source should be transferred based on time and place?
- What is the application target and its requirements?
- What is the operating frequency where input RF power and output DC power levels are sufficient?
- Which components and topology boost the sensitivity and DC power versus input low power level?
- What is the effect of using more than one source?
- Is there a practical application that needs it?
- Where can we use a WPT system?

- What is the practical and added value of this research system for the RF field?

The answers to these research questions will help to support the implementation of the RF-WPT system, and may also uncover some reasonable trade-offs. Figure 1.4 illustrates the necessary pillars for building WPT.

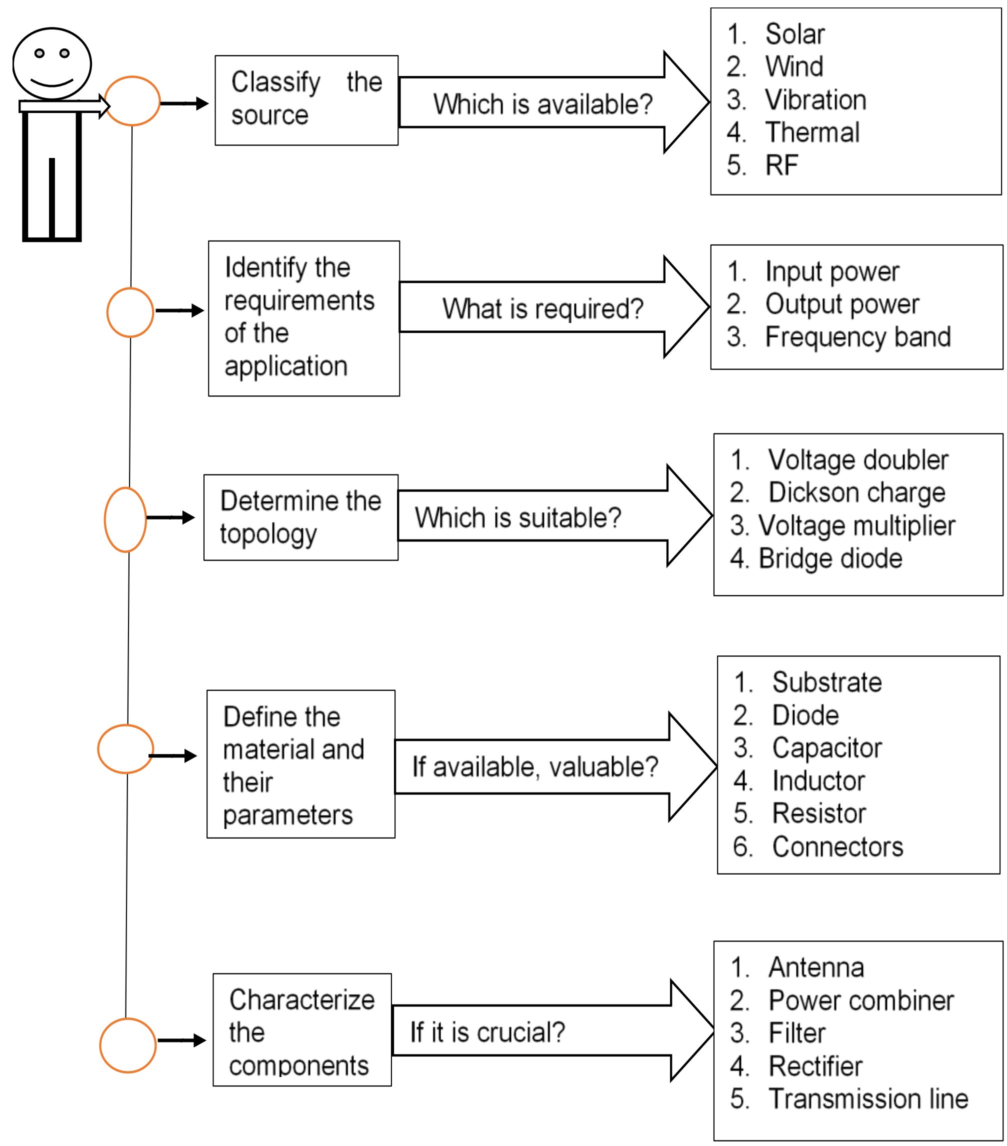

Figure 1.4. Activity diagram for implementation of an RF-WPT-EH system.

1.1.4 Objectives

The overall goal is to design prototype systems for wireless power transfer and energy harvesting from the ambient under 6 GHz. Such systems will be useful in industrial, scientific, and medical (ISM) applications.

The specific objectives are to determine the energy source, components, materials, and design, realizing the trade-offs with some restrictions.

- To identify, design, and fabricate the rectenna system to deal with low RF power for WPT with high efficiency.
- To scavenge sufficient DC power and increase the reception angle for the required applications.
- To analyze the factors that affect the improvement of sensitivity, broadband, and efficiency.

1.1.5 Thesis Overview

This thesis highlights the study of RF-WPT to be prospective in telecommunication systems. It also focuses on the considerations of DC output power to use in IoT or RFID over 5G applications. WPT is a backbone because all electronic devices are becoming dependent on it. The research outcomes with high efficiency and a sense of low RF power level from ambient BTS and cellular signals could be used in industrial, scientific, medical, etc., environments. The final product will feature a small-sized receiver circuit that is ideal for use in wireless device systems.

1.1.6 Research Scope

RF and microwave signals are currently being transmitted through urban and suburban areas in applications such as wireless communications, including cellular phone networks, radio frequency identification (RFID) and the Internet of things (IoT).

These applications consume relatively low amounts of energy (i.e., between microwatts and milliwatts). The present thesis proposes several prototypes to achieve more bandwidth, higher efficiency, and greater compactness in addressing this research gap. The WPT in particular focuses on specific requirements for ISM developments, as illustrated in Table 1.1.

Table 1. 1. Illustrates the pillars of RF-WPT_EH.

RF-WPT EH pillars	Implementation requirements	Selection reasons
Energy source	RF	Available and free cost
Operating frequency	L, C bands	Attenuation less affect, no need FCC license, covered ISM, and short wavelength comparing to broadcasting services
Application applied	IoTs, RFID, 5G	More capacity, plenty devices, and less energy consumption
Components	Antenna/ power combiner/ couplers	Crucial component, can reap energy, easy (integrated, fabricated), cheap
Material elements substrate	RO3010, RO4350	Availability, cheap, and low loss
Material elements components	L-lumped	Simple to install and performs properly with lower frequencies
Material active components	Diode such as HSMS-286K, SMS-7630-006LF	High sensitivity, and can operate over L, S, C bands
Tools	Advanced Design System (ADS) software	Integrated design circuits, and design RF devices

1.1.7 Innovative Contributions

A. The main contribution of this thesis is to analyze the extraction of the energy from RF and microwave for WPT and EH. Nowadays, technology is moving towards WPT, for example, we need to charge devices wirelessly from RF sources. Similarly, some devices need a change of batteries to recharge it, therefore; charging these devices wirelessly may bring comfort.

B. The novel contributions presented in this research can be summarized as follows:

(I) A rectenna circuit using a 90° hybrid coupler with a transformer and full-wave differential rectifying component is proposed. The rectenna circuit essentially integrates a single patch antenna with a 90° coupler to facilitate the connection between the antenna and the differential rectifier circuit. The isolation between the two antennas is enhanced through the $\lambda/4$ transformer and the 90° hybrid coupler.

(II) A rectifier 180° hybrid coupler for a full-wave differential rectifying component is presented. It is used to treat the analysis and design. The proposed circuit is able to convert AC to DC.

(III) A simple T-junction coupler rectifier circuit is also proposed. This circuit basically combines RF signals and produces an output voltage that is double the combined signals.

(IV) A rectenna Wilkinson coupler circuit is presented. This circuit integrates a patch antenna with a Wilkinson rectifier to minimize losses, enhance isolation, and increase broadband.

(V) A dual T-junction rectifier circuit is proposed as well. This circuit consists of a two-layer power combiner to boost output, which is essentially achieved by integrating the differential rectifier with the power combiner. Thus, two corresponding sub-rectifiers in parallel combinations are proficient for enhancing efficiency and allowing the strength of the DC output.

Broadband operates in S, L, and C bands to cover 3G, 4G, and 5G applications. It obtains a high efficiency of 75% in low input power, and high load resistance of 5 KΩ, reaching -30 dBm in sensitivity parameters.

As mentioned, the contribution of originating either an RF full-wave or two-layer power combiner is the improvement of the output and efficiency. This is basically accomplished by using the differential feeding from the power combiner.

1.1.8 Publications

1.1.8.1 List of Journals

1. R. Agwil, S. Tatu, Dual Antenna Power Detector Operating over L, C Bands for Power Harvesting Application in 3G, and 5G, International Journal of Advanced Research in Electrical, Electronics and Instrumentation Engineering, Vol. 8, Issue 11, DOI:10.15662/IJAREEIE.2019.0811001 November 2019, Published.

2. R. Agwil, S. Tatu, Combine RF Ambient for Power Harvesting using Power Detector for Sensor Application over L, S, C Bands, International Research Journal of Engineering and Technology (IRJET), Volume: 07 Issue: 01-Jan 2020, Published.

3. R. Agwil, S. Benchikh, H. Djillali, S. Tatu, Antenna rectifier using quadrature hybrid coupler for power-harvesting applications, International Journal RF Microwave Computer Aided Engineering, DOI: 10.1002/mmce.22279 24 April 2020, Published.

4. R. Agwil, S. Tatu, Quadrature Sandwich Rectenna for Wireless Power Transfer, WSEAS TRANSACTIONS on COMMUNICATIONS, Volume 19, 2020, E-ISSN: 2224-2864, DOI: 10.37394/23204.2020.19.19, Published.

1.1.8.2 List of Conferences

1. R. Agwil, S. Tatu, 180° Hybrid Coupler for a Full-wave Power Rectifier Detector for Wireless Power Transfer, ITT2020(Seventh International Conference on Information Technology Trend (ITT2020), IEEE *Xplore.* DOI: 10.1109/ITT51279.2020.9320787, November-26-2020, 978-1-7281-8380-0, Published IEEE.

2. R. Agwil, S. Tatu, Voltage Doubler Rectenna for Broadband Power Harvesting Applications, Poster STARaCOM March 2020, November-17-2020, Presented.

1.2. Literature Review

1.2.1 Initial investigation of rectenna

Nikola Tesla presented the concept of wireless electrical energy transmission in 1905 [1], stating that energy could be wirelessly transmitted to any earthly space. Tesla further stated that his "World System" was theoretically derived from his three inventions: the transformer, the magnifying transmitter, and the Wireless System transmission of electrical energy without wires. His work has encouraged research during the last century into the development of WPT.

Historically, rectennas were introduced by W. C. Brown in 1964, when a microwave-powered helicopter via a transmitting antenna achieved flight 18.28 meters above ground level [2]. The device gathered additional required RF energy from the surrounding environment, showing RF collecting converting to DC power. Based on this and other research, the goal in this work is to increase the efficiency of the rectenna for self-powering wireless system applications.

A rectenna is a process for converting electromagnetic energy into DC. It can be used in WPT systems to transmit power by radio waves, as shown in Figure 1.5.

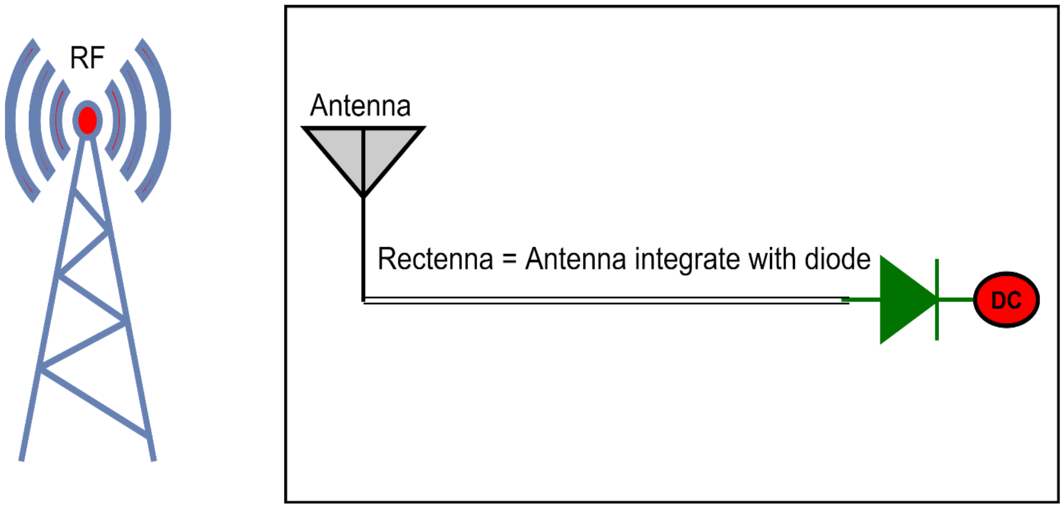

Figure 1.5. Diagram of rectenna.

Research conducted in [3] presented energy harvesting for wireless networks, but the received signals have limited use in EH because they are restricted by energy causality. The problem is harvested energy is less than that required for sufficient powering.

In [4], the researchers compared two aspects of EM radiation in WPT: Omnidirectional, and Unidirectional (microwave/laser). The advantage of Omnidirectional is the tiny size of the receiver. However, its disadvantage is the rapid drop of power transfer efficiency over distances and ultra-low power reception. Omnidirectional transfer can be used in applications charging a WSN for environmental monitoring (temperature, moisture, light, etc.). Unidirectional transfer is an effective power transmission over long distances (up to kilometer range), but it requires line-of-sight (LOS) and complicated tracking mechanisms, meaning it is only suitable for inherently large-scale devices. For instance, Unidirectional transfer can be applied to unmanned planes known as Stationary High Altitude Relay Platform (SHARP).

A microstrip antenna is a crucial element for transmitting or receiving waves that can be easily integrated in planar circuits. Collecting energy from the surrounding environment through wide band frequency, it is more benefit for energy harvesting. The authors in [5] presented a study on bandwidth widening techniques for directive antennas, using radiating energy for resonant antennas. However, the authors found that bandwidth impedance is often insufficient to cover effective frequencies in wireless telecommunication systems.

Another RF circuit can be used to cover a wideband microwave application for the rectifier. In [6], the researchers proposed a ring power divider that offers a filtering response in the operating frequency. For the harmonic, stepped impedance resonators are employed, with the frequency operating in a bandwidth of 1.7 GHz to 4.6 GHz. However, the size (5.1 × 5.5 cm) is an issue, though this may be modified to decrease dimensions and increase bandwidth [6].

1.2.2 Energy Sources

The sun emits the energy and vitality required for all activities on Earth, producing power for the sustainment of physical life. Other sources (vibration/motion, thermal energy, and radiofrequency [RF]) operate as modes of energy transmission. With the recent arrival of the Internet of Things (IoT), the number of devices requiring power has increased. Most of these devices are currently battery-operated, but advanced technologies are trending towards self-powering.

RF is one of the sources being discussed in the literature for use in EH and WPT. For example, the authors in [7-8] have summarized current energy harvesting/scavenging results and their power management. The classified sources of energy are presented in Table 1.2.

Table 1. 2. Illustrates the characteristics of various sources of energy [7-8].

No	Source of Energy	Source Power	Output Power	Usability
1	Ambient light Indoor Outdoor	 0.1 mW/cm^2 100 mW/cm^2	 10 µW/cm^2 10 mW/cm^2	Sun light
2	Vibration Human Industrial	 0.5m@1Hz 1 m/s^2@50 Hz 1m@5Hz 10 m/s^2@1 KHz	 4 µW/cm^2 100 µW/cm^2	Depends on the movement
3	Thermal Human Industrial	 20 mW/cm^2 100 mW/cm^2	 30 µW/ cm^2 1-10 mW/cm^2	Continue
4	RF	0.3 µW/cm^2	0.1 µW/cm^2	Available day, night, indoor, and outdoor

Sunlight is considered the most viable energy source, since it records the highest amount of energy compared with other sources, as shown in Table 1.2. Ambient light measures 0.1 mW/cm^2 indoors and 100 mW/cm^2 outdoors, while output power measures 10 µW/ cm^2 indoors and 10 mW/cm^2 outdoors, respectively. However, the main disadvantage of ambient energy from sunlight is that it is not available at night or during all seasons. Therefore, especially in countries farthest from the equator, numerous solar panels must be used to harvest ambient energy. This approach can be complex and costly.

Other alternative sources are energy scavenged from the human body and energy from industrial vibrations. However, in the latter case, the output power harvesting variable has a wide range, depending on the factory operations. This energy source is also not cheap. Human motion energy is measured at 0.5 m/s^2@1Hz, 1 m/s^2@50 Hz, while energy from vibration industrial source is measured at 1 m/s^2@5 Hz, 10 m/s^2@1 kHz. The output power for these two sources is 4 μW/cm^2 and 100 μW/cm^2, respectively.

Thermal energy comprises generator power based on available temperature. Like industrial vibration energy, there are enormous variations in the output power. Thermal energy also requires a large area. In comparing thermal, industrial and human energy output, we see that thermal energy reaches up to 20 mW/cm^2, while industrial one reaches 100 mW/cm^2, and human output reaches around 30 μW/ cm^2.

Telecommunication systems and broadcasting are abundant RF sources in the environment. Despite having relatively low energy output harvesting compared to other energy sources, RF is virtually everywhere on Earth and constantly emits energy. In fact, RF has become essential for connecting information and carrying energy due in large part to its ready availability and low cost. The next section discusses the use of ambient RF for energy harvesting.

1.2.3 Ambient RF Energy Harvesting

Base transceiver stations (BTSs) of RF universally transmit information and carry energy. Radio transmitter and receiver signals process between BTSs and circuit receiver systems, and can operate wireless power transfer. The function of BTSs is to widely broadcast through the environment to sensitive electronic apparatuses such as cellular phones [7-8].

Signals distributed through the ambient can carry information and energy for transceivers. This process is useful for green sustainability and drives wireless systems by scavenging energy. The radiated energy at the top of an antenna tower is approximately 60 W, 100 W (50 dBm), but the density reduces rapidly with increasing distance [9] [55] 56].

The researchers in [10] studied ambient backscatter-assisted wireless-powered communication for IoT networks. They found that pervasive ambient RF resources relay for dual manner operation using various mode selection protocols based on stochastic geometry analysis. Two RF-points within unobstructed line-of-sight of one another can successfully achieve transmission. The challenge, however, is aligning the signal detector from the ambient backscatter communication system to be line-of-sight. The authors also found that some parameters, such as bandwidth, transmit power, and waveform, are lacking [10].

1.2.4 Rectifier Topologies

The authors in [11] reviewed several designing methodologies for rectifier topologies. As shown in Table 1.3, these include a half-wave, a full-wave, a bridge diode, and a voltage multiplier. Rectifiers consist of one or more diodes that enable the current to flow in one direction and convert AC into DC. It can form in different shapes in semiconductor switches, silicon-controlled rectifiers, space pipe diodes, etc. In a half-wave rectifier, the AC connects at the diode. Specifically, the output is visible during the positive half-cycle but invisible during the negative half-cycle. Furthermore, a single-phase feeding requires a single diode, whereas a three-phase supply requires three diodes. Therefore, this topology is incompetent due to having only half waveforms, which is a low peak wave [11].

Conversely, a competent topology is a full-wave rectifier for both half cycles, with the AC feeding the diode's input and current stream into the load in the same direction. This topology crops a higher output voltage to fluctuate the DC during positive and negative half-cycles of the input AC. As both a full-wave rectifier and full-wave bridge rectifier, the two circuits' topology of voltage doubler is utilized to obtain the same way of the current flux to the load resistor [11].

Converting from AC to DC involves referring to rectifying. A diode element is a rectifier in terms of power harvesting, and the antenna then collects the signal. This is then required to be rectified and boosted for powering the application. At this stage, a suitable topology and diode must be carefully chosen [11].

Table 1. 3. Various topologies of the rectifier stage [11].

Rectifier stage	Output Signal	Input Signal (AC)
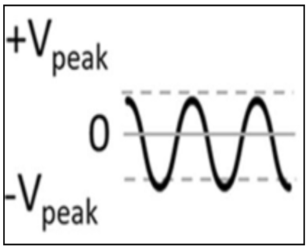	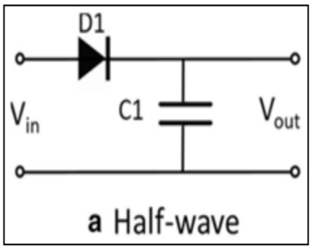	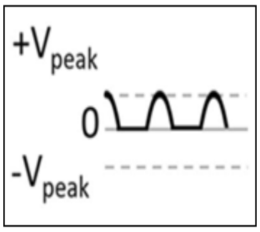
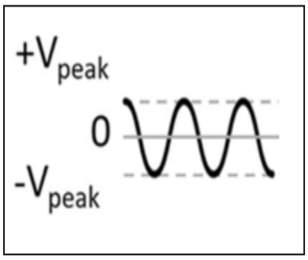	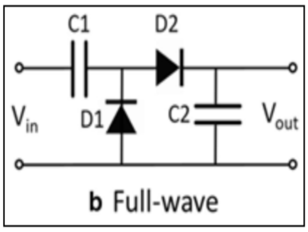	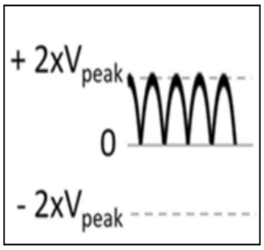
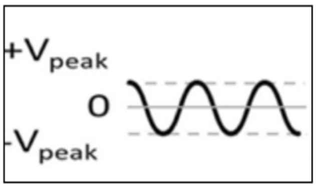	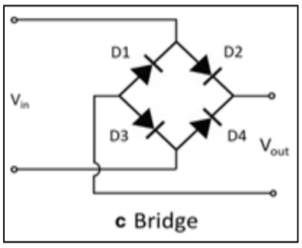	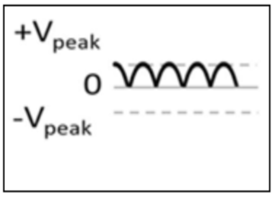

1.2.5 Antenna Rectifier for Energy Harvesting

WPT aims to communicate to the most places with compact devices while also reducing battery use. It is possible to harvest energy when the EIRP is higher. Frequencies below 6 GHz are unlicensed and service mobile bands for 5G, with maximum output voltage of 1.970 V and 1.784 V for 2 GHz and 4.8 GHz, respectively, being obtained in [12]. A Schottky diode HSMS-2850 was employed and achieved an efficiency of 30% at 2 KΩ RL, but with a relatively high input power level of 250 mW (24 dBm). The use of a high input power level is not recommended, for safety reasons.

A study proposing a novel sickle-shaped antenna was presented in [13], with a dual-band rectenna being used. In the work, a single Schottky diode (HSMS-2860) was employed for the rectifier stage, reaching an output voltage of 2.6 V. Efficiency of 63% and 54.8% was obtained at 2.4 GHz and 5.8 GHz operating frequencies, respectively, utilizing an R_L of 600 Ω, and a highest input power of 12 dBm [13].

In [14], the authors designed two arrays of dual microstrip antennas for 5.8 GHz ISM applications. They utilized a Dickson charge pump to light up a light-emitting diode (LED) from 50 cm away. A high at 1 W (30 dBm) of input transmitted power was observed within a narrow band of radiation pattern [14].

In [15], the authors used an operating frequency of 5.8 GHz, with the rectifier showing an efficiency of 60.6%. A Schottky diode was placed as a shunt diode among short-circuited second and third harmonics used by the oscilloscope. In the study, the input energy level was 9 dBm, and there were 1.3 KΩ loads besides the DC-pass capacitor with 0.28% ripple amplitude. The space between the transmitting and receiving antennas was 1.22 m, and the receiving antenna gain was 10.5 dBi. Further, the DC voltage was 1.5 V, not accounting for loss factors such as impedance mismatch loss and polarization loss. The authors concluded that 56.3% efficiency and 1.71 V DC voltage were obtained at 6 dBm input power level. However, this design uses high input power, and the diode HSMS-286B has breakdown characteristics limited to 7 V.

A technique of harmonic control Class-F using a voltage doubler to improve the conversion of RF to DC was applied in [16]. In the research, a Schottky diode was mounted for a 5.8 GHz rectifier, which obtained efficiency of 64.1%. The output voltage was 5.1 V, the RL was 1150 Ω, and the high input power level was 24 dBm.

In [17], a circuit improvement of an internal wireless system (IWS) for satellites was proposed. The authors presented a method that used two radial stubs designed in parallel. The main purpose of the experiment was improving sensing applications in space, with the results optimized for dual-frequency impedance termination. The study used a class-F load, which was able to function with third harmonic components. The operation frequency was 5.8 GHz, the output voltage was 5 V, and the R_L was 1.3 KΩ. The PCE achieved 71% at an input power of 30 dBm. This input power, however, is too high.

In [18], the researchers presented a dual-band rectifying circuit for WPT, using it to perform an RF-to-DC experiment. The power level incident chosen was 10 dBm. Their results showed 2.6 V and 66.8% and 2.3 V and 51.5%, at 2.4 GHz and 5.4 GHz, respectively, at R_L=1050 Ω. High efficiency was obtained due to the relatively high input power level. However, the amount of power density available from an ambient environment is much lower [18].

The researchers in [19] proposed a compact rectenna for WPT at a frequency of 5.8 GHz. Their input power ranged from −10 to 25 dBm, which achieved 50% to 70% efficiency using R_L = 220 Ω. A multimeter was used to measure the output DC voltage, with values of 2.8 V, 1.1 V, and 0.45 V being obtained when the input power level was 17, 9.5, and 2.5 dBm, respectively, using an HSMS2850 diode. This design could be implemented in the design of the rectifier topology and could be improved with lower input power in consideration of the energy amount from ambient wireless for WPT applications.

The authors in [20] presented an integrated antenna to build a compact rectenna for the 1.2 to 5 GHz band. They used an input power of 9 dBm with a load RL = 1 KΩ. The total measured RF-DC conversion efficiency was maintained above 30% in [20]. The authors selected this frequency band in order to operate with ISM, WLAN, 5G, LTE, and GPS applications for wireless devices, and implemented a design of a combined broadband differential rectifier (DR). While the design is preferable for RF-EH, it has a complicated circuit. Moreover, the multi-band operation is too complex to support the matching network of the antenna.

1.2.6 Technologies and Components Rectifier for WPT-EH

As a result of significant technological advances, radio frequency (RF) and microwave (MW) are used for energy harvesting (EH). Both technologies increase research on rectifying wireless power transmission [21]. In [22] a circuit-implemented complementary metal oxide semiconductor technology, operated at 5.8 GHz, is integrated in time-division multiplexed wireless sensors. Research on the design and implementation of a frequency of 2.4 GHz using an SMS7630 Schottky rectifier for two stages, and two stages of L-type matching network, was conducted.

Other authors have proposed a rectifier comprising of a 3 dB quadrature hybrid coupler (QHC) with an isolation port, the outputs of which are connected with two matching networks to injecting two sub rectifier circuits, including two filters and a load resistor [23]. In an experiment carried out by [24], they design, at 2.72 GHz, a unit cell that reaches near-unity radiation-to-RF.

Furthermore, the experiment showed in [25] that increasing wireless power has presented a circuit, which contains a series diode, a rectifier, and two transmission lines including two short circuit stubs. According to [26] research has paid attention to the input power for matching the rectifier and for providing high conversion efficiency at frequencies of 2.1 GHz and 2.45 GHz.

The Greinacher full-wave rectifier circuit topology, combined with a 180° hybrid ring (rat-race) coupler, was shown in [27]. Their work obtained a 125-MHz bandwidth at a center frequency of 1850 MHz, with 51% efficiency at 6.5 dBm under the load (Rload = 4.7 kΩ). In [28], a compact dual-band rectenna is used, namely, a slot-loaded dual-band folded dipole antenna proposed 915 MHz and 2.45 GHz, respectively, for a load resistor of 2.2 kΩ with an efficiency of 37% and 30% when irradiated by an MW signal of available power of −9 dBm.

RF sources have emerged as a vital part of research on power harvesting from ambient and are very significant to autonomously powering up standalone low-power systems, as concluded. They displayed the RF-based system as being challenging due to the very low incident RF power, power consumption, and losses by its components. It verified that their power harvesting is possible, provided a very efficient rectenna and very low-leakage capacitors are used [29]. An experiment [30] developed a circuit with a Wilkinson power combiner (WPC) that utilizes two different RF inputs. It permits the broadband operation of the multisector Chebyshev impedance matching technique, which was used in parts of the WPC circuit. The size of the circuit is large for electronic devices; hence, it dissipated much energy. Its range of operation was 0.4-0.81 GHz, 1.54-1.84 GHz, and 2.2-2.89 GHz, with 1.65 V output voltage.

A method is presented that was developed based on the novel rectifying circuit in [31]. It integrated the Cockcroft Walton rectifier in series with the Dickson rectifier organized in parallel and operated at a center frequency of 900 MHz center frequency. It used seven pairs of Schottky diode HSMS-285C with 14 capacitors, which are numerous elements. In [32] a microstrip patch rectenna connected wirelessly with ambient RF to harvest energy from GSM-900, GSM-1800, and UMTS-2100 bands. Their results favor its application for the Internet of Things presented.

A work formulating the design of the triple-port pixel antenna was proposed as a binary optimization challenge with an objective purpose related to harvested RF power in the GSM-1800 band for specified power angular spectrums [33], without the need for antenna matching components. The RF energy harvesters by [34] is considerably more compact than standard board designs but are challenged with lower input power level.

The IMN adapts to maximize power transmitted from source to the load by [35]. A rectifier in [36] is used to exploit the isolation resistor of the Wilkinson power combiner to reuse the power that might at first be wasted in the isolation resistor. A strategy for reusing the isolation resistor of a Wilkinson power combiner is introduced when the information RFs are not matching. It is seen that only one rectifier circuit is used, and the application is to build the proficiency of power amplifiers (PAs) configured, subsequently; it doesn't change the RF attempts to DC.

According to [37] the different RF wireless applications require power harvesting via integrated system components for recycling harvesting, from ambient power that offers direct wireless communications. The applications such as RFID sensors; these sensors are widely used in smart city, for instance smart parking, for low power consumption, cheaper, and comfort of deployment. Also, the disposal of the battery [37] decrease maintenance costs and some other environmental situations. RF energy harvesting has been an advent field of research [38]. However, the in-progress approaches of energy harvesting from RF signals are not sufficient, it is a perspective that more innovative technologies will be improved presently.

The research in [39] presented an integrated rectifier receiver (IRR) for lower power consumption, which employs the AC collecting signals. Their system for signal modulation using double signals has the potential to transfer a constant DC power to the sensor. Another experiment performed in [40] integrated energy rectifier at four bands to harvest the ambient electromagnetic energy in low and large-range energy density setting. It measured high conversion efficiency at 47.8%, 33.5%, 49.7%, and 36.2% of four two frequencies 0.89, 1.27, 2.02, and 2.38 GHz, respectively. The input power was −10 dBm. The rectifier has also a huge input strength.

The study in [41] presented a receiver circuit that integrated an antenna and rectifier using a single diode. Its frequency of operation was from 2 to 18 GHz at an input power of between −17 and 15 dBm. It obtained an efficiency of 20% with a resistance load of 100 Ω at 3 GHz. In [42], a dual-frequency scheme was proposed with ultralow-power, using a single diode rectifier topology. The input power levels were −11 and −13.5 dBm at 915 and 2450 MHz, respectively. The output DC voltage was 200 and 313.5 mV, respectively, with a resistance load of 2200 Ω.

Another article presented a new rectenna topology to improve power handling [43]. It increased the number of rectifying branches with a single collected DC output, and the topology was tested using a two-branch rectifier. The power conversion efficiency was 57% at 17 dBm, for an operating frequency of 2.1 GHz. The work in [44] demonstrated the concept of dual-band resistance compression networks (RCNs) for rectifier circuits with enhanced performance. Its proposed rectifier circuits changed the input power level and variations in the rectifier load. Further, the frequencies were a dual-band 915 MHz and 2.45 GHz rectifier based on an RCN. This reduced the sensitivity to variations in the output load and input power.

In another work, the researchers in [45] considered the time domain superposition coding technique, adding on the G3-PLC standard and performing reproduction tests. Their outcomes show that the framework had a gain of up to 4 dB when the G3-PLC standard was added with time area superposition coding. However, the calculations could be challenged on the obstruction of high commotion and the adequacy of multipath impact. A method was presented in [46] to reuse current for a wideband low noise amplifier (LNA) and ultra-wide band (UWB) purposes. It was completed by the wideband input matching and represents a collection of degenerative parallel LC circuit and resistive returns in a shunt-shunt connection. Additionally, the cascaded LC method was applied to obtain results matching.

The targeted parameters to wireless power transfer are related in ISM applications [47]. In [48] a broad-band rectenna 1×4 quasi-Yagi antenna array is formed with a T-junction power divider for GSM-1800 and UMTS-2100 band.

1.2.7 Summary of the Literature Review

In the above review of the pertinent literature, several state-of-the-art rectennas were discussed for the fields of WPT and EH. These designs, however, faced some challenges in the RF and microwave bands. One of the main issues was finding a way to effectively integrate passive with active components for WPT, as the element's behavior can be linear or non-linear. A second key issue was that standard frequency operation and incident power level are variable functions of transmitted power and distance from the base station. An additional challenge was making the system suitably compact while still being able to obtain microwave frequencies. Such a system would have to contend with lower input power levels due to increased free space attenuation, in accordance with the Friis equation [51].

Chapter 2 – Integrated Rectenna Prototype using Patch Antennas and 90º Hybrid Coupler Combiner

2.1 Introduction

The proposed rectenna incorporates two rectangular patch antennas integrated with a full-wave rectifier maybe a block diagram would be good providing at this point. This section focuses on the design of some components in order to combine signals and rectify them. These components are integrated on the printed circuit board (PCB). Each component serves a specific task. The Dual patch antennas receive RF energy from space. The 90º hybrid coupler is suitable to combine signals from antennas for RF collecting. The matching network maximizes the output power. The rectifier converts the AC signal into a DC signal. Ultimately, the load component including the storage capacitor eliminates voltage ripples.

The 5.8 GHz ISM frequency band (5.725 - 5.875 GHz), which does not require an FCC license [20], is chosen to harvest energy. In addition, this band is commonly used for WLAN bands in urban areas (802.11/a standard). Moreover, it can operate among 5G technology in sub-6 GHz operating frequencies, which has recently been launched.

For implementing the prototype, the substrate relative permittivity ε_r = 10.2 is considered to avoid a larger circuit size for antennas and 90° hybrid coupler components. Low permittivity leads to a larger dimension design than is considered reasonable in modern devices [49]. It causes a narrow space between the two λ/4 arms of the 90º hybrid coupler, increasing the undesired coupling. Therefore, the prototype is designed based on the trade-off in terms of size and mutual coupling.

Advanced Design Systems software (ADS) from Keysight Technologies was used for the design and simulation of the circuits. The Printed Circuit Board uses a Rogers RO3010 substrate [50]. The parameters of the substrate are shown in Table 2.1.

2.2 Antenna

Microstrip antennas, called patch antennas, can have different shapes: circular, elliptical, rectangular, square, triangular, etc. One of the most used is the rectangular patch. The advantages of microstrip antennas - low profile, simplicity, ease of use integrate by along with other planar components of a compact low-cost module.

The bandwidth can be increased by increasing the height of the substrate [51]. However, a trade-off must be considered, because increasing the height will simultaneously increase the width of the microstrip lines, making the circuit implementation very difficult.

Three parameters (f, ε_r, and h) are required in the design of the rectangular microstrip patch antennas. According to [51], patch antenna dimensions are calculated, which determines the width (W) and the physical length (L).

Table 2.2 displays the parameters and variables, related to equations (2.1) to (2.5), which are used to calculate the width, length, effective dielectric constant, and length extension. The feeding method is a microstrip line, which is commonly used in microstrip antennas.

Table 2.1. Parameters of substrate RO3010.

The relative permittivity (ε_r)	The thickness (*h*)	The thickness of copper line (*T*)	The loss tangent (tan *D*)
10.2	0.64 mm	17.5 μm	0.001

Equations (2.1) – (2.5) are used for estimating the dimensions of patch antenna. We used the following formulas as in [51].

Width patch antenna (Wp)

$$(Wp) = \frac{C}{2 \cdot f \cdot \frac{\sqrt{\varepsilon r+1}}{2}}\ 15.5\ \mathrm{mm} \tag{2.1}$$

Table 2.2. Parameters and variables required in equations (2.1) to (2.5).

Speed of light (*c*)	Frequency (*f*)	Wavelength (*λ*)
3×10^8 m/s	5.8 GHz	0.0517 m

Effective dielectric constant (ε_{eff})

$$= \frac{\varepsilon r+1}{2} + \frac{\varepsilon r-1}{2} \cdot [1 + 12 \cdot \frac{h}{W}]^{-\frac{1}{2}} = 9.4 \tag{2.2}$$

Correction factor $(\Delta L) = h \cdot 0.412\ \frac{(\varepsilon eff+0.3)\cdot\left(\frac{W}{h}+0.264\right)}{(\varepsilon eff-0.258)\cdot\left(\frac{W}{h}+0.8\right)} = 0.274$ (2.3)

The actual length of patch antenna (L) is calculated by equation (2.4)

$$L = \frac{\lambda}{2} - 2 \cdot \Delta L = 0.295 \tag{2.4}$$

The effective length is (L_e) $= L + 2 \cdot \Delta L = 8.4\ \mathrm{mm}$ (2.5)

The original design of this patch antenna depends on the conventional equations above. The parameters have been optimized using the ADS software. Table 2.3 shows the original, and optimization dimensions of the patch antenna. Figure 2.1 shows the simplified schematic of the patch antenna.

Table 2.3. The dimensions of microstrip antenna (mm).

Calculations	Width (Wp)	Width (Wp)
Optimization	16.18	7.82

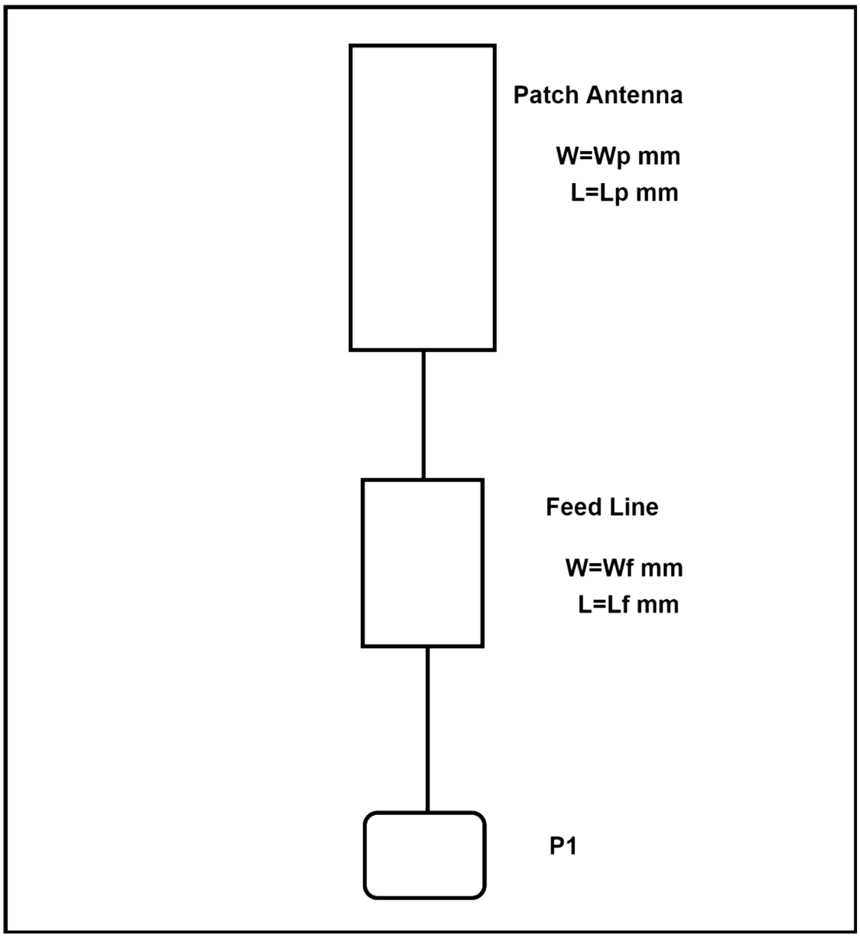

Figure 2.1. Schematic of Patch Antenna design.

Figure 2.2 shows the layout of the patch antenna based on the dimensions that were optimized.

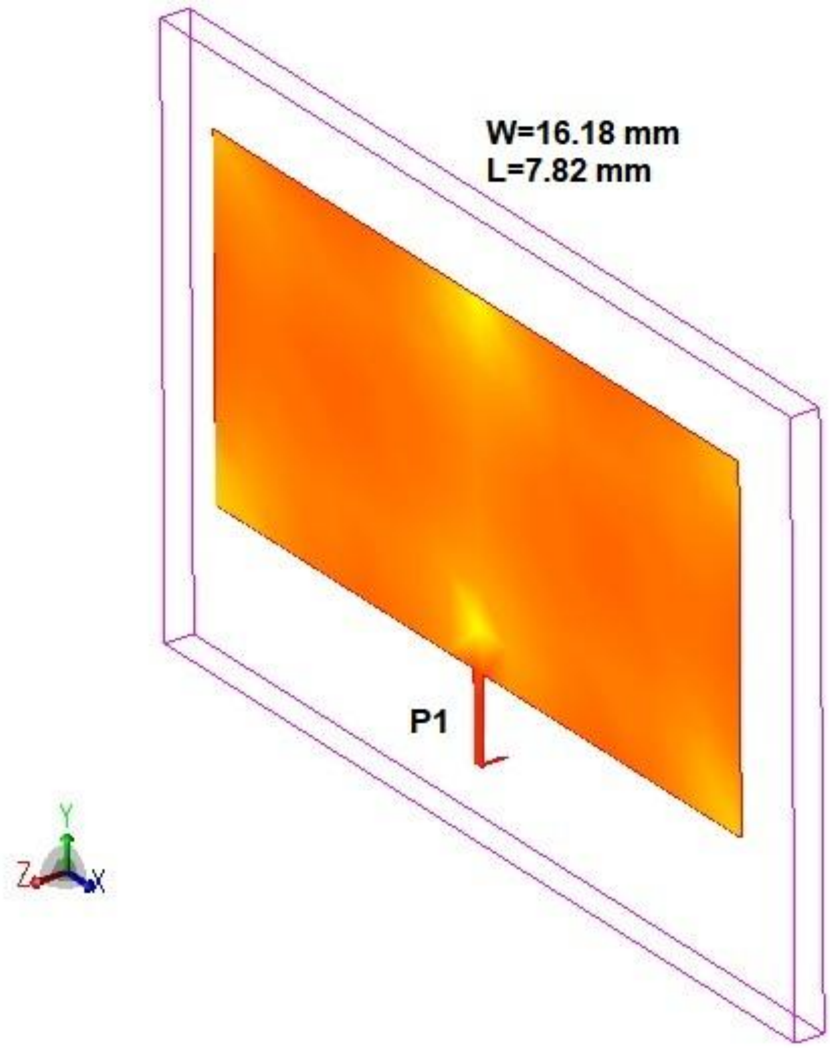

Figure 2.2. E-field distribution of patch antenna.

Figure 2.3 displays the input return loss. The simulation shows that the return loss is approximately 27 dB at 5.8 GHz. The 10 dB bandwidth is approximately 100 MHz, representing 2 % of the central frequency, a common result for a patch antenna.

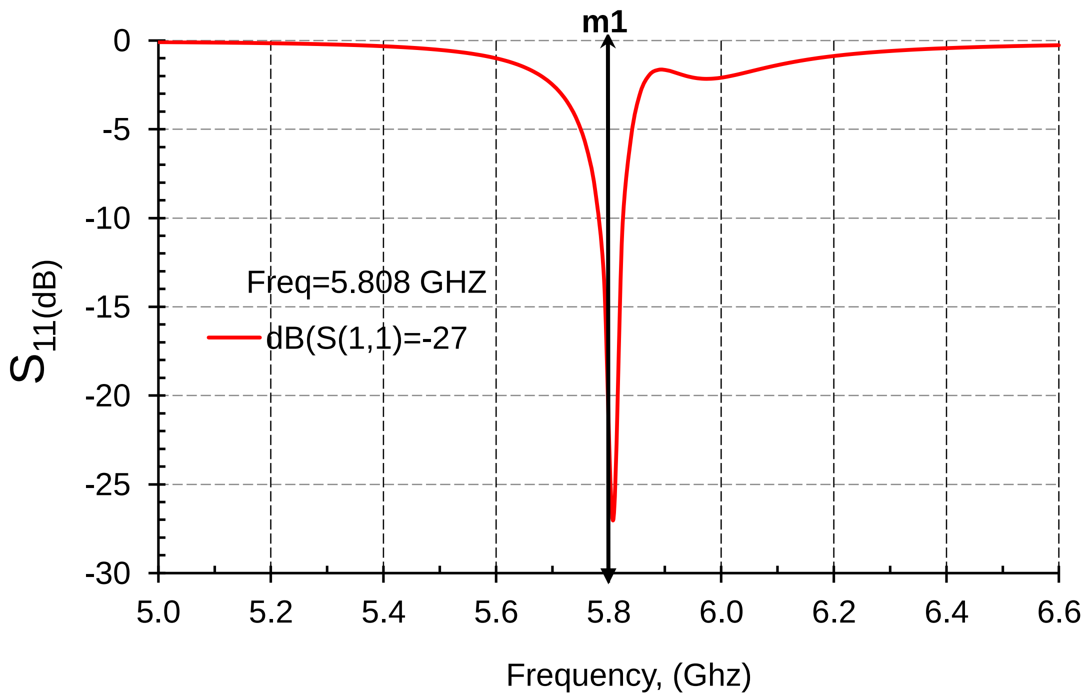

Figure 2.3. Simulated S_{11}(dB) of the patch antenna.

The rectangular patch antenna component collects F signals. It has a radiation attribute and a low cross-polarization radiation. Accordingly, the three-dimensional radiation in Figure 2.4 depicts the energy distribution.

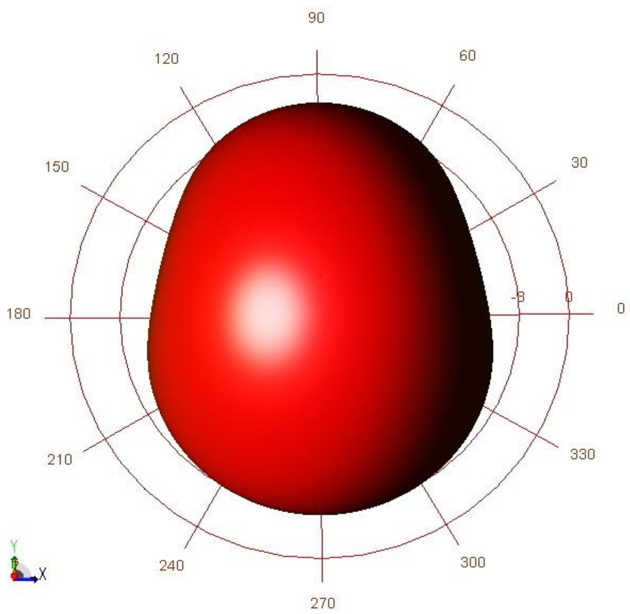

Figure 2.4. Three-dimensional radiation pattern of patch antenna.

The simulated patch antenna directivity is 5.7 dBi, the simulated gain is 4.5 dB, and the efficiency by divide the gain over directivity is 79% as seen in Figure 2.5.

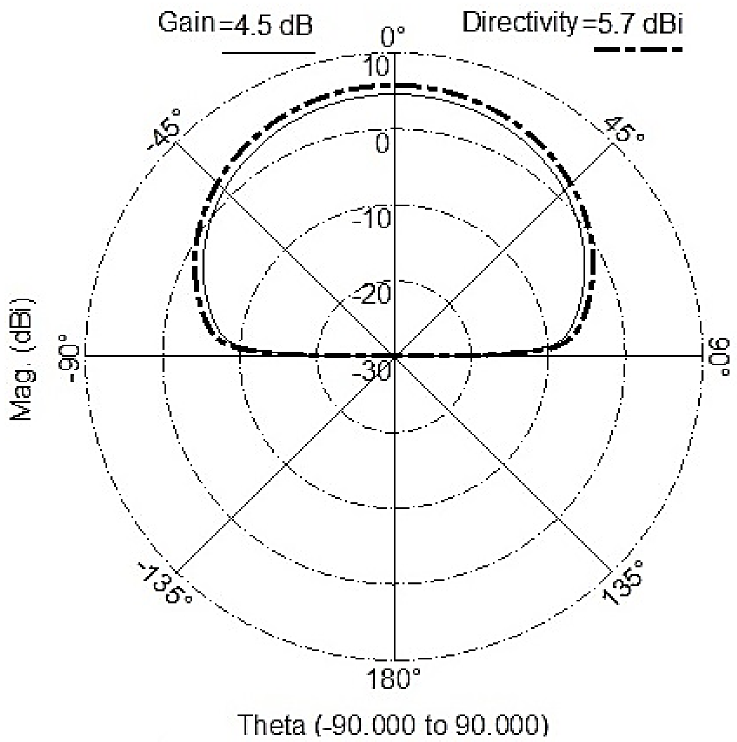

Figure 2.5. The simulated directivity and gain of patch antenna.

2.3 90º Hybrid Coupler

We designed the 90º hybrid coupler according to [52], as shown in Figure 2.6, to combine signals from two patch antennas. It is used, with a 90° phase shifter added to the coupled port, for feeding in a differential way the rectifier stage. Using LineCalc program in ADS, the dimensions of the transmission lines for the design of the 90º hybrid coupler are calculated. The substrate parameters and variables are listed in Tables 2.1 and 2.2. We set the electrical effective length at 90º for quarter wavelengths used in the coupler layout, and the characteristic impedance Z_0 is 50 Ω. The width (W), and length (L) dimensions of Z_0 = 50 Ω transmission lines (TL1, 2, 3, 4, 5, and 6) and of $Z_o/\sqrt{2}$ = 35.36 Ω ones (TL7, and 8) are listed in Figure 2.6.

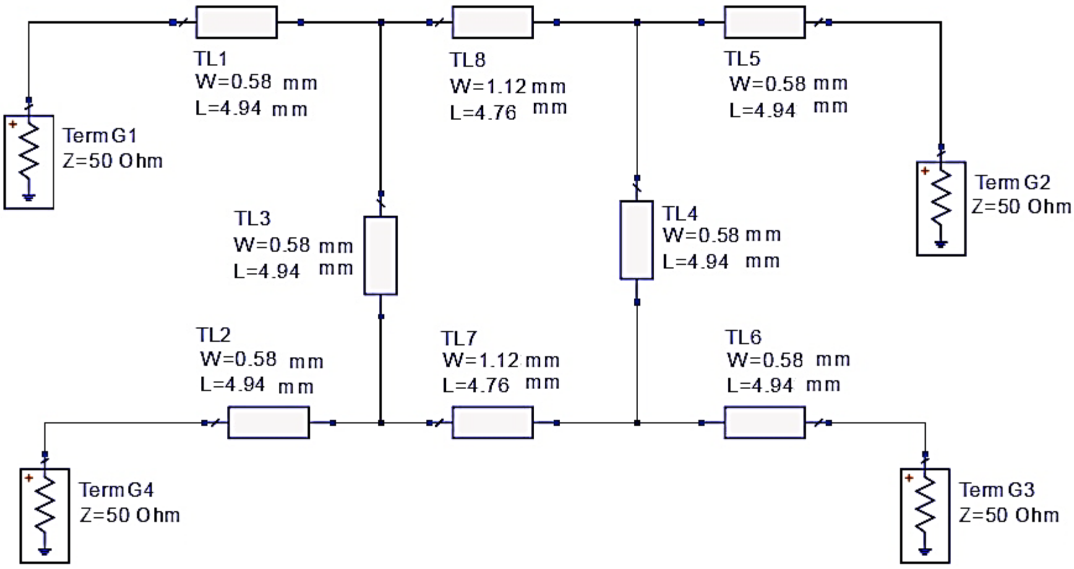

Figure 2.6. 90º hybrid coupler design.

Figure 2.7 shows the layout and energy distribution if the coupler is fed at port 1 (EM Momentum of ADS). Port 4 is ideally isolated, and a 3 dB coupling with a 90º phase shift difference between Port-2 and 3 is obtained. When the coupler is excited at both inputs (P_1 and P_4) from the patch antennas, it will combine the energy to the outputs (P_2 and P_3), keeping the inputs isolated from each other. By symmetry, the inputs can be P_2 and P_3 and the outputs P_1 and P_4.

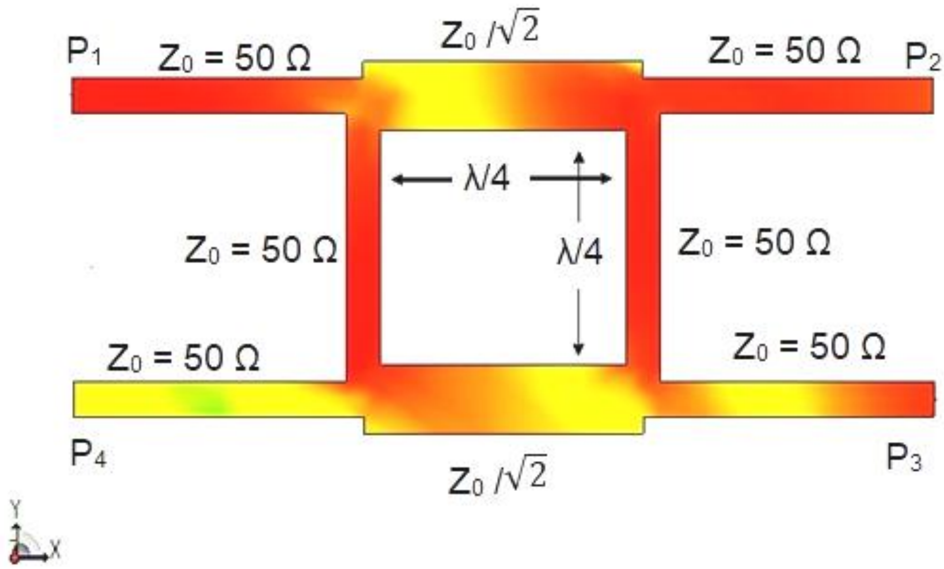

Figure 2.7. The layout of 90º hybrid coupler.

Figure 2.8 shows the S-parameter simulation results for the 90º hybrid coupler in ADS EM Momentum. The (EM) setup form defines the dielectric and conductor properties. Optimization tools are used. If a bandwidth under −10 dB is considered, the circuit operates from 5 to 6.6 GHz. Minimum S_{11} is – 56 dB at central frequency, where S_{12} = -3 dB and S_{13} = -3 dB. The maximum isolation S_{14} is around − 63 dB at 5.818 GHz. It is wholly matched at all four ports. It is apparent that the S-parameters are very good in the operating band.

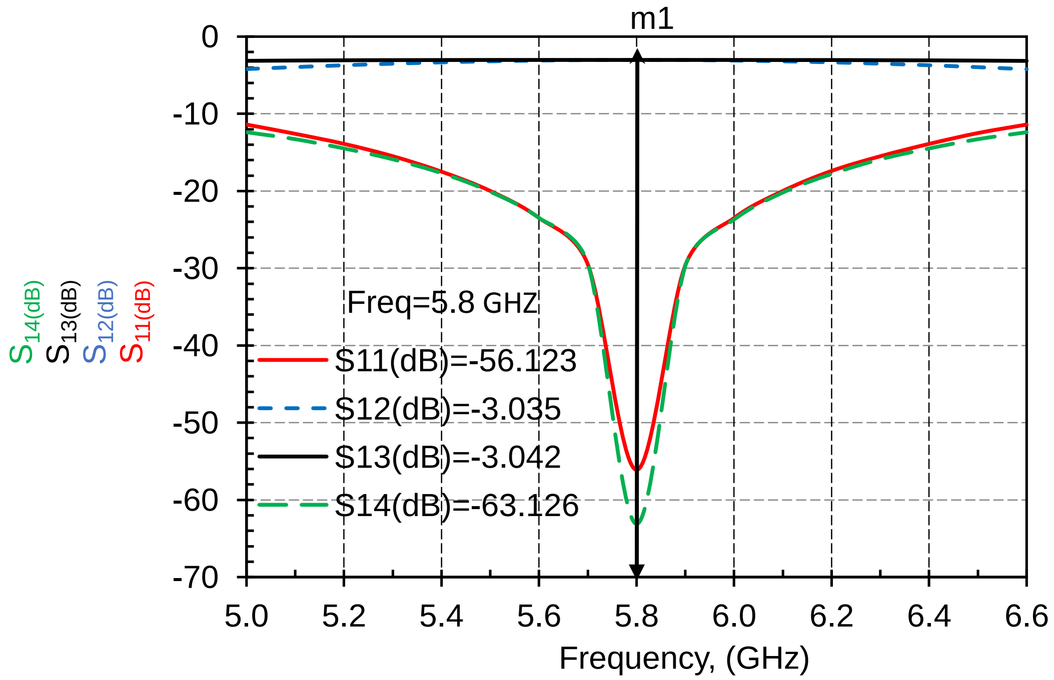

Figure 2.8. Simulated S-parameters of a 90º hybrid coupler.

The patch antennas are feeding the 90º hybrid coupler to combine the input signals RF. Figure 2.9 shows the dual patch antennas integrated with the 90º hybrid coupler. Transmission Lines are defined as the dimensions of dual passive rectangular patch antennas.

The antenna is a reciprocal device. In order to obtain its radiation pattern, the RF signal is applied to P_1. In the receiving mode, the input ports are P_2, and P_3, that are connected with two patch antennas. The signals are combined properly, considering the need of differentially feeding the rectifier, by adding a λ/4 transmission line (90° phase shift) between one of the two antennas (Ant_2) and the input port P_2 of the 90º hybrid coupler, as seen in Figure 2.9.

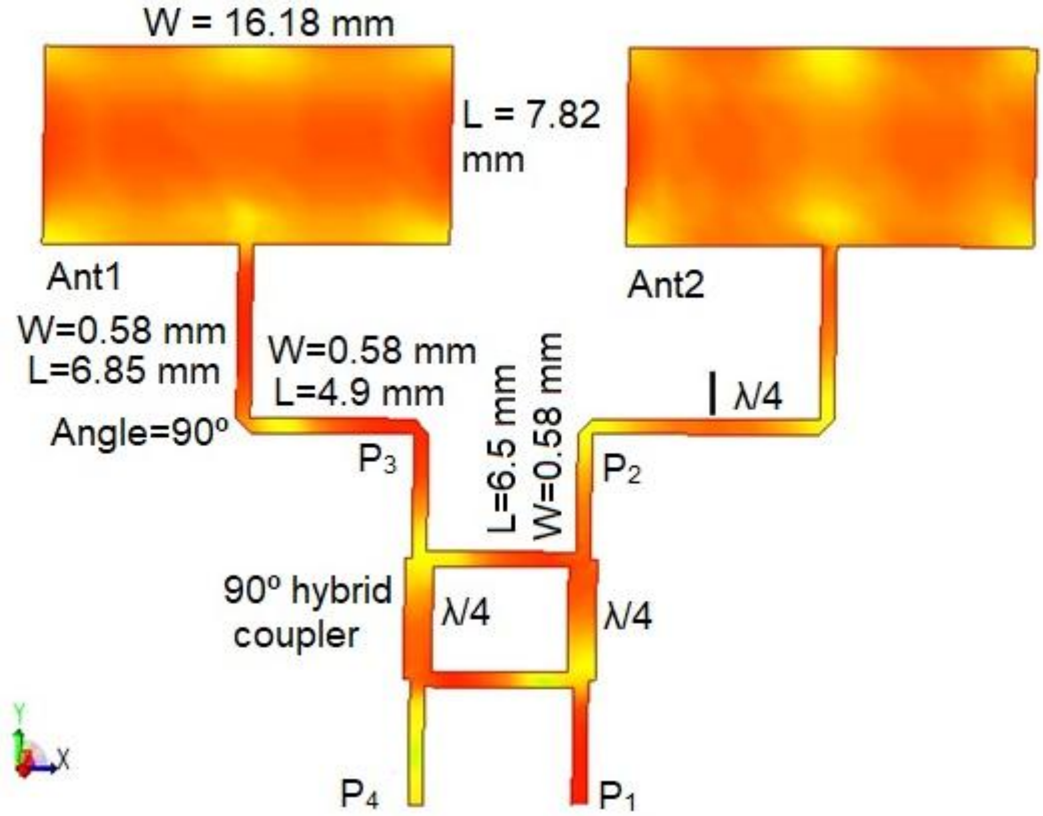

Figure 2.9. Layout of the 90° hybrid coupler integrated with two patch antennas.

ADS EM Momentum simulated results of the gain, directivity, and power radiation are shown in Figure 2.10. The obtained directivity and gain are 7.1 dBi and 6.2 dBi, respectively. The half-power beam width (HPBW) is approximately 45°.

The designed rectangular patch antenna is integrated with the 90º hybrid coupler on the same dielectric substrate. The layout is on the top and another part is the ground plane.

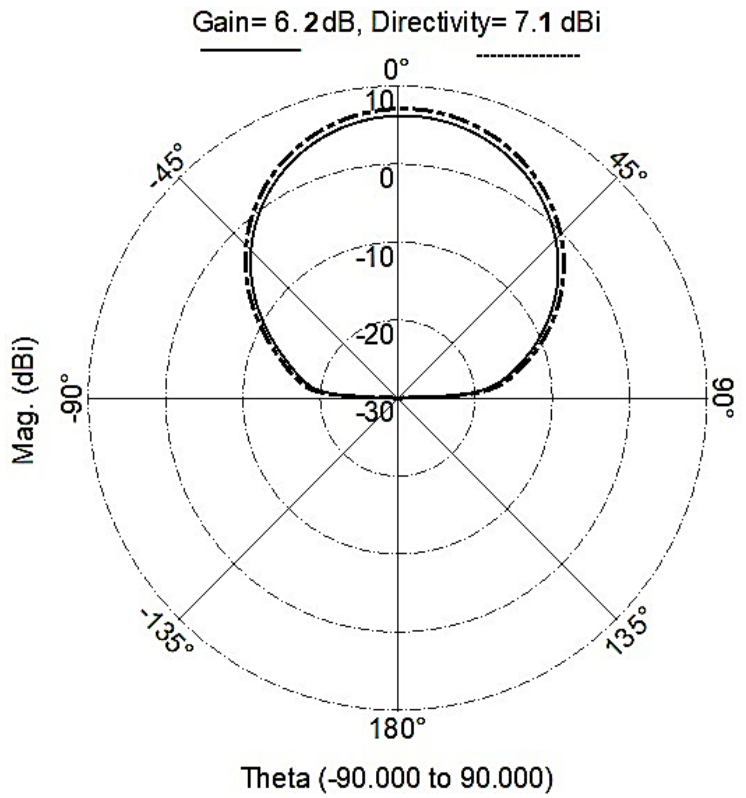

Figure 2.10. The directivity and the gain of Figure 2.9 layout patch antennas and 90º hybrid coupler.

Combined Figure 2.11 shows the three-dimensional radiation of dual patch antennas combined with the 90º hybrid coupler. The 3D diagram is obtained from the ADS Momentum using Electro Magnetic Design Solver. The main lobes on 90º and 270º with nulls at 0º and 180º are apparent.

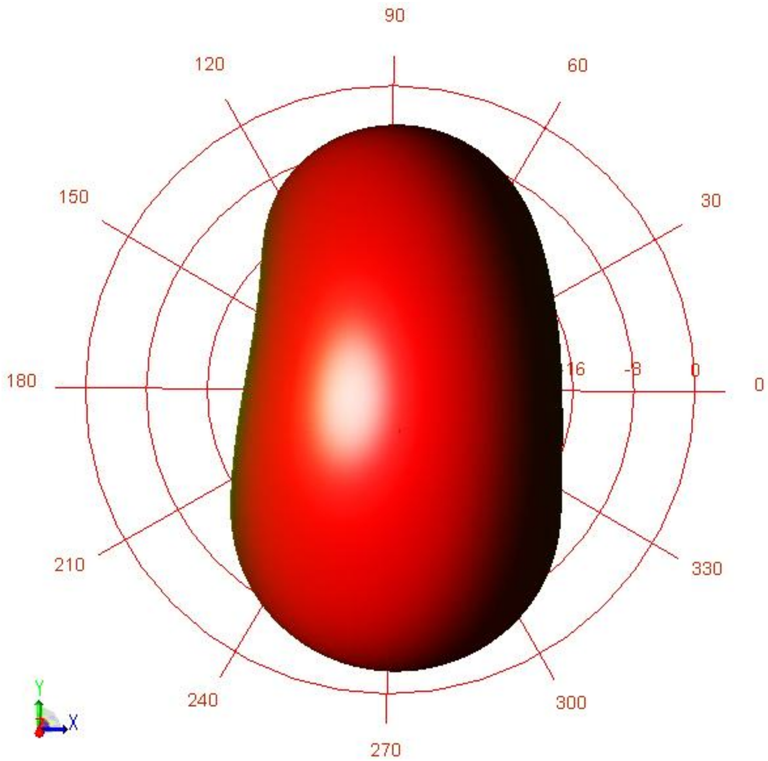

Figure 2.11. Three-dimensional radiation of dual patch antennas with the 90º hybrid coupler.

The efficiency of the two-antenna system (including hybrid coupler in Figure 2.9 displayed in Figure 2.12) is divided the gain over the directivity. It is shown greater than 50% for most frequencies

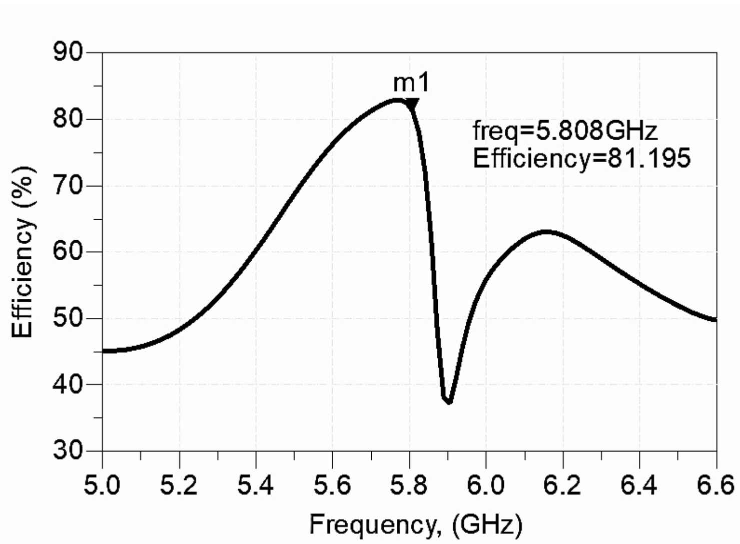

Figure 2.12. The EM Momentum simulation of efficiency (%) versus the frequency (GHz) of the layout of the dual patch antennas integrated the 90º hybrid coupler.

2.4 Rectifier

Rectification is converting the AC signal into DC using one or more diodes to allow the current to flow in one direction to the load, blocking the current in the opposite direction. A common type of rectifier uses only the positive or negative half of the wave. Another rectifier type is a full-wave rectifier which is a circuit that converts both halves of the wave into DC.

- **Full-Wave Diode Bridge**

This proposed circuit uses a bridge diode in the rectifier stage. It is a full-wave rectifier that uses four diodes, as seen in Figure 2.13. During the positive half-cycle D_1 and D_2 are forward-biased, and D_3 and D_4 are reverse-biased, as aforementioned in chapter 1 (Section 1.2.4). When the current flows through the positive path through D_1, it creates a voltage across the load. The current enters D_2 through the ground and, after that, it returns to the negative side of the input.

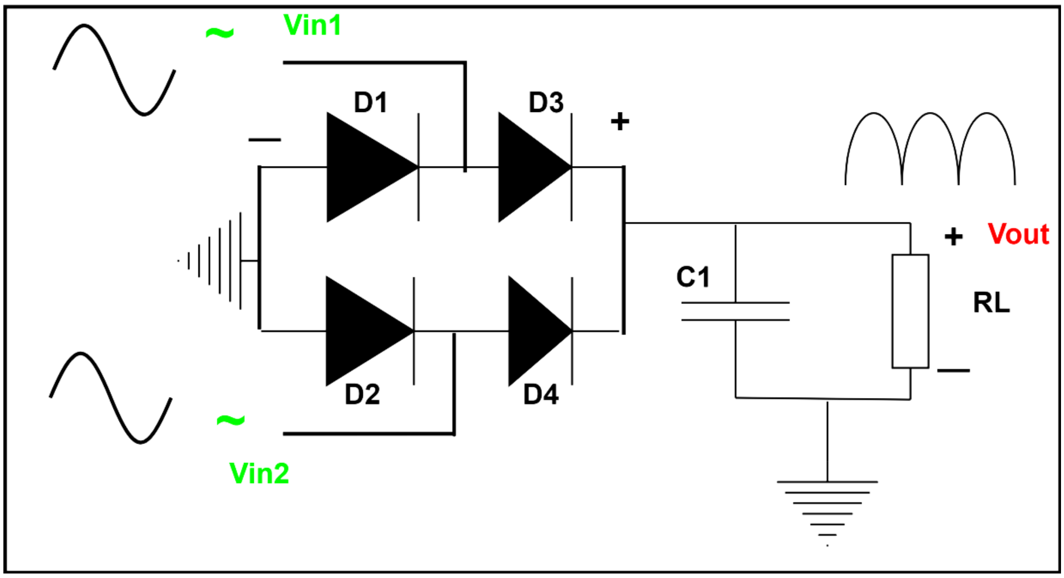

Figure 2.13 Full-wave rectifier of typical bridge diode circuit.

- **Practical implementation**

The diode is ideal for RF/ID applications, as well as large signal detection, modulation, RF to DC conversion or voltage doubling. Another advantage is the compact packaging, two diodes being available in one package. This led to a smaller number of required solder joints. It combines advanced semiconductor technology with low-cost packaging technique. Figure 2.14 lists the parameters for the AVAGO HSMS286K diode pair [53].

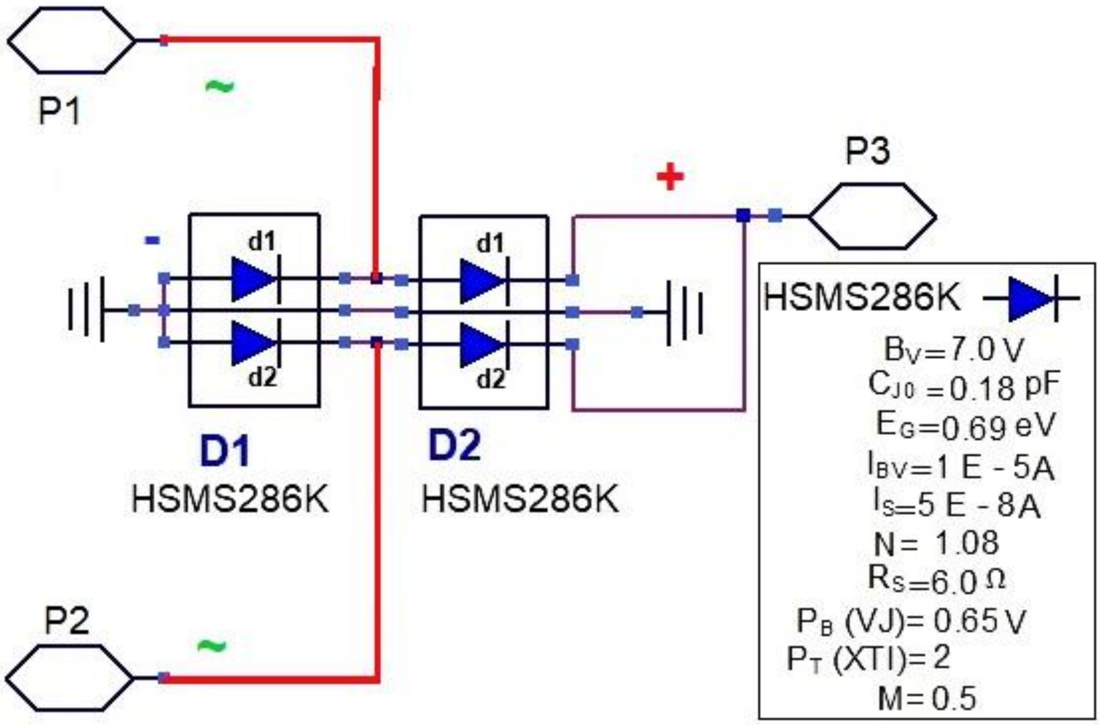

Figure 2.14. Figure 2.7. Diagram of HSMS286K diode.

2.5 Matching network

The impedance matching network (IMN) is placed between source load and eliminates the power reflections from diodes. The target input impedance in the IMN is Z_0 [54]. In the rectenna circuit, the output of the coupler is the source input of the IMN. Its output is connected to the input of the rectifier stage, as the load impedance. A mismatch between the source and the load causes reflected power flow in the circuit, which minimizes the system's efficiency. The IMN uses reactive components for its implementation.

- **Types of Impedance Matching Network**

There are a number of standard configurations for matching networks such as L, T and Π types, as shown in Figure 2.15. (B), and (C). The T and Π matching configurations are more complex than the L type network, respectively [54]. In Figure 2.15, the (A) L-type matching network circuit is used to match the impedance between the passive circuits. On the other side, the IMN is connected to the bridge diode rectifier. The L-type matching network elements contain two components: the inductor (L) and the capacitor (C). More elements can also be used to enhance the efficiency and output power of the rectennas.

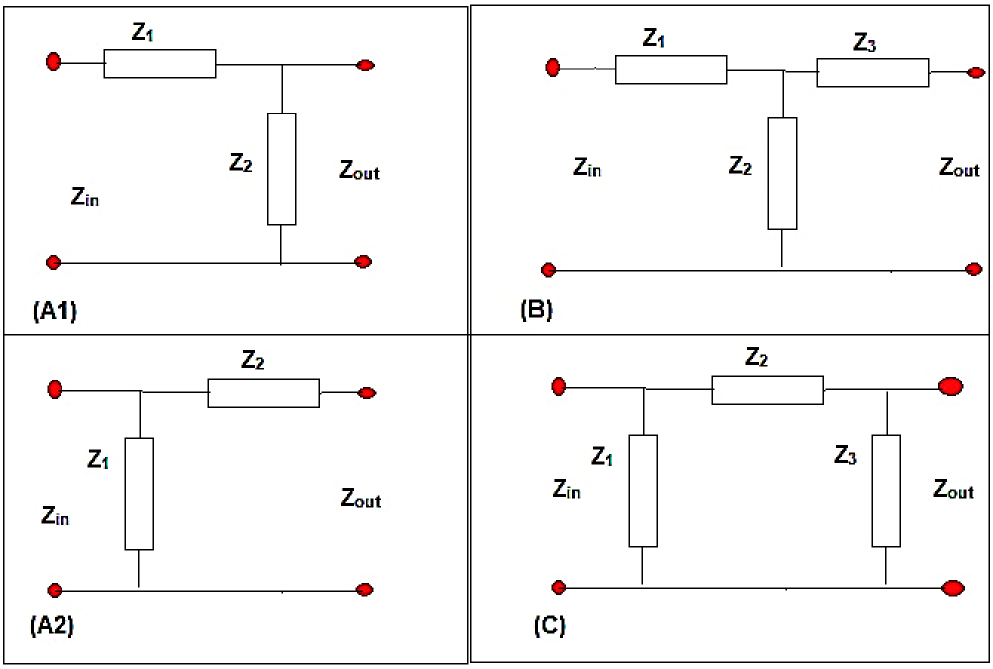

Figure 2.15. Types of impedance matching network (A) L-type, (B) T, and (C) Π [54].

- **Design of Impedance Matching Network**

Using a single L-network section depends on the conditions offered by the source and load impedances. The maximum power transfer condition $Z_S{}^*=Z_{IN}$ is based on the equations described in [54]. The essential purpose is to match an arbitrary complex load impedance, $Z_L = R_L + j \cdot X_L$, to complex source impedance, $Z_s = R_s + j \cdot X_S$, using a matching network.

The matching between source and load can be solved with the equations of B, X parameters and C, and L elements, with the conditions shown in Tables 2.4 and 2.5. More than one solution can be obtained. The matching solution is related to four factors: (complexity, bandwidth, implementation, and adjustability). From equation

(2.7) the real and imaginary parts can have two pairs of solutions, B_1, X_1 and B_2, X_2, as shown in equations (2.8) and (2.9).

$$Rs - j \cdot Xs \ = \frac{1}{jB + (\frac{1}{jX + RL - j \cdot XL})} \tag{2.7}$$

$$B_1 = \frac{RL \cdot Xs + \sqrt{RL \cdot Rs \cdot (Rs^2 + Xs^2 - RL \cdot Rs)}}{RL \cdot (Rs^2 + Xs^2)} \tag{2.8}$$

$$X_1 = \frac{RL \cdot Xs - Rs \cdot XL}{Rs} + \frac{Rs - RL}{B_1 \cdot Rs} \tag{2.9}$$

Also, the next equation B_2 replaces the negative sign before square root as shown in (2.10). The equation (2.11) X_2 is the same as X_1, but B_1 is replaced by B_2.

$$B_2 = \frac{RL \cdot XL - \sqrt{RL \cdot Rs \cdot (Rs^2 + Xs^2 - RL \cdot Rs)}}{RL \cdot (Rs^2 + Xs^2)} \tag{2.10}$$

$$X_2 = \frac{RL \cdot Xs - Rs \cdot XL}{Rs} + \frac{Rs - RL}{B2 \cdot Rs} \tag{2.11}$$

Equation (2.12) for the second configuration is:

$$Rs - j \cdot Xs \ = jX + \frac{1}{jB + (\frac{1}{RL + j \cdot XL})} \tag{2.12}$$

In equation (2.12) the real and imaginary parts can be separated to obtain two solutions for (2.13) B_3, (2.14) X_3 and (2.15) B_4, (2.16) X_4:

$$B_3 = \frac{Rs \cdot XL + \sqrt{RL \cdot Rs \cdot (RL^2 + XL^2 - RL \cdot Rs)}}{Rs \cdot (RL^2 + XL^2)} \tag{2.13}$$

$$X_3 = \frac{Rs \cdot XL - RL \cdot Xs}{RL} + \frac{RL - Rs}{B_3 \cdot RL} \tag{2.14}$$

$$B_4 = \frac{Rs \cdot XL - \sqrt{RL \cdot Rs \cdot (RL^2 + XL^2 - RL \cdot Rs)}}{Rs \cdot (RL^2 + XL^2)} \quad (2.15)$$

$$X_4 = \frac{Rs \cdot XL - RL \cdot Xs}{RL} + \frac{RL - Rs}{B_4 \cdot RL} \quad (2.16)$$

The equations (2.8), (2.10), (2.13), and (2.15) are valid when the square roots are positive or zero.

Table 2.4. The valid conditions of equations for valid solutions.

No equations	Conditions of the equations valid matching complex impedance circuits
(2.9), (2.11)	$R_S^2 + X_S^2 - R_L \cdot R_s > 0$ and $R_L^2 + X_L^2 - R_L \cdot R_s < 0$
(2.13), (2.16)	$R_S^2 + X_S^2 - R_L \cdot R_s < 0$ and $R_L^2 + X_L^2 - R_L \cdot R_s > 0$
(2.8), (2.11), (2.14), (2.16)	$R_S^2 + X_S^2 - R_L \cdot R_s > 0$ and $R_L^2 + X_L^2 - R_L \cdot R_s > 0$

Table 2.5. The real values of B, and X to calculate capacitor and inductor.

Values	Positive	Negative
B	$C = \frac{B}{2 \cdot \pi \cdot f}$	$L = -\frac{1}{2 \cdot \pi \cdot f \cdot B}$
X	$L = \frac{X}{2 \cdot \pi \cdot f}$	$C = -\frac{1}{2 \cdot \pi \cdot f \cdot X}$

$$\mathrm{B}_4 = \frac{48.703 \cdot (-29.342) - \sqrt{1.153 \cdot 48.703 \cdot (1.153^2 + (-29.324)^2 - 1.153 \cdot 48.703)}}{48.703 \cdot (1.153^2 + (-29.342)^2)} = -0.04$$

$$\mathrm{X}_4 = \frac{48.703 \cdot (-29.324) - 1.153 \cdot (35.091)}{1.153} + \frac{1.153 - 48.703}{-0.04 \cdot 1.153} = -243.5$$

$$C = -\frac{1}{2 \cdot \pi \cdot f \cdot \mathrm{X}_4} = 1 \text{ pF} \quad (2.17)$$

$$L = -\frac{1}{2 \cdot \pi \cdot f \cdot \mathrm{B}_4} = 6 \text{ nH} \quad (2.18)$$

2.6 Simulation of the rectenna

The 90º hybrid coupler splits the signal into two paths, which can be individually handled by two L type matching network components during signal conversion and can be recombined into a single signal thereafter. The signals are combined properly at the bridge input: one output port is grounded, and another one doubles the signal, as shown in equations (2.19) - (2.20). The outputs (b_i) are normalized waves and are given by:

$$b_2 = a\,[(-j)^2 + (-j)^2] = -2a. \qquad (2.19)$$

$$b_3 = a\,[(-j) + (-j)^3] = a\left[(-j) + (-j)\right] = 0. \qquad (2.20)$$

As seen in Figure 2.16, V_{in1}, and V_{in2} are injected into the 90º hybrid coupler. The two differential voltages at the output of the matching network are feeding the HSMS286K bridge diode inputs. The DC output is obtained at the load, which is connected in parallel with the storage capacity C_2.

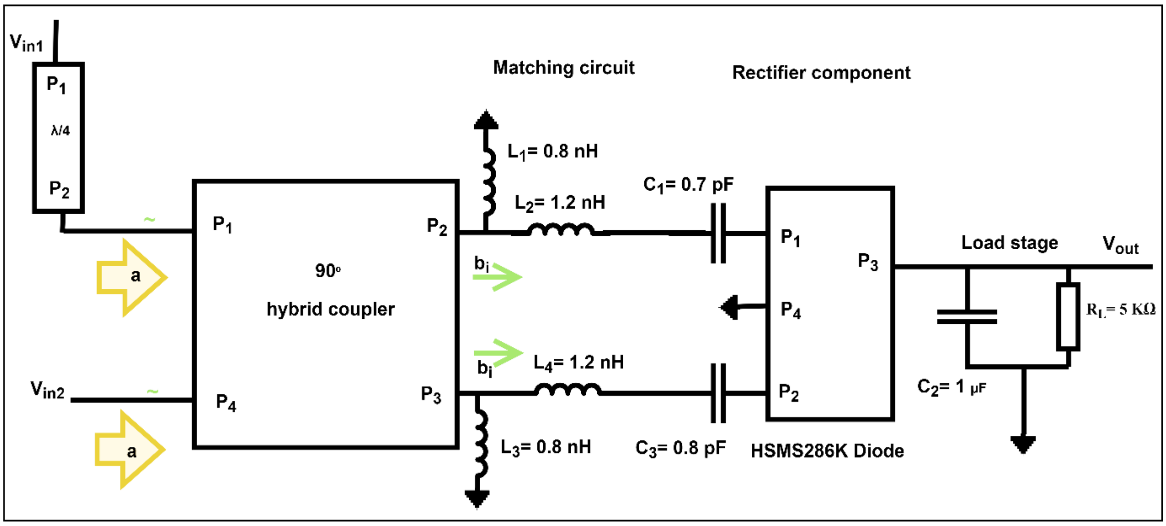

Figure 2.16. Schematic of 90º hybrid coupler, integrated matching network and bridge diode with the load stage.

The circuit shown in Figure 16 has been simulated, and the results for S_{11} and S_{44}, are shown in Figure 2.17. It is apparent that S11 and S44 are both less than -10 dB for a 1 GHz bandwidth ranging from 5 GHz to 6 GHz. The S_{11} and S_{44} are approximately -24 dB at 5.8 GHz. This central frequency is identical to those of patch antennas. The coupler itself covered a wider band, as seen in Figure 2.17.

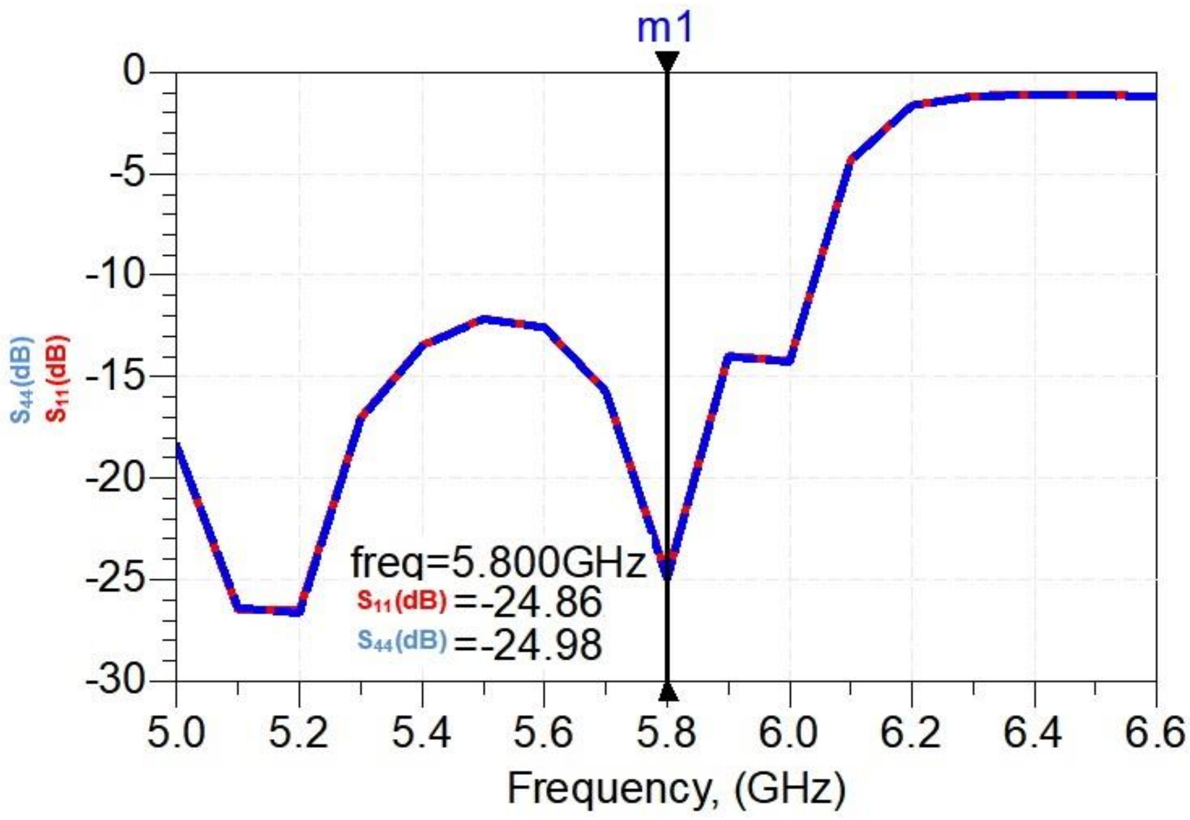

Figure 2.17. S_{11}, S_{44} of 90º hybrid coupler, with integrated matching network and bridge diode with the load stage.

Figure 2.19 shows that there is no RF component at rectifier is output, when a power of 0 dBm is applied at the two input terminals at 0 Hz.

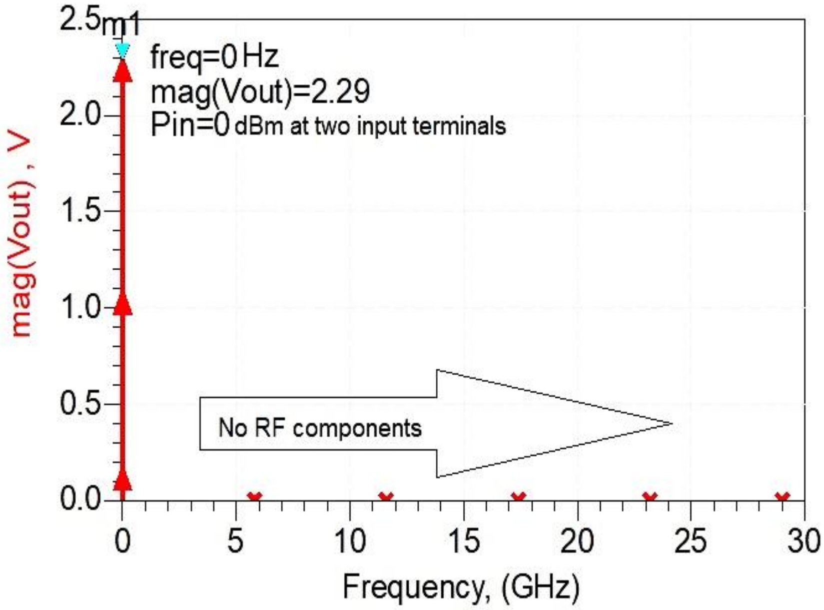

Figure 2.18.Output power of the schematic shown in Figure 2.16.

Figure 2.19 shows DC output voltages (V_{out}), (0.17, 1.08, and 2.29 V) versus time, expired in psec, at different input power levels (-10, - 5, and 0 dBm respectively at two input terminals). The test condition uses the schematic given in Figure 2.16, with two generators being connected to the inputs.

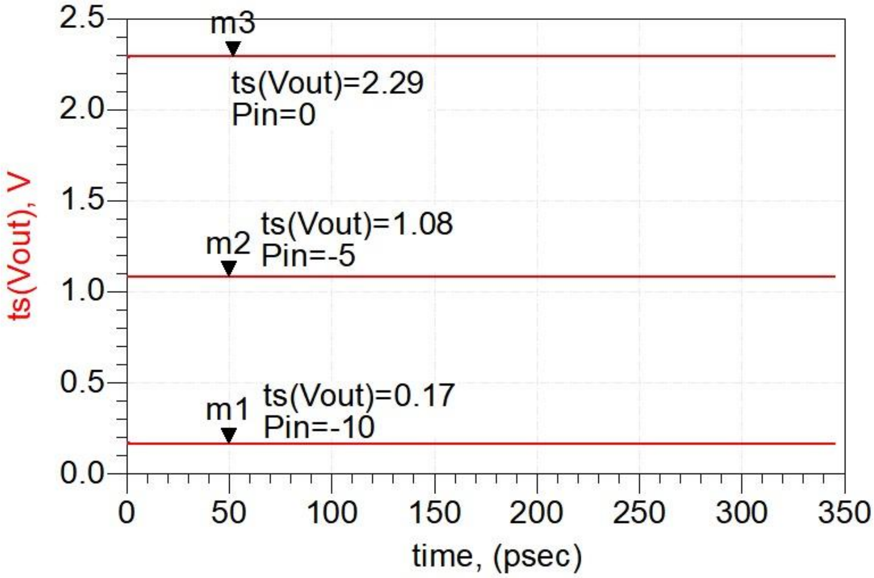

Figure 2.19. Simulation of output voltage Vout in (V) of the schematic 90º hybrid coupler, integrated with rectifier.

The schematic of the 90º hybrid coupler, integrated matching network and bridge diode with the load stage is shown in Figure 2.20. An efficiency of about 40% was obtained when -5 to 0 dBm is applied at two input power terminals. The two input power signals of the 90º hybrid coupler are transferred to the rectifier stage. The efficiency results are given by equations (2.21) and (2.22).

$$Pdc\_Watt = real\ (Vout\ [0] \cdot I_{load}[0]) \qquad (2.21)$$

$$The\ efficiency\ (\eta) = \left(\frac{Pdc\_Watt}{\text{Input power 1+Input power 2}}\right) \cdot 100\% \qquad (2.22)$$

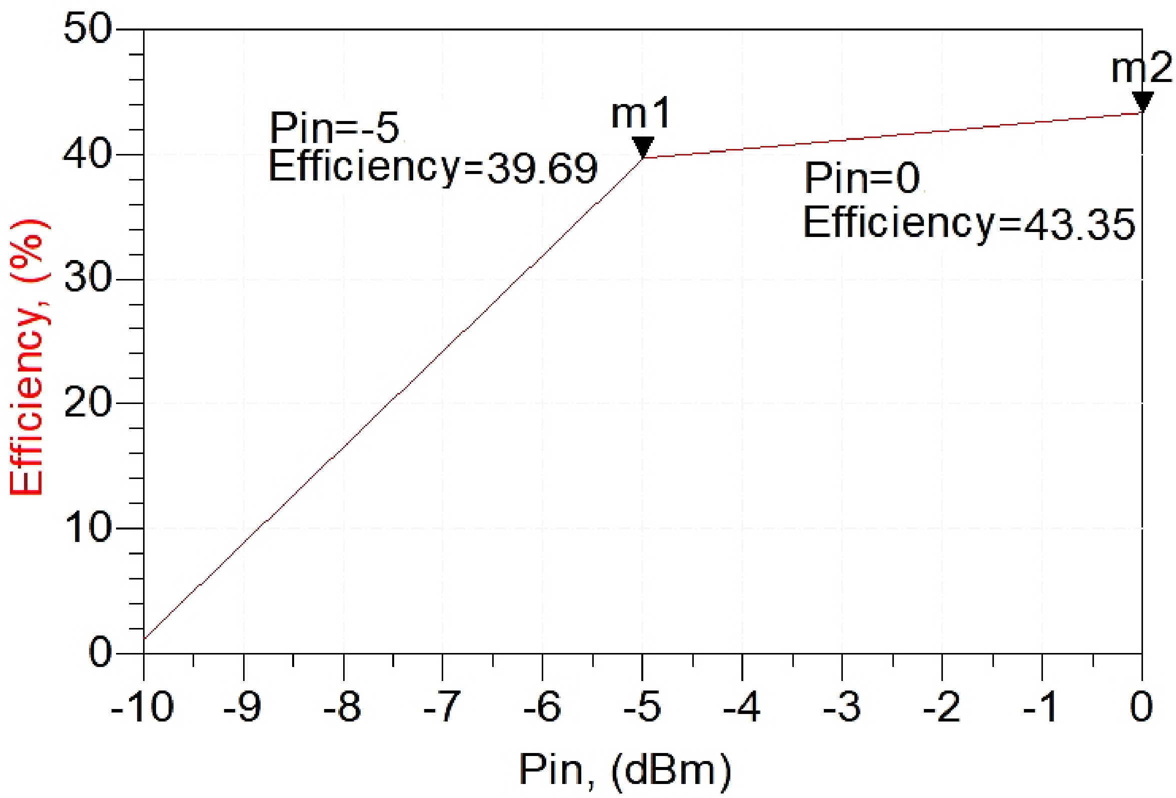

Figure 2.20. The result of efficiency versus input power of Figure 2.16.

2.7 Fabrication

The fabricated compact prototype is shown in Figure 2.21. It comprises dual patch antennas connected to the 90º hybrid coupler which are integrated with the matching network and rectifier stage. The additional λ/4 line between the antenna and the upper input of the 90º hybrid coupler is required to obtain out-of-phase signals at the bridge input, as explained earlier in the beginning of section 2.6. The PCB dimensions are 5.5 cm × 5.5 cm.

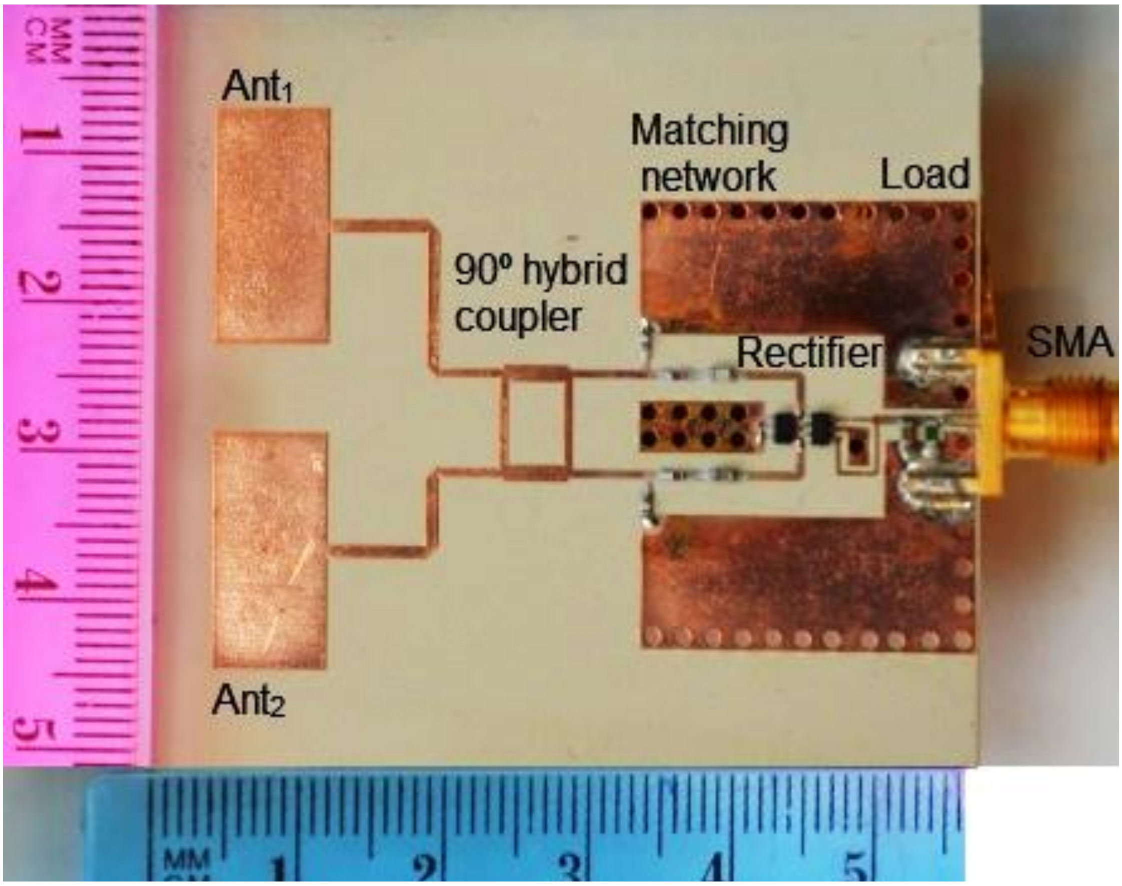

Figure 2.21. Photo of the fabrication circuit 90º hybrid coupler integrated with matching network and rectifier stage.

2.8 Measurement

The measurement set-up is presented in Figure 2.22. It uses a signal generator model DS SG6000LDQ connected to an antenna that is shown in Figure 2.23 (transmitter side). On the reception side, the DC output signal of the device under test (DUT) is measured using an Agilent 34401A Digital Multimeter.

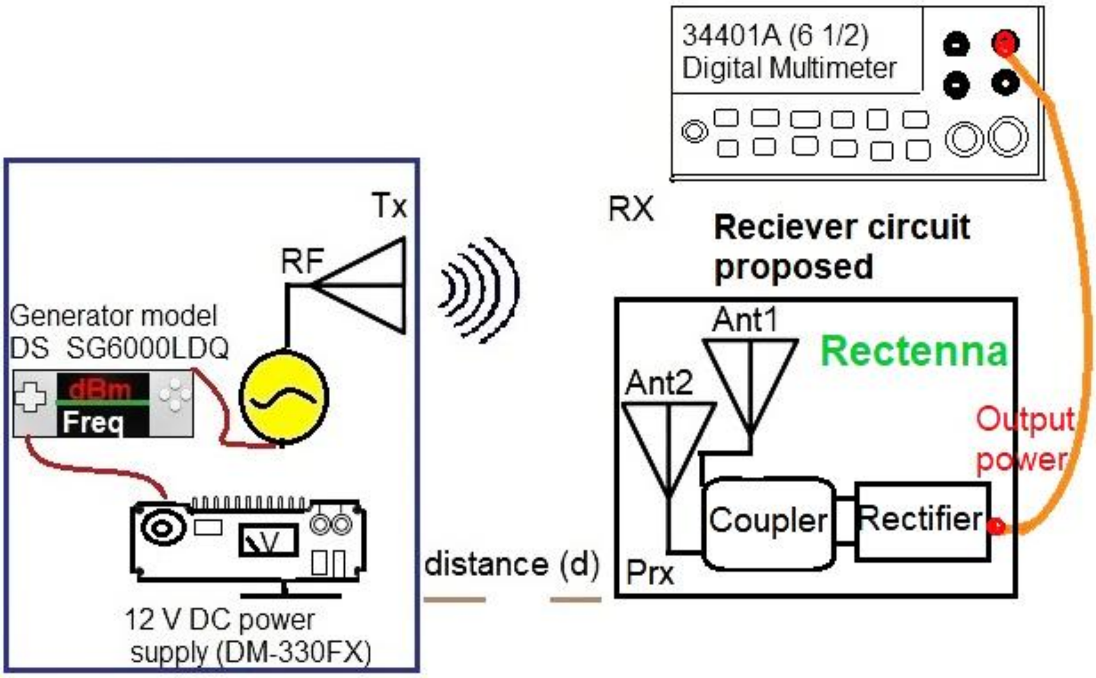

Figure 2.22. The diagram of the measurement set-up.

In Figure 2.23, the transmitter antenna is used as a reference for transmitting the signal to the receiver circuit. The RF signal power is 7 dBm, the gain of the transmitting antenna is 6 dBi, receiver gain is 6 dB, and distance is 0.55 m. The receiver’s output power is −25.5 dBm, and the bandwidth is 5380 MHz to 5450 MHz.

The dimension of the transmitter antenna is chosen to determine the far-field using the equation (2.23), where D = 0.12 m and λ = 0.56 m. The distance (d) between transmitter and receiver antennas is chosen to be at the beginning of the far-field. The parameters are used to calculate the estimation power receiver (P_{rx}) in (2.24), power transmitter (P_{tx}), gain transmitter (G_{tx}), and gain receiver (G_{rx}).

$$\text{Far field (d)} \geq \frac{2 \cdot D^2}{\lambda} = 0.56\, m. \tag{2.23}$$

When d = 0.56 m, and frequency = 5.8 GHz.

$$Prx = Ptx + Gtx + Grx + 20 \ \cdot log10 \ \cdot (\frac{\lambda}{4\pi d}) \tag{2.24}$$

$$= 7 + 6 + 6 + (-\ 42.7) = -\ 23.7 \text{ dBm}.$$

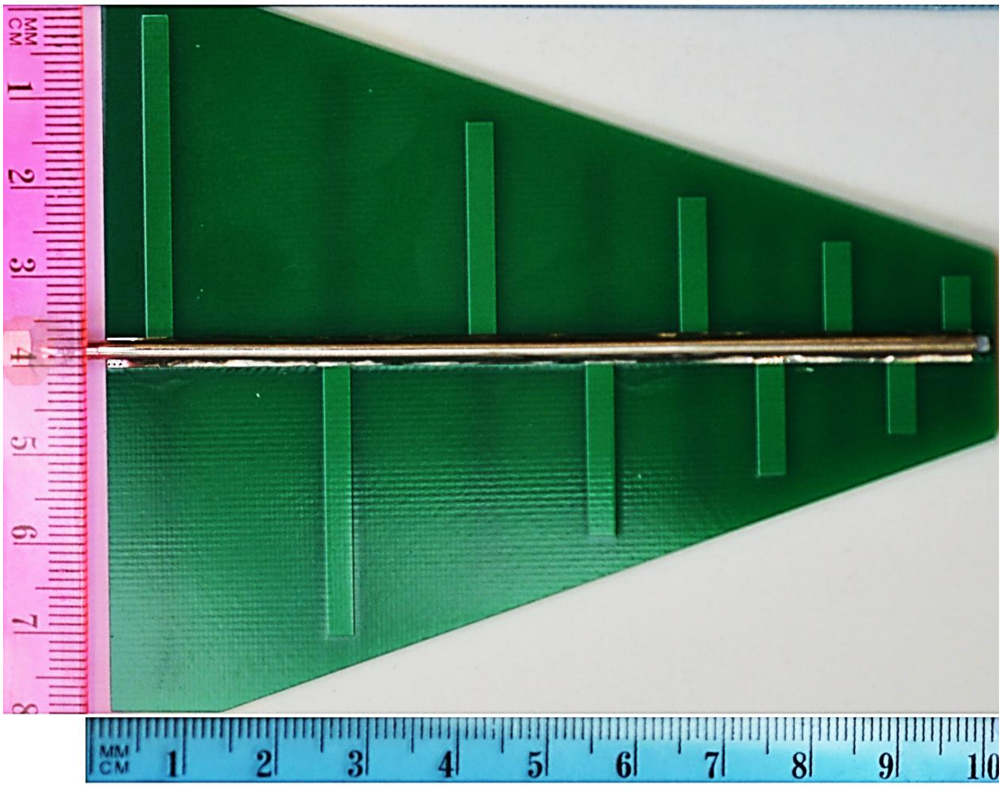

Figure 2.23. The dimensions of transmitter antenna (D = 0.12 m).

The measurement has been performed on a full-bridge rectifier with dual receiving antennas for wireless RF charging of an electronic device. Also, the rectifier's topology is a simple and compact structure. This PCB can be easily integrated within the ambient electromagnetic radiation for WPT applications.

FCC [55], [56] stated that most cellular base transceivers in urban and suburban areas transmit signals to wireless electronic devices at a sufficient radiated power equal to or less than 100 W (50 dBm) per channel.

2.9 Conclusion

This rectifier circuit shows the implementation of rectenna for wireless power transfer and energy harvesting by the RF-DC method. Due to RF availability, the energy that is harvested is appropriate to power wireless sensors. The 90° hybrid coupler is the backbone of the proposed receiver and is implemented here with dual micro-strip antennas, full-wave rectifier bridge, and matching network. This circuit proposed covers 5.8 GHz (WLAN) and offers power for 4G and 5G sensors in certain conditions. The advantages of the designed circuit are small size, lightweight, and easiness to install. Future work will focus on improving the power of the detector.

Chapter 3 – Integrated Rectifier Prototype using 180º Hybrid Coupler

3.1 Introduction

The 180º hybrid coupler is commonly used as a power combiner or splitter in RF and microwave circuits [52]. An 180º hybrid coupler is a four-port circuit. In this prototype, the two input ports are connected to antennas through SMA connectors. It offers 180º phase shift between the two output ports, properly balancing the circuit for feeding a rectifier.

3.2 Design and simulation of the 180º hybrid coupler

The ADS tool provides the LineCalc program that is used for the design of the 180º hybrid coupler. The RO4350 substrate is chosen due to its low dielectric tolerance, high frequency effectiveness, steady electrical features versus frequency, and low dielectric thermal drift. The Datasheet of RO4350 is given in [57], and the properties of the substrate are summarized in Table 3.1. Also, Table 3.2 shows the parameters and variables required for the design of the 180º hybrid coupler.

The permittivity and thickness of the material are shown in Table 3.1, for increasing the efficiency and bandwidth. A 5.8 GHz ISM band is chosen for testing (no license required). It can also operate with 5G sub 6 GHz signals.

Table 3.1. Parameters of substrate RO4350.

The relative permittivity (ε_r)	**The thickness (*h*)**	**The thickness of copper line (*T*)**	**The loss tangent (tan *D*)**
3.48	1.524 mm	17.5 μm	0.0009

Table 3.2. Parameters and variables required for the design of the 180º hybrid coupler.

Speed of light (*c*)	Frequency (*f*)	Wavelength (λ)	Characteristic impedance (Z_0)
3×10^8 m/s	5.8 GHz	5.17 cm	50 Ω

Figure 3.1 shows the schematic and dimensions of the transmission lines. LineCalc, which is an analysis and synthesis program in ADS, was used to calculate the dimensions of the component. The circular layout has a length of 6λ/4. Its characteristic impedance is equal to $Z_0 \cdot \sqrt{2} = 70.7$ Ω. Connected to the ports, each of the three curves has a length of λ/4 and the longer one has a length of 3λ/4. The characteristic impedance $Z^0 = 50$ Ω is set of four transmission lines. The electrically effective length of 90º, is also connected to the coupler ports.

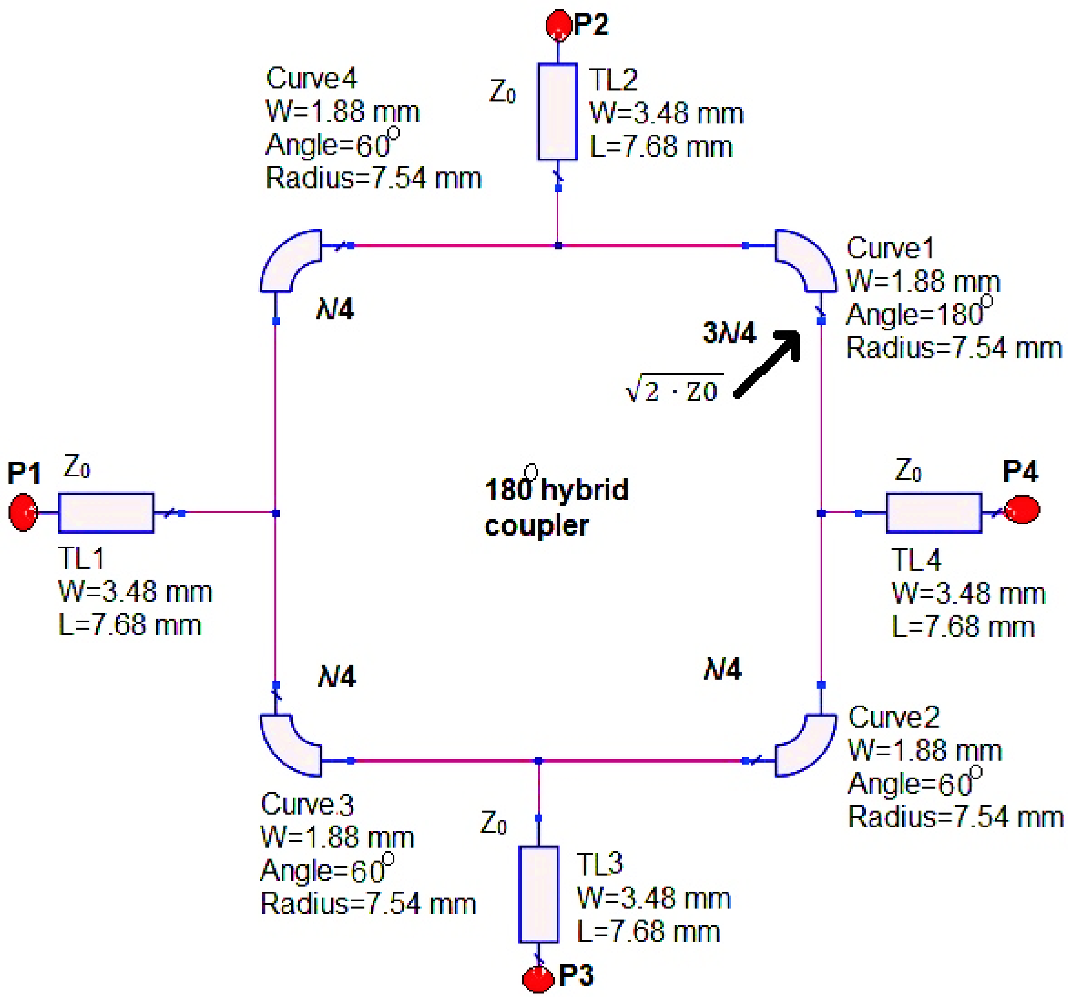

Figure 3.1. Schematic of 180° hybrid coupler.

Figure 3.2 shows a simulation of the S-parameters of the 180º hybrid coupler. Around 42 dB of return loss is obtained at the center frequency of 5.8 GHz. In addition, the S_{12}, and S_{13} transmission coefficients are around −3 dB at the center frequency, which correspond to an approximately half power level. Near-perfect isolation is achieved, since S_{14} reaches 56 dB at the same frequency. It is adequate to report the performance over frequency.

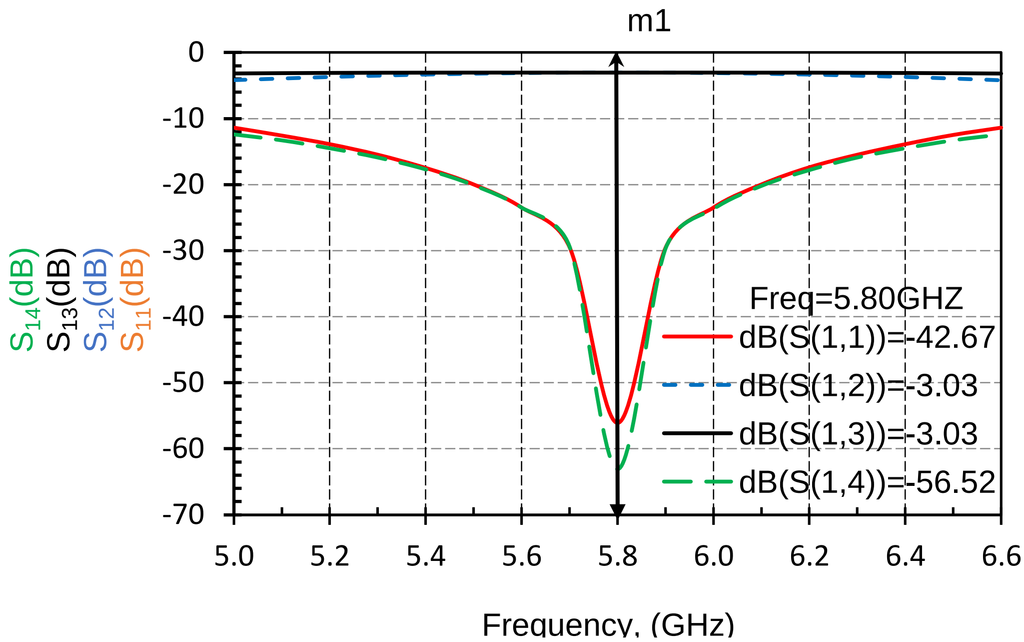

Figure 3.2. Simulated S-parameters of a 180° hybrid coupler.

The phase shift is shown in Figure 3.3. It is apparent that the difference between the Phase S_{24} and the phase S_{31} is approximately 180º, which is suitable for feeding the diode bridge out of phase.

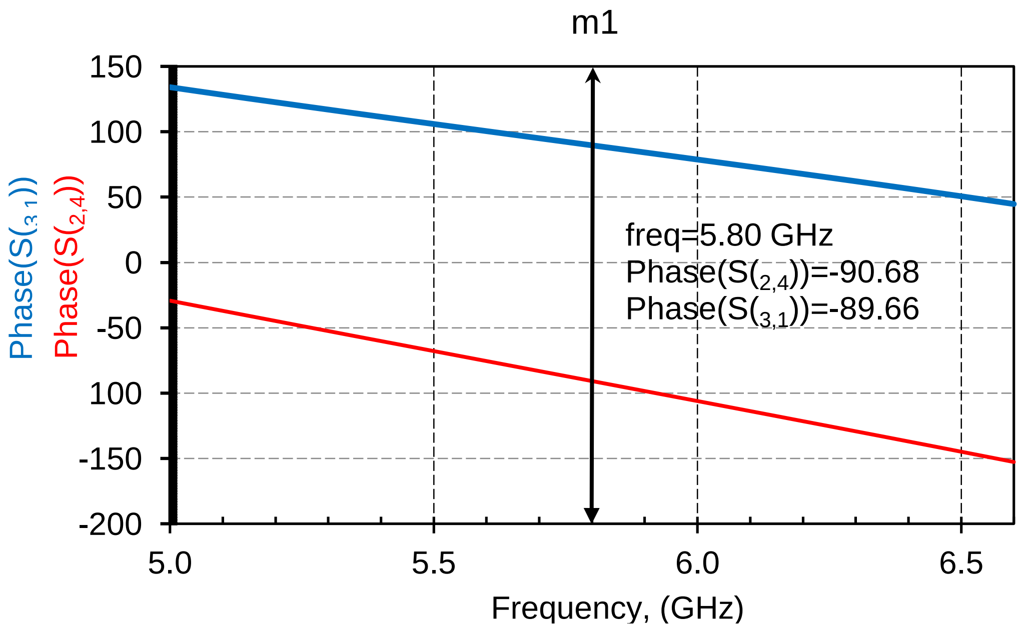

Figure 3.3. Simulated phase shift of a 180° hybrid coupler.

The layout of the 180º hybrid coupler is shown in Figure 3.4. The coupler is fed at port 3, and, as seen, the signals are split between ports 1 and 3. The port 2 is isolated (green means low energy, red means high energy on the EM simulation). The ports 1,4 and 2,3 are isolated, as also seen in the previous simulation results.

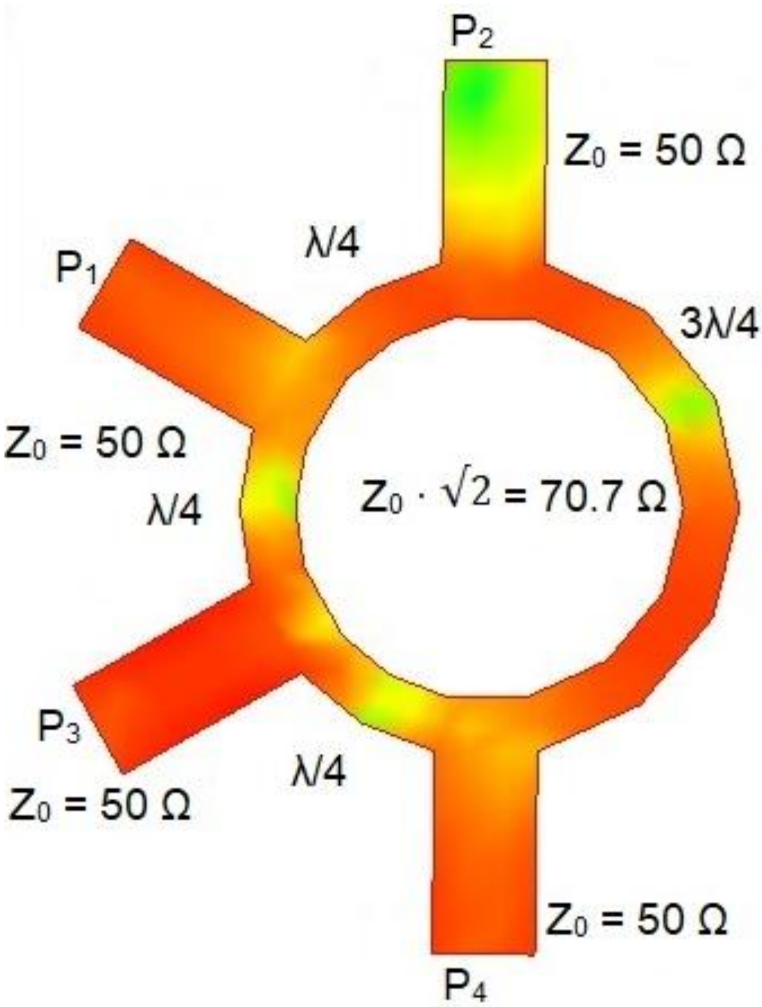

Figure 3.4. Layout of a 180° hybrid coupler with electrical field distribution.

3.3 Rectifier component

The rectifier uses a full-wave method to convert AC to DC. Pairs of HSMS286K diodes, are mounted in a bridge diode topology in the rectifier. The Diode's specifications are aforementioned in chapter 2, section 2.4. This diode is placed between the L type matching network and the load stage. It receives the signals from two 180º hybrid coupler outputs through the differential input.

3.4 Matching circuit

The purpose of the matching circuit is to transfer the maximum power from the source to the load, as described in detail in chapter 2, section 2.5. This circuit uses a single L matching section to connect the 180º hybrid coupler output with the input of the diode bridge rectifier. The equations giving the solutions for B (3.1) and X (3.2) are:

$$B_4 = \frac{22.005 \cdot (-17.265) - \sqrt{1.245 \cdot 22.005 \cdot (1.245^2 + (-17.265)^2 - 1.245 \cdot 22.005)}}{22.005 \cdot (1.245^2 + (-17.265)^2)} = -0.070 \qquad (3.1)$$

$$X_4 = \frac{22.005 \cdot (-17.265) - 1.245 \cdot 35.208}{1.245} + \frac{1.245 - 22.005}{-0.070 \cdot 1.245} = -104.574 \qquad (3.2)$$

Based on the solutions (3.1) and (3.2), the capacitor (C) and inductor (L) are determined in equations (3.3), and (3.4) under the conditions mentioned in Table 2.4.

$$C = -\frac{1}{2 \cdot \pi \cdot f \cdot X_4} = 2.6 \text{ pF} \qquad (3.3)$$

$$L = -\frac{1}{2 \cdot \pi \cdot f \cdot B_4} = 3.9\, nH \qquad (3.4)$$

3.5 Schematic rectifier integrated with 180º hybrid coupler

Figure 3.5 shows the connection of two antennas with a 180º hybrid coupler. The schematic consists of four stages: (i) the 180º hybrid coupler connected with a (ii) matching network, (iii) a full-wave rectifier using two pairs of HSMS-286K Schottky detector diodes connected to the storage capacitor C = 1 µF to eliminate the ripples, and (iv) the resistance load R_L = 5 KΩ.

There are clear advantages of using the 180º hybrid couplers [52]: isolation is excellent, and all ports are matched. Subsequently, it has a flat amplitude characteristic, a low phase error from an ideal value of 180º, and low losses.

In addition, the characteristic impedances of the lines are convenient to realize, and easy to fabricate. Moreover, the design provides high bandwidth (2800 MHz), which is suitable for matching networks. The applications of this design include high-power combiners, electronic components, like antenna beam forming networks, especially for low-side lobe antennas.

The two input ports of the diode bridge receive the signals suitably combined from the 180º hybrid coupler. The 180º hybrid coupler provides two signals of equal amplitude and a constant 180° phase differential for feeding the rectifier. One output port is grounded, and another one doubles the signal from the 180º hybrid coupler as shown in equations (3.5), and (3.6). The outputs (b_i) are normalized waves and given by:

$$b_1 = a \cdot [(-j)^2 + (-j)^2] = -2 \cdot a. \quad (3.5)$$

$$b_4 = a \cdot [(-j) + (-j)^3] = a \cdot [-j + j] = 0. \quad (3.6)$$

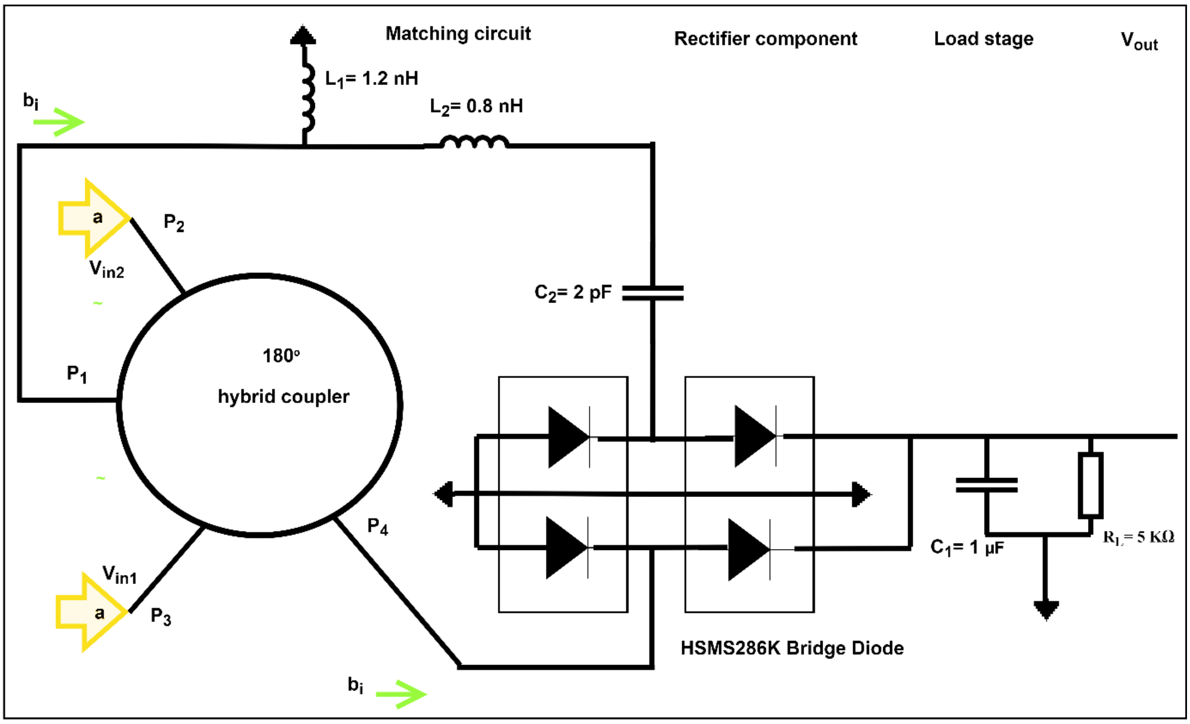

Figure 3.5. The schematic of the circuit 180º hybrid coupler integrated with rectifier

According to Figure 3.5, the values 1.2 and 0.8 nH were used.

The simulation results of the schematic shown in Figure 3.5 are plotted in Figure 3.6. Port 1 return loss is equal to 29 dB and at port 2 return loss is equal to 26 dB. The operating return loss, which is under 10 dB, covers the bandwidth from 5250 MHz to 5600 MHz. Also, the inputs (P_2, and P_3) are connected to antennas. P_1 and P_4 as output ports have transmitted the signals in differential 180º phase to the inputs rectifier stage.

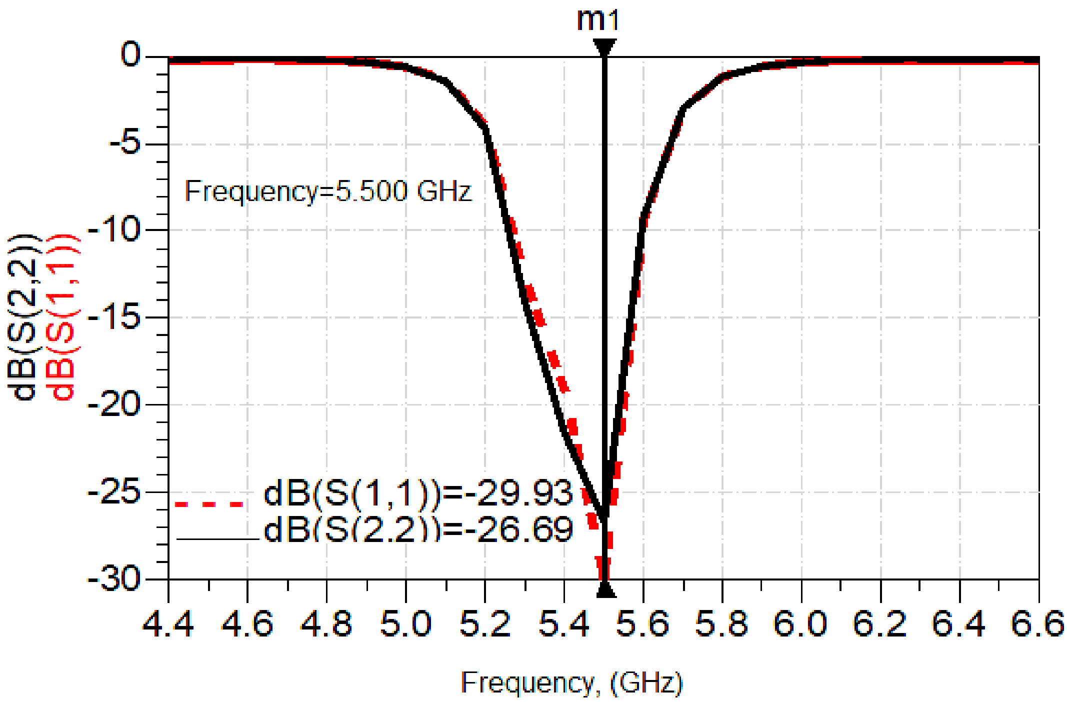

Figure 3.6.Simulation of S11, S22 parameters of Figure 3.5.

Figure 3.7 shows that the output rectifier signal is free from RF components and has only a DC component. At the load, the storage capacitor C1 = 1 µF is used to reduce the ripples.

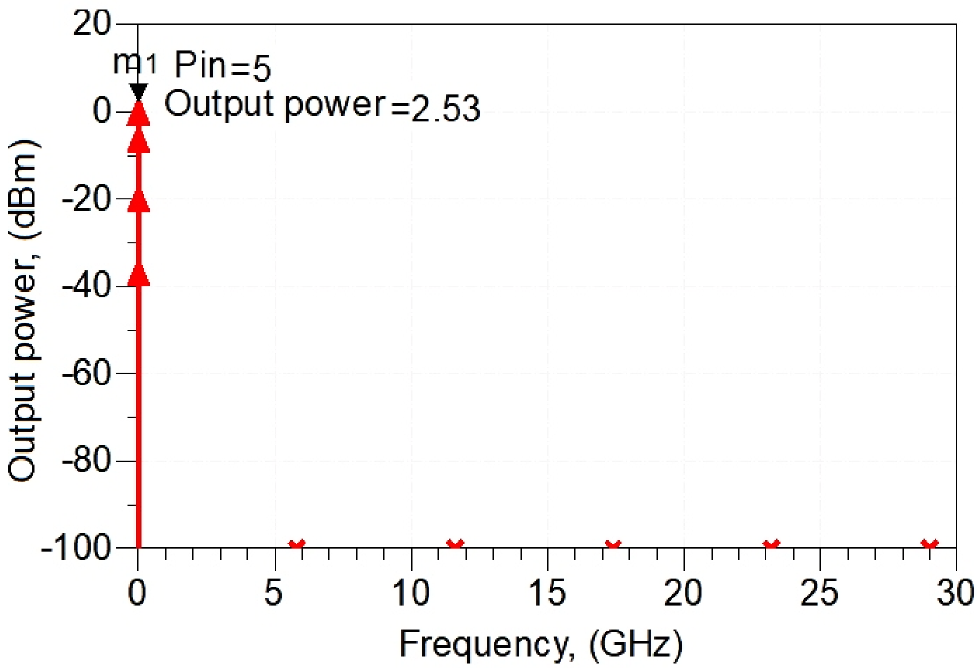

Figure 3.7. Output power of the schematic rectifier in Figure 3.5.

Figure 3.8 shows three output voltage levels (Vout) 0.52, 2.36, and 4.32 (V) versus the (psec) that are obtained at the two terminals input power levels -5, 0, and 5 (dBm), respectively.

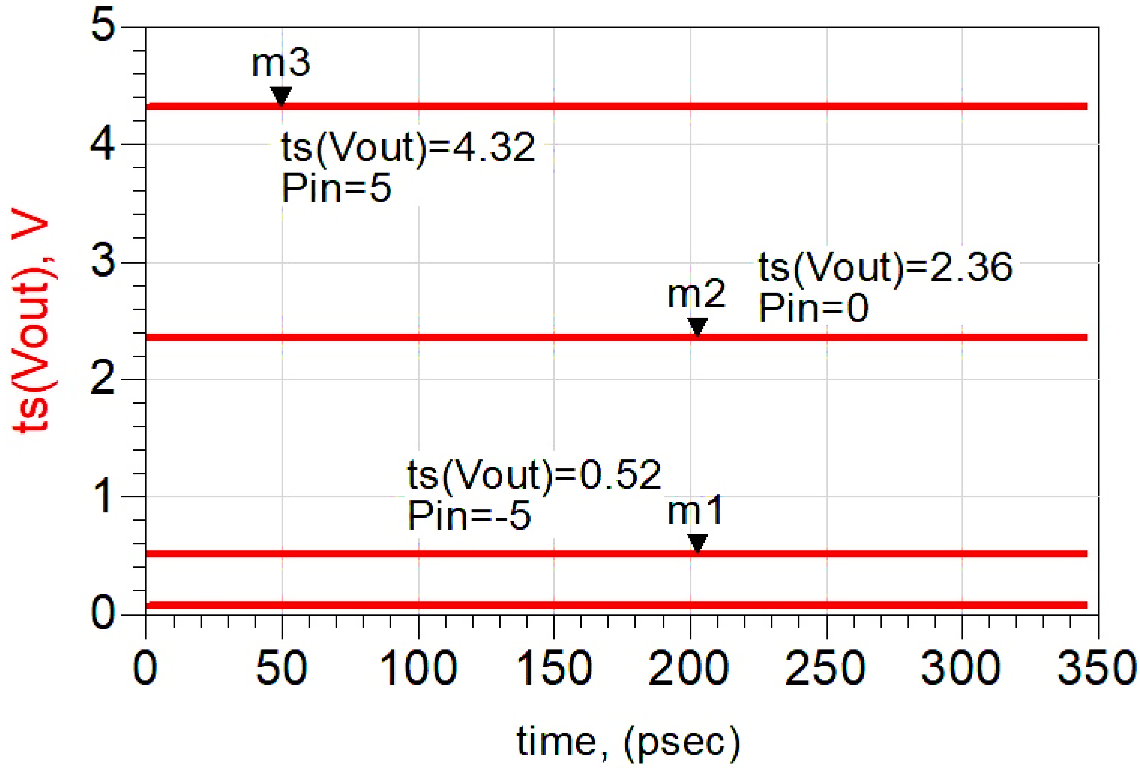

Figure 3.8. Output Vout (V) of schematic rectifier circuit using 180° hybrid power combiner coupler.

In Figure 3.9 it is apparent that the efficiency of 180º hybrid coupler integrated with rectifier is: 50.76% at 0 dBm, and 54.11% at 5 dBm from two terminals input power.

Equations (3.7) and (3.8) have been used to calculate the efficiency.

Output power $P_{dc\_(Watt)}$ in DC is:

$$Pdc\_{Watt} = real \cdot (Vout[0] \cdot I_{\_load}[0]) \tag{3.7}$$

$$The\ efficiency\ (\eta) = \left(\frac{Pdc\_Watt}{\text{Input power 1+Input power 2}}\right) \cdot 100\ \% \tag{3.8}$$

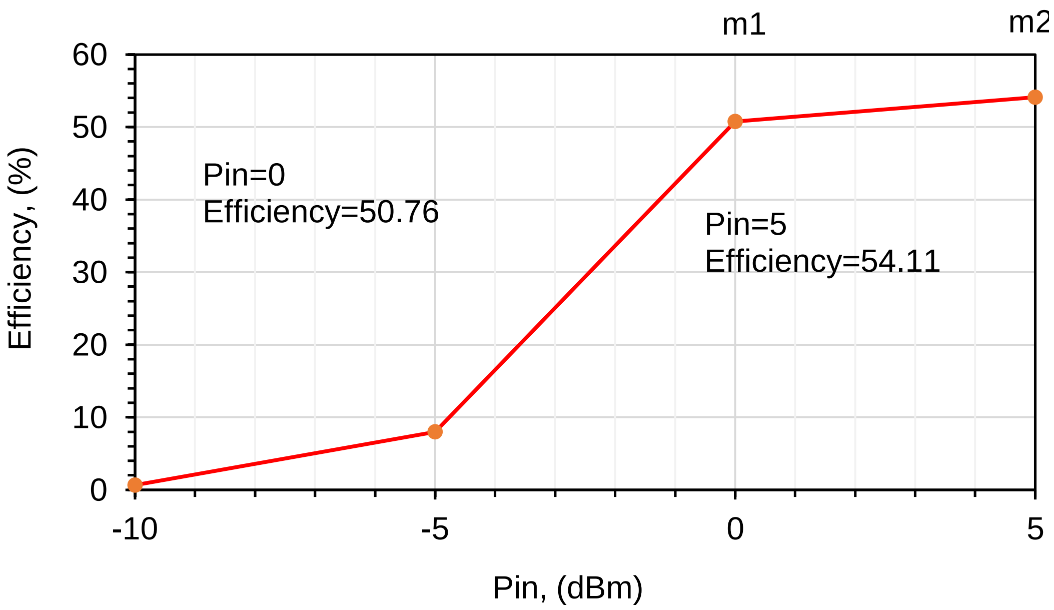

Figure 3. 9. The efficiency of the Figure 3.5.

3.6 Fabrication

The prototype has been fabricated, and pictures are shown in Figure 3.10. Its physical size is (6 cm × 8 cm). It includes the 180º hybrid coupler, lumped elements, HSMS286K for bridge diode rectifier, and the load.

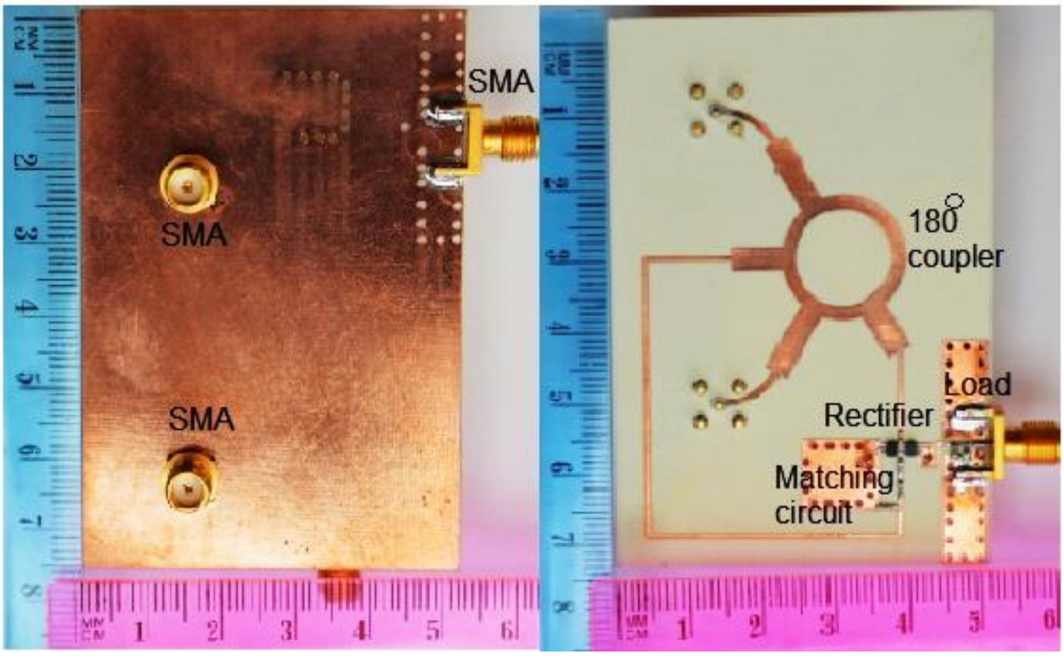

Figure 3.10. Photo of the prototype: 180º hybrid coupler integrated with matching network and rectifier stage.

3.7 Measurement

The measurement set-up is presented in Figure 2.22. It uses a signal generator model DS SG6000LDQ connected to an antenna, which plotted in Figure 2.23 in the transmitter side. On the reception side, two antennas are connected to the inputs of the 180º hybrid coupler. The output signal of the device under test (DUT) is measured using an Agilent 34401A Digital Multimeter.

The parameters of the transmitter are input power level P_{tx} (5dBm), the gains G_{tx} (6dB), and the distance (d=0.5m). The power at the receiver (P_{rx}) is measured over the whole bandwidth. The peak measurement result for the receiver is -10dBm in the bandwidth (1540-1630MHz), -5 dBm in the bandwidth (1830-2200MHz), -18dBm in the bandwidth (3000-3030MHz), and -24dBm in the bandwidth (5330-5370MHz).

The Friis equation [52] (3.9) is applied to calculate the P_{rx} when d = 0.50m, and frequency = 5.8GHz.

$$Prx = Ptx + Gtx + Grx + 20 \cdot log10 \cdot (\frac{\lambda}{4 \cdot \pi \cdot d}) \tag{3.9}$$

= 5 + 6 + 8 + (-35.7) = − 16.7 dBm.

From the ambient, the RF source can capture the energy, which is used in WPT and PH applications. However, it is based on the power of the transmitter, and the distance between the transmitter and the receiver circuit. The receiver circuit provides -10 dBm output DC power at the input power of 0 dBm (1 mW) at 1 m distance between T_x and R_x. The design shows 50% efficiency at 0 dBm, proving the ability of harvesting ambient RF energy to boost the application to the IoT.

3.8 Conclusion

This contribution, 180º hybrid coupler, RF to DC can be improved for feeding flipping the rectifier stage. The obtained efficiency is 50% at two terminals input power of 0 dBm for a resistance load of R_L = 5 KΩ. The output DC conversion depends on collecting even more RF energy. Through the rectifier, additional components will be considered, such as a voltage multiplier to increase rectenna efficiency.

Chapter 4 – Integrated C-Band Rectifier using T-junction Power Combiner

4.1 Introduction

T-junction power combiner/divider are passive microwave components, widely used to combine or divide the energy [52]. These types of dividers are simple, and easy to fabricate. There are several kinds of transmission lines that could be used for the implementation of these components. Microstrip lines are low-cost, and lightweight compared to waveguides counterparts. Our design combines two input RF signals from receiving antennas into an output, connected to a rectifier.

4.2 Design and simulation of T-junction power combiner coupler

ADS software was used for the design and analysis of the proposed T-junction power combiner coupler. The length (L) and width (W) for a quarter-wave transformer are calculated through the LineCalc program. The parameters and variables are shown in Tables 3.1 and 3.2. Table 4.1 shows the original dimensions of the T-junction power combiner coupler, and Figure 4.1 shows the corresponding schematic. The microstrip lines are used to implement 70.7 Ω lines, using both L and W values for a quarter-wave transformer. The 50 Ω lines use the calculated W, and L of a quarter-wave transformer. Curve1 and curve2 use to connect the 70.7 Ω lines with the 50 Ω lines. The width of the curves matches the 70.7 Ω line. Each curved bend has an angle of 90° and a radius of 1.52 mm.

Table 4.1. The dimensions of TLs T-junction (mm).

Transmission Line	1, 6, 7 (W)	1, 6, 7 (L)	2, 3, 4, 5 (W)	2, 3, 4, 5 (L)	Curve1, 2 Angle	Curve1, 2 (W)
Original	3.5	7.7	1.9	3.9	90º	1.9
Optimization	As shown in Figure 4.1					

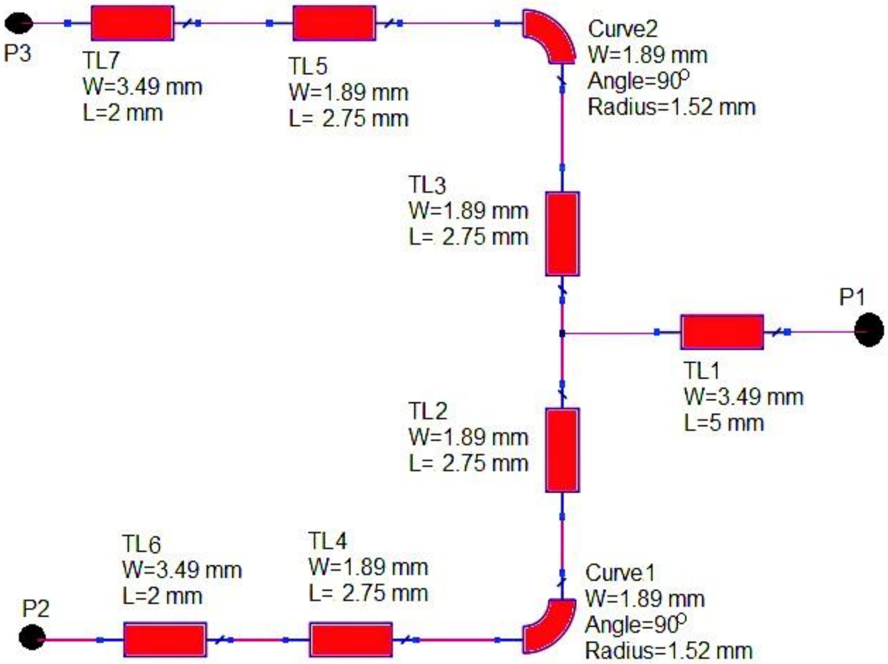

Figure 4.1. Schematic of the T-junction power combiner coupler.

Figure 4.2 displays the simulation results. A wideband performance is obtained from 2-9 GHz with S_{11} less than -10 dB. The S_{11} value is less than – 53 are having dB at 5.8 GHz. Also, magnitudes of S_{12} and S_{13} have identical values reaching -3.06 dB.

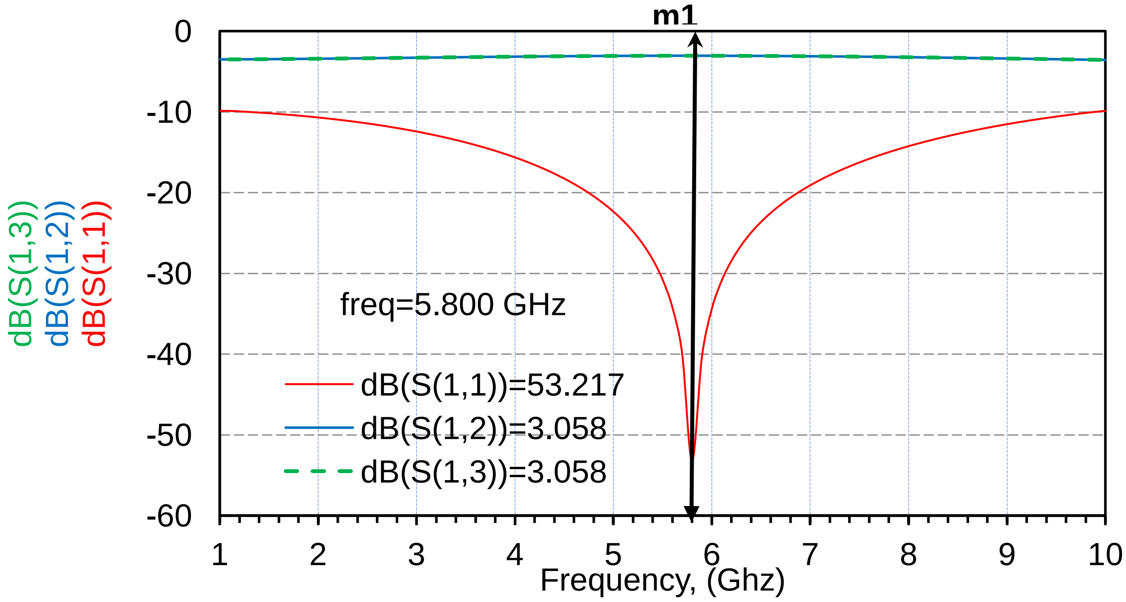

Figure 4.2. Simulated S-parameters of a T-junction power combiner coupler.

This T-junction component provides equal phase shift, as it is apparent in Figure 4.3 for S_{21} and S_{31}.

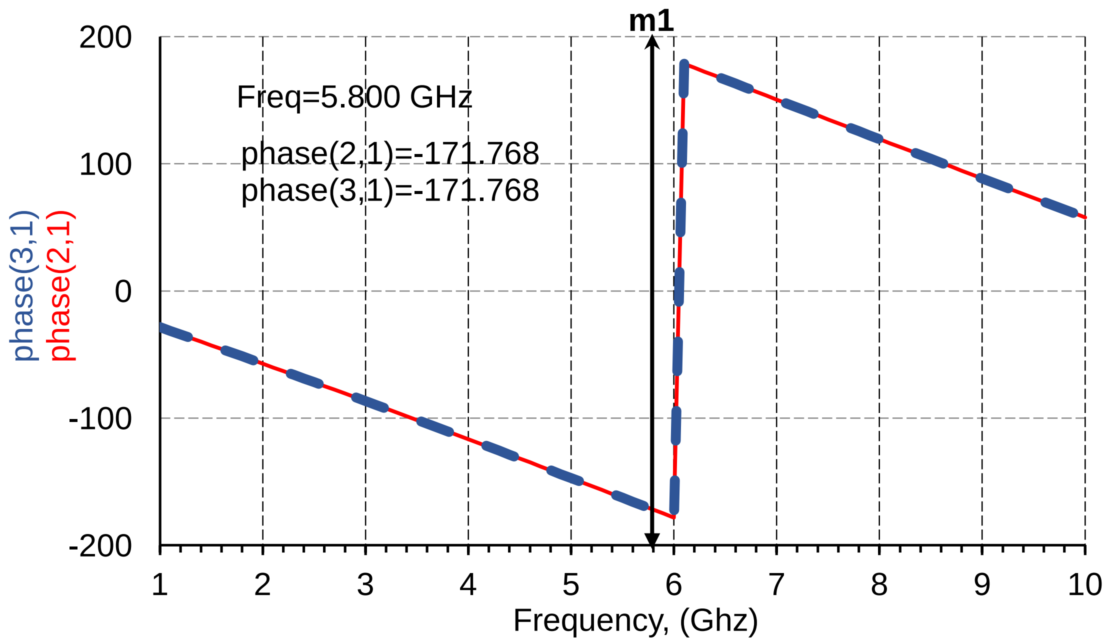

Figure 4.3. Simulated phase shift of T-junction power combiner coupler.

Figure 4.4 shows the layout of the T-junction power combiner with three 50 Ω ports. The 70.7 Ω curved transmission lines connect these three ports together.

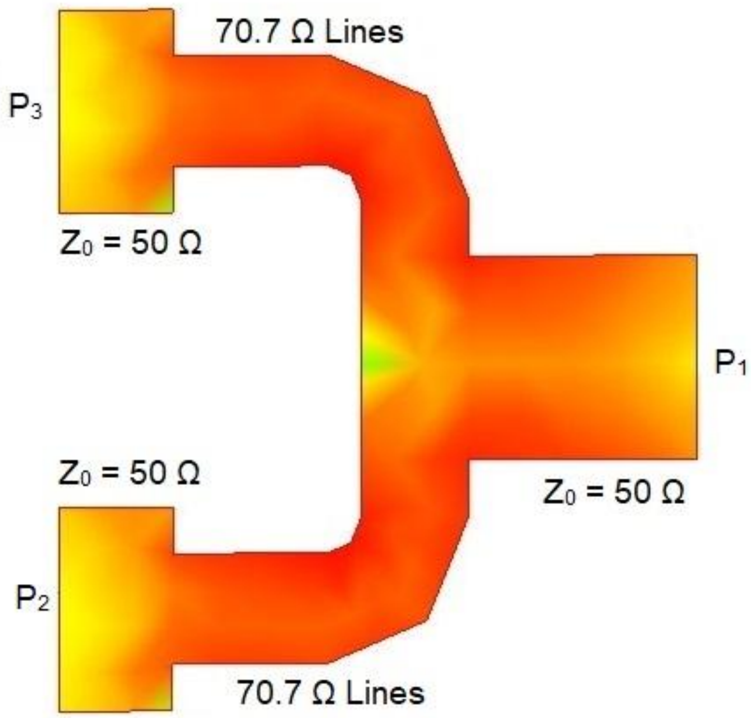

Figure 4.4. Layout of the T-junction power combiner.

4.3 Rectifier components

As mentioned in chapter 1 section (1.2.4), a common practical rectifier topology is a full-wave voltage doubler, and it is preferred when increasing the output DC voltage is required. Therefore, in this section, we will discuss the full-wave voltage doubler topology.

- **Topology of the Full Wave Voltage Doubler**

The schematic of the voltage doubler is shown in Figure 4.5. This doubler uses two diodes that conduct during the positive half cycle when the signal is above zero.

Similarly, the diodes act as an open circuit when the negative half cycle signal is less than zero. The voltage doubler is used to charge the capacitors C1 and C2, and it ideally doubles input voltage (Vin) at the output (Vout), i.e., $V_{out} = 2 \cdot Vin$.

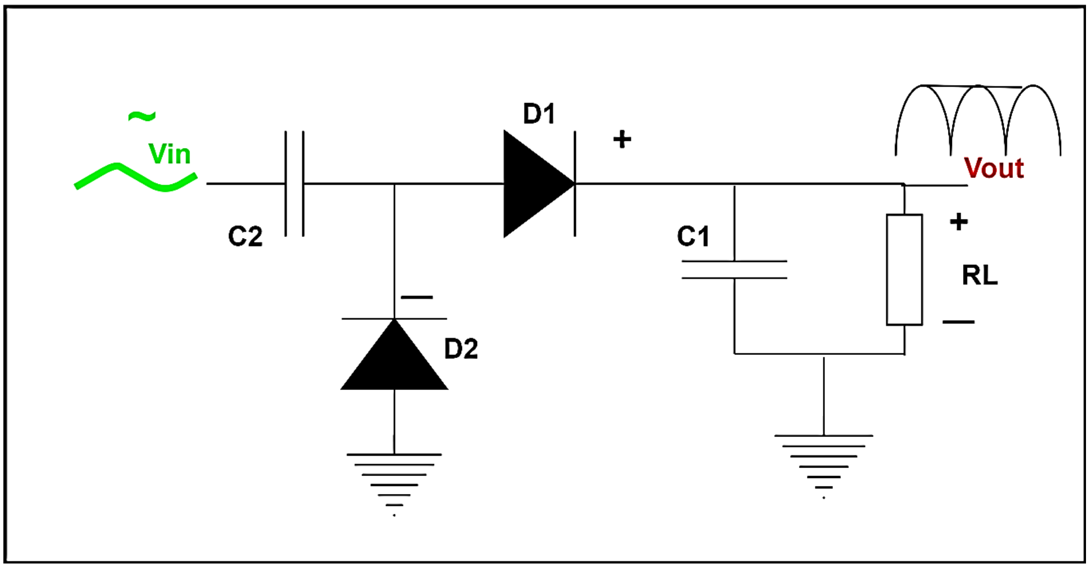

Figure 4.5. Full-wave rectifier of typical voltage doubler diode circuit.

- **Practical implementation**

Figure 4.6 shows the Spice Model diagram of SMS7630_006LF diode taken from the datasheet [58]. These diodes can be used in sensitive RF and microwave detectors, sampling and mixer circuits, high-volume wireless Wi-Fi, and mobile, and low-noise receivers. Low-cost, surface-mountable, and plastic-packaged silicon Schottky diodes are used in RF and microwave technologies [58].

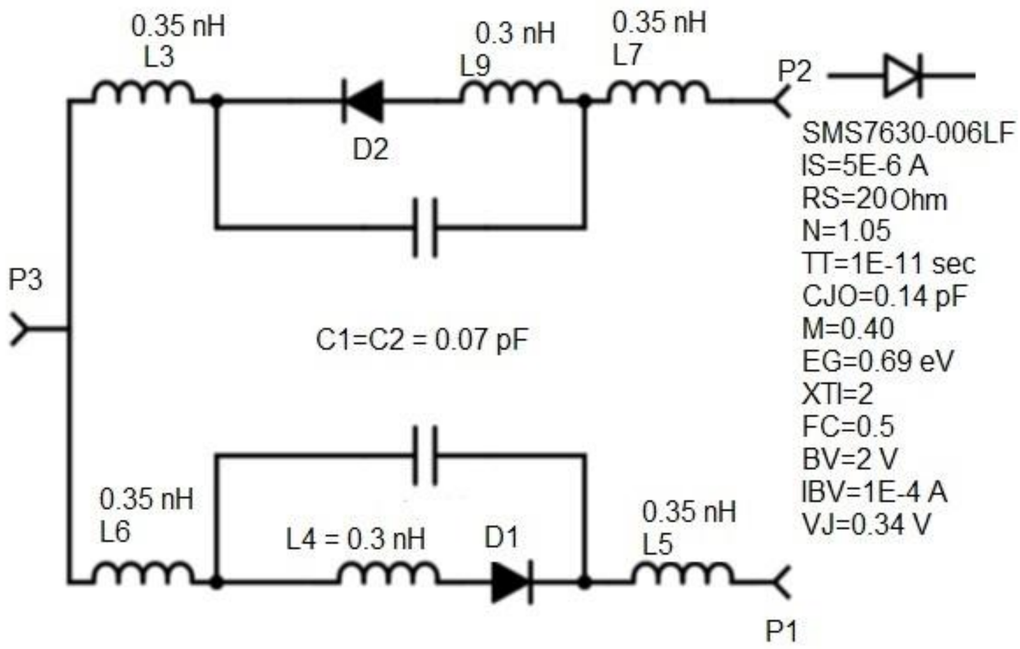

Figure 4.6. Diagram of pairs SMS7630-006LF diode model [58].

4.4 Matching circuit

T-junction power combiners and voltage doubler rectifiers are matched to maximize the output power. L-type matching network circuit is used in this circuit because it is compact. According to the theory, matching way have more than one solution. The capacitors and inductors can be placed in series or shunt. Furthermore, instead of a capacitor and inductor, we can employ two capacitors or inductors as well.

Equation (4.1) separates the real and imaginary parts to obtain two solutions. The equations for B_4 and X_4 are shown below in (4.2) and (4.3) [54].

$$Rs - j \cdot Xs = j \cdot X + \frac{1}{jB + (\frac{1}{RL + j \cdot XL})} \tag{4.1}$$

From equation (4.1), the solution for B_4 is determined, whereas that for X_4 is obtained through equation (4.3).

$$B_4 = \frac{Rs \cdot XL - \sqrt{RL \cdot Rs \cdot (RL^2 + XL^2 - RL \cdot Rs)}}{Rs \cdot (RL^2 + XL^2)} \quad (4.2)$$

$$\mathrm{B}_4 = \frac{49.630 \cdot (-50.338) - \sqrt{6.247 \ \cdot 49.630 \ \cdot (6.247^2 + (-50.338)^2 - 6.247 \cdot 49.630)}}{49.630 \ \cdot \ (6.247^2 + (-50.338)^2)}$$

$$= -\ 0.026$$

$$X_4 = \frac{Rs \cdot XL - RL \cdot Xs}{RL} + \frac{RL - Rs}{B_4 \cdot RL} \quad (4.3)$$

$$\mathrm{X}_4 = \frac{49.630 \ \cdot \ (-50.338) - \ 6.247 \ \cdot \ (-0.762)}{6.247} + \frac{6.247 \ - \ 49.630}{-0.026 \ \cdot \ 6.247} = -133.319$$

As the values of B_4 and X_4 are negative, therefore; the capacitor and inductor equations are given below in equations (4.4) and (4.5).

$$C = -\frac{1}{2 \cdot \pi \cdot f \cdot X_4} = 2.059\ pF \quad (4.4)$$

$$L = -\frac{1}{2 \cdot \pi \cdot f \cdot B_4} = 1.055\ \mathrm{nH} \quad (4.5)$$

After analytic solutions have been determined, optimization and tuning techniques were employed to improve these results through simulations. The elements of the L-type matching network contain two inductors and the capacitor.

4.5 Simulation results for the rectifier with T-junction power combiner coupler

Figure 4.7 shows the across simplified schematic of the rectifier. The T-junction combines the dual RF input to feed the L-type matching network of the RF rectifier element. The voltage doubler drives the rectifier component to convert the (RF) signal into DC. A DC voltage for powering sensors is obtained with the storage capacitor (C_1) connected in parallel with the load resistor (R_L). The element values are provided in Figure 4.7. The tuning performed in ADS has as an initial solution with the values obtained previously in section 4.4, for matching C_1, and C_2. Likewise, the ideal R_L = 5 kΩ is chosen as a trade-off between the output voltage and relative efficiency. The R_L is in parallel with C_1 =1 µF, which is used for eliminating the voltage ripples of the output.

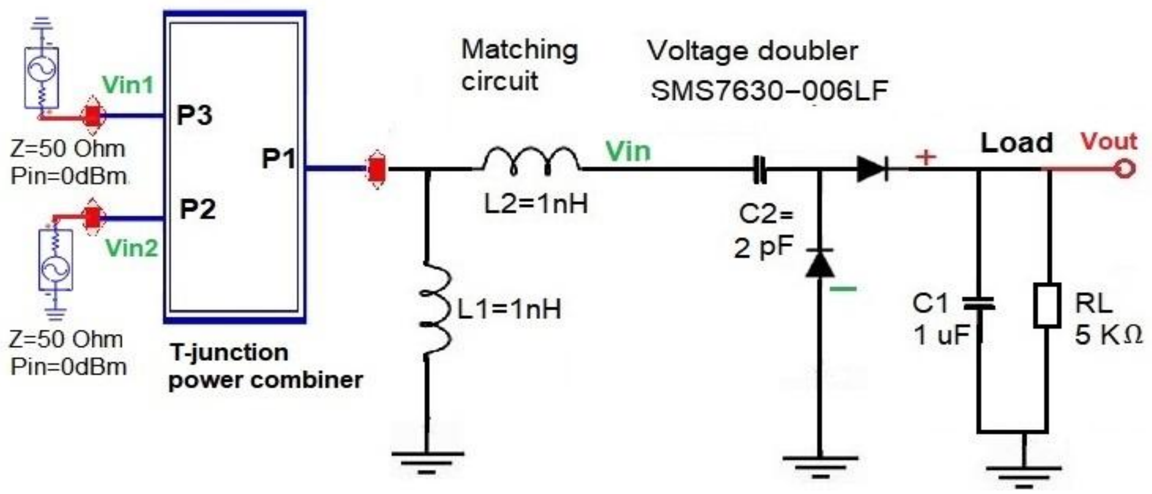

Figure 4.7. Schematic of the T-junction power combiner coupler integrated matching network, and voltage doubler with the load stage.

The voltage doubler rectifier generates the DC output and eliminates the AC components at the fundamental frequency and all its harmonics. Therefore, the output power is obtained using equation (4.6). Figure 4.8 shows an output power of -3.29 dBm for an input power level of 0 dBm at each RF input (P_2 and P_3) as shown in Figure 4.8.

Output power $Pdc_{\_(Watt)}$ in DC is:

$$Pdc_{\_Watt} = real \cdot (Vout[0] \cdot I_{\_load}[0]) \tag{4.6}$$

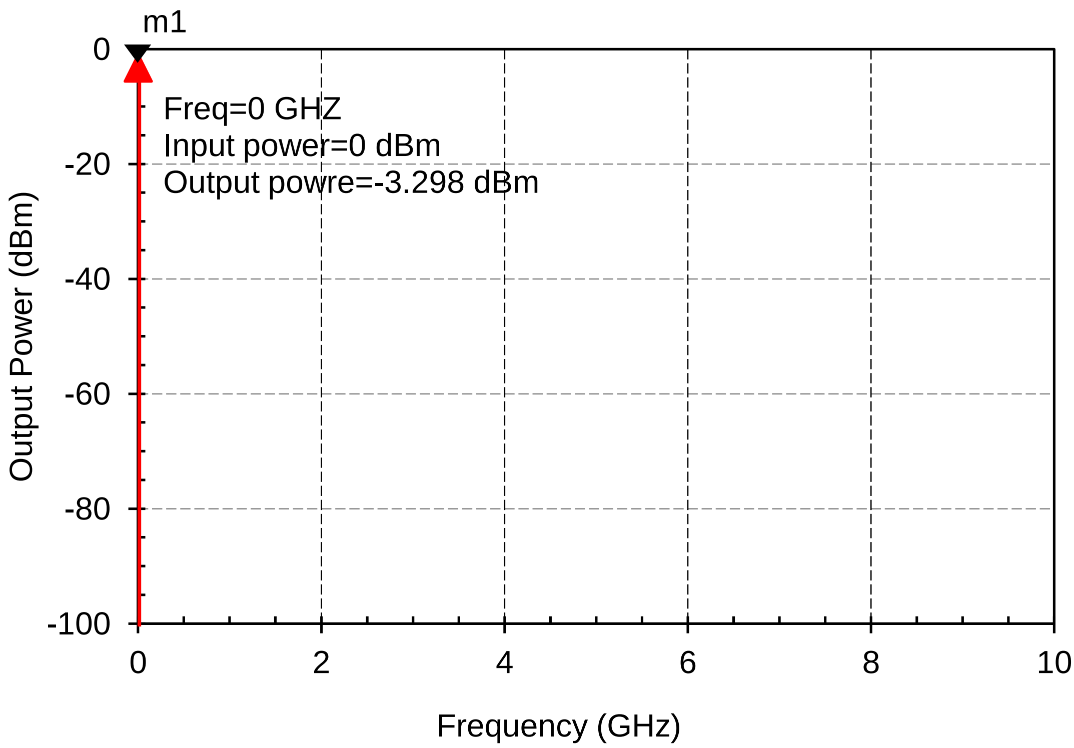

Figure 4.8.Output power of the schematic shown in Figure 4.7.

Vin, the input voltage, which is feeding the voltage doubler, is plotted in Figure 4.9. (a). The output voltage is maximized by using a voltage doubler. It is also increasing the load resistance for a given optimized result. Within the rectifier stage, the AC signal of double amplitude is converted into a DC signal. Figure 4.9, (b) shows the results for the output rectified voltage Vout in (V). The output voltage reaches 0.10, 0.57 V, and 2.16 V for input power levels of -20, -10, and 0 dBm, respectively.

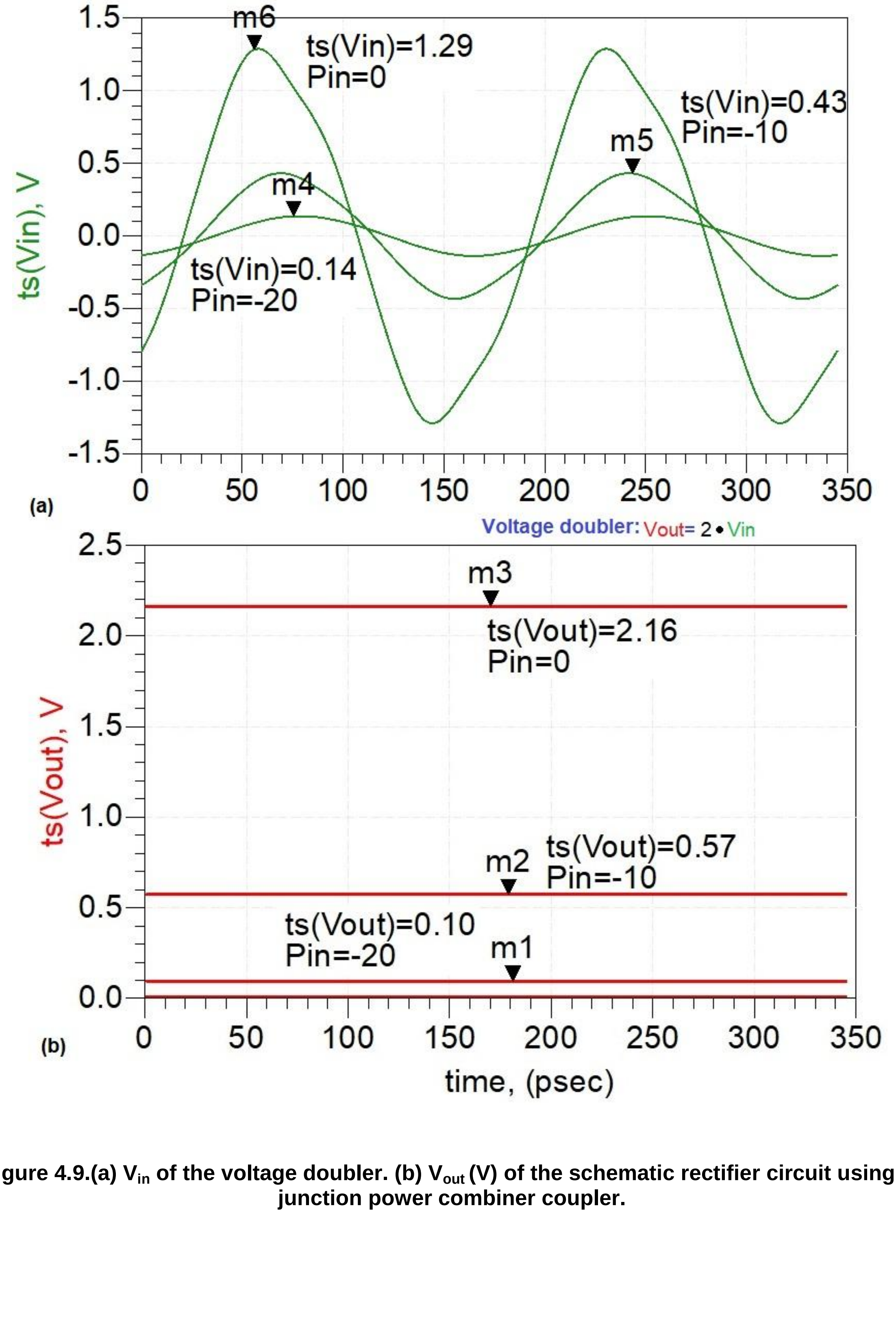

Figure 4.9.(a) V_{in} of the voltage doubler. (b) V_{out} (V) of the schematic rectifier circuit using T-junction power combiner coupler.

Equation (4.7) calculates the efficiency of the T-junction power combiner coupler, integrated matching network, and voltage doubler at the load stage. It is obtained by dividing the output DC power over the total dual input power. The efficiency of the designed system reaches 11.52%, 30.50%, and 43.60% for an input power level applied at the two inputs of -20, -10, and 0 dBm, respectively.

$$The\ efficiency\ (\eta) = \left(\frac{Pdc\_Watt}{\text{Input power 1+Input power 2}}\right) \cdot 100 \quad \% \tag{4.7}$$

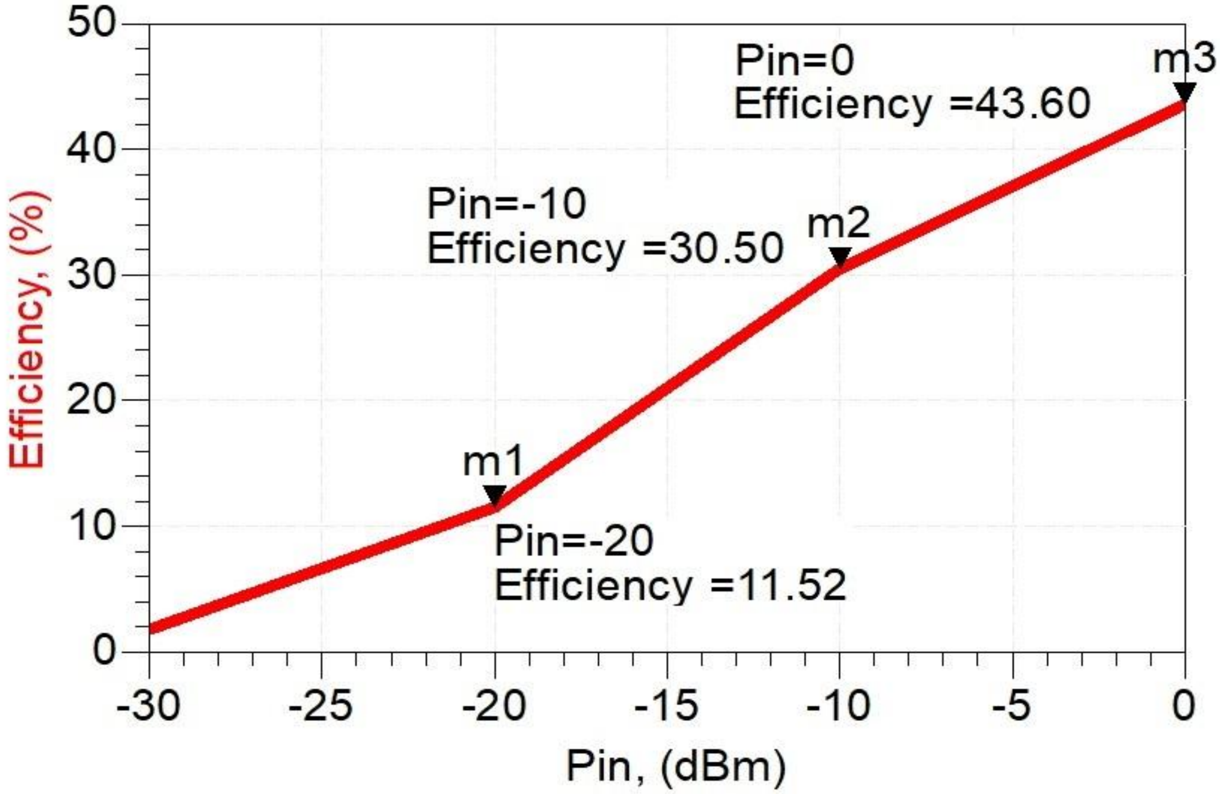

Figure 4.10. The efficiency of the Figure 4.7.

Figure 4.11 displays the layout consisting of a T-junction power combiner coupler connected through a matching network to the voltage doubler and load stage.

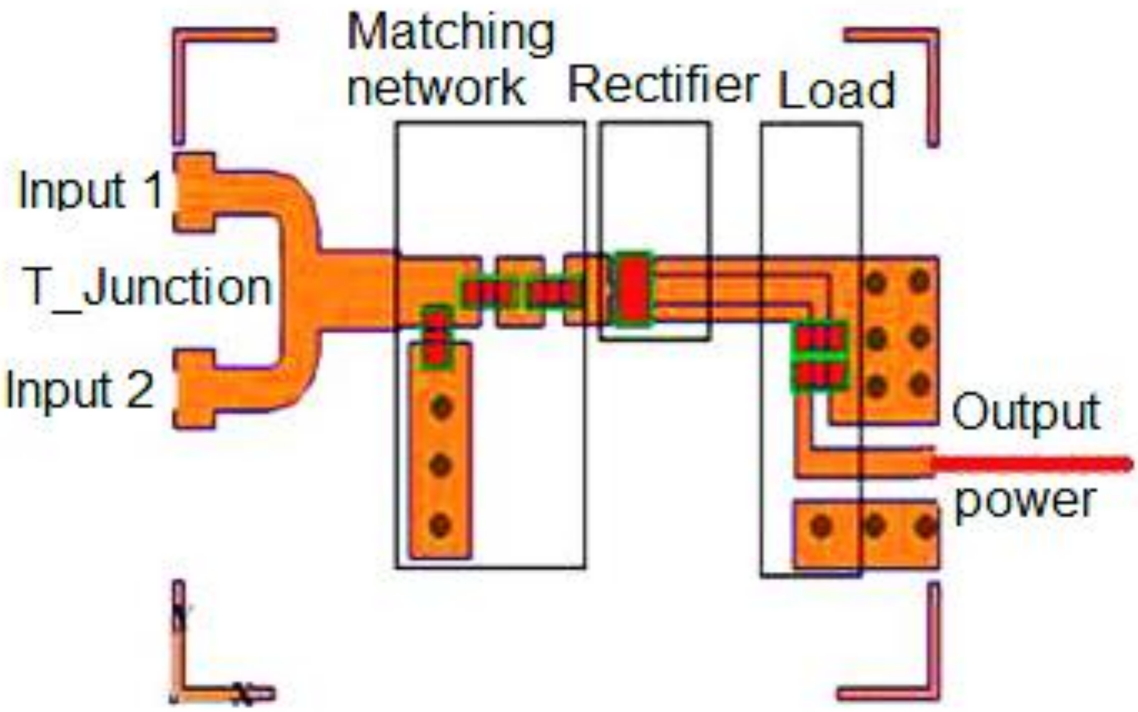

Figure 4.11. Layout of the designed T-junction power combiner coupler circuit integrated with other components.

4.6 Fabrication

The proposed system which comprises a T-junction power combiner coupler, an L-type matching network, a voltage doubler, and a load resistance was fabricated, as displayed in Figure 4.12. The proposed system has a size of (4cm x 3cm).

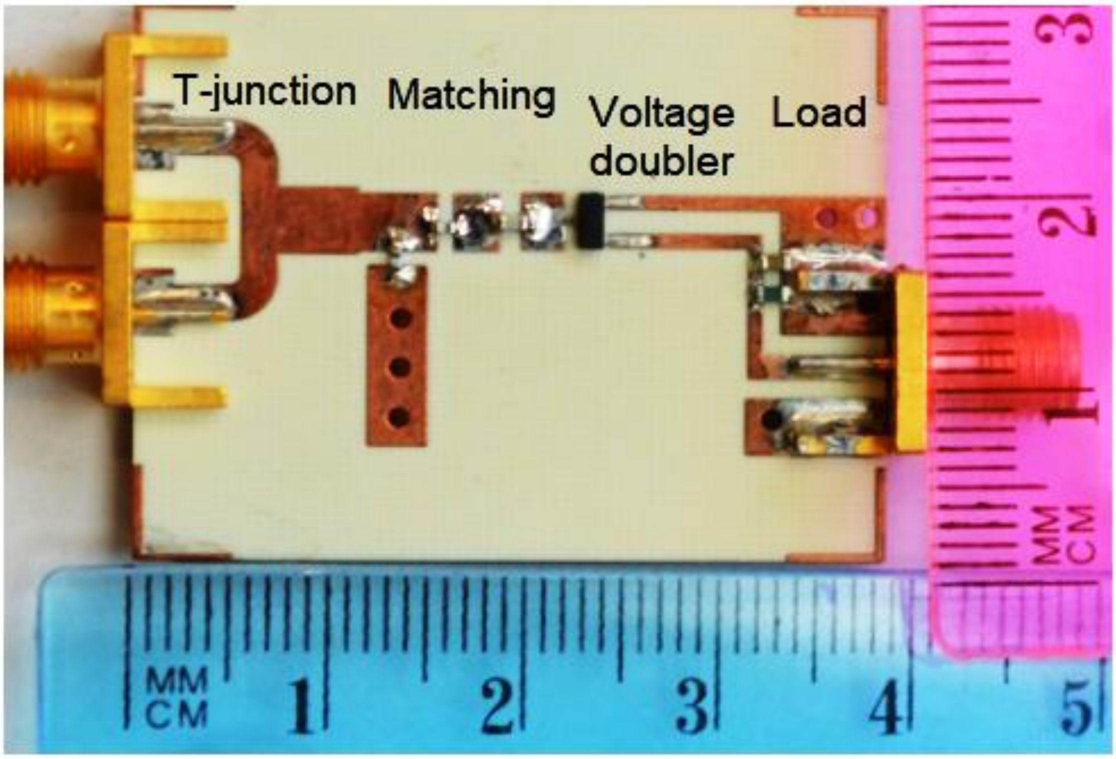

Figure 4.12. Photo of the fabricated prototype of the proposed system.

4.7 Measurement

As already shown in Figure 2.22, the measurement setup includes a signal generator model DS SG6000LDQ connected to a transmitter antenna. Similarly, two receiver antennas are attached to the input terminals. The photo of the antenna employed during our measurements is shown in Figure 2.23. Table 4.2 shows the calculated far field regions for the corresponding frequencies and wavelengths. The output signal of the device under test (DUT) was measured using an Agilent 34401A Digital Multimeter.

Table 4.2. Calculate wavelengths (λ) for the three frequencies (f) with far-field (d).

f (GHz)	2	5	7.5
λ (m)	0.15	0.06	0.04
Far-field d (m) $\geqq \frac{2\, D^2}{\lambda}$	0.19	0.48	0.72

Three far-field regions of 0.19 m, 0.48 m, and 0.72 m for λ = 0.15, 0.06, and 0.04 m, respectively, are obtained while keeping a distance of d = 1 m. The Friis equation (4.8) is applied to calculate the received power estimation.

$$Prx = Ptx + Gtx + Grx + 20 \cdot log10 \cdot (\frac{\lambda}{4 \cdot \pi \cdot d}) \quad (4.8)$$

= 0 + 5 + 8 + (−38.46) = -25.46 dBm,

= 0 + 5 + 8 + (−46.45) = -33.45 dBm,

= 0 + 5 + 8 + (−49.94) = -36.94 dBm.

During the measurements, the transmitter input power was set to P_{in} = 0 dBm and the distance d = 1 m. The obtained output powers were –17 dBm for a bandwidth of (1650-2000 MHz), – 20 dBm for a bandwidth of (3000-3400 MHz), - 24 dBm for a bandwidth of (2050-2500 MHz), and -24 dBm for a bandwidth of (6550- 6950 MHz).

The measurement results, which were verified through the Friis equation (4.9), are given below; a good agreement was found between the measured and calculated data.

$$Prx = Ptx + Gtx + Grx + 20 \cdot log10 \cdot (\frac{\lambda}{4 \cdot \pi \cdot d}) \quad (4.9)$$

When d = 250 m, and λ identified in Table 4.2 above.

= 47 + 15 + 8 + (-86.42) = - 16.42 dBm.

= 47 + 15 + 8 + (-94.37) = - 24.37 dBm.

= 47 + 15 + 8 + (-97.89) = - 27.89 dBm.

These results can be applied to industrial, scientific, and medical electronic devices. When the input power is 0 dBm, then the output voltage can reach approximately 2 V, which is a practical value for powering sensors**.** Therefore, the circuit can be very useful for wireless power transfer.

4.8 Conclusion

This receiver circuit uses a T-junction power combiner coupler for a dual input RF voltage doubler via an L-type matching network. These components are integrated into a simple and small size circuit. The output DC voltage is maximized at the load stage. Starting with -30 dBm, the efficiency increases with the input power from a few percent to about 43 % at 0 dBm input power level from two terminals, and 5 kΩ load resistance. The measured results give the confidence to power sensors and could be in this chapter applied to 3, 4, and 5G of wireless communication systems. The idea presented can be applied in a wider range of applications.

Future work will improve a dual RF with multi power detector to increase the power scavenging.

Chapter 5 - Integrated Rectifier Prototype using Wilkinson Power Combiner

5.1 Introduction

The Wilkinson power coupler is a three-port equally split divider or combiner, widely used in microwaves and RF [52]. There are clear advantages in using the Wilkinson coupler: it has higher isolation and better return loss compared to a T-junction. The Wilkinson coupler is employed in this prototype in order to collect the power received from dual rectangular microstrip antennas. This power is then passed to a rectifier component.

A voltage doubler is mounted at the Wilkinson coupler output before the rectifier stage. An L-type impedance matching network is integrated between the Wilkinson coupler and the rectifier to secure maximum power transfer from source to load. This circuit is designed, fabricated, and measured. The goal is to scavenge direct current, with improved efficiency and sensitivity. The proposed circuit can operate over multiple bands, L and C. The ISM 5.8 GHz band is covered by the prototype. The prototype is implemented on the same 1.524 mm thickness substrate as the patch antennas. Subsequently, a larger bandwidth leads to collecting more signals, which in turn enhances WPT.

5.2 Antenna

The rectangular patch antenna is calculated using the equations (5.1) to (5.5). The parameters and the variables are displayed in Tables 3.1 and 3.2.

The width of the patch antenna (Wp) is calculated according to [51].

$$(\mathrm{Wp}) = \frac{\mathrm{C}}{2 \cdot \mathrm{f} \cdot \frac{\sqrt{\varepsilon r + 1}}{2}}\ 24.44\ \mathrm{mm} \tag{5.1}$$

The effective dielectric constant (ε_{eff}):

$$= \frac{\varepsilon r + 1}{2} + \frac{\varepsilon r - 1}{2} \cdot [1 + 12 \cdot \frac{h}{W}]^{-\frac{1}{2}} = 3.17 \tag{5.2}$$

The correction factor (ΔL):

$$= h \cdot 0.412\ \frac{(\varepsilon\mathrm{eff} + 0.3) \cdot \left(\frac{W}{h} + 0.264\right)}{(\varepsilon\mathrm{eff} - 0.258) \cdot \left(\frac{W}{h} + 0.8\right)} = 0.724 \tag{5.3}$$

The actual length of the patch antenna (L) is calculated by equation (5.4)

$$\mathrm{L} = \frac{\lambda}{2} - 2 \cdot \Delta \mathrm{L} = 0.005 \tag{5.4}$$

The effective length (L_e) is:

$$= \mathrm{L} + 2 \cdot \Delta \mathrm{L} = 14.5\ \mathrm{mm} \tag{5.5}$$

Tuning and optimization stages have been conducted for obtaining the ideal result. Table 5.1 shows the original and optimization dimensions of the microstrip antenna.

Table 5.1. The dimensions of microstrip antenna (mm).

Calculations	Width (Wp)	Length (Lp)
Original	24.44	14.5
Optimization	25.63	13.10

The ADS software has been used to design the schematic of the microstrip antenna, as illustrated in Figure 5.1.

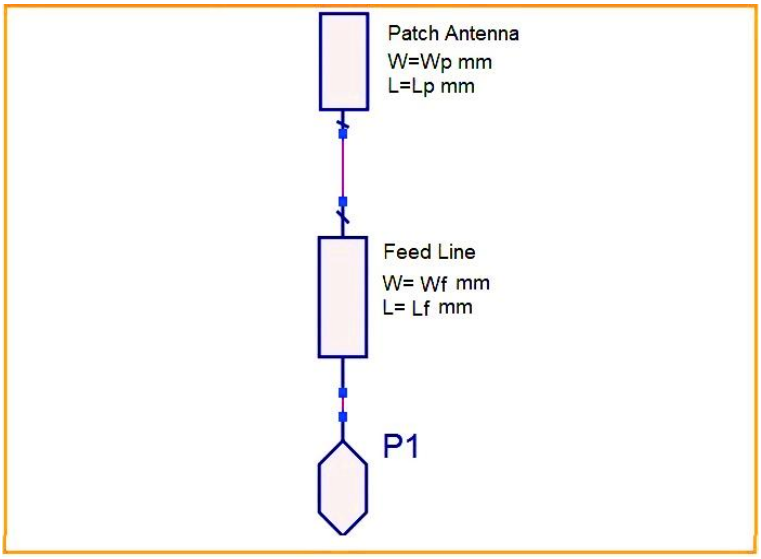

Figure 5.1. Schematic of patch antenna design for the Wilkinson rectifier.

Figure 5.2 shows the simulation result of S11(dB). The 10 dB return loss band ranges from 5.660 GHz to 5.910 GHz, which corresponds to a bandwidth of 250 MHz. The S11 is around – 30 dB at the central frequency of 5.800 GHz.

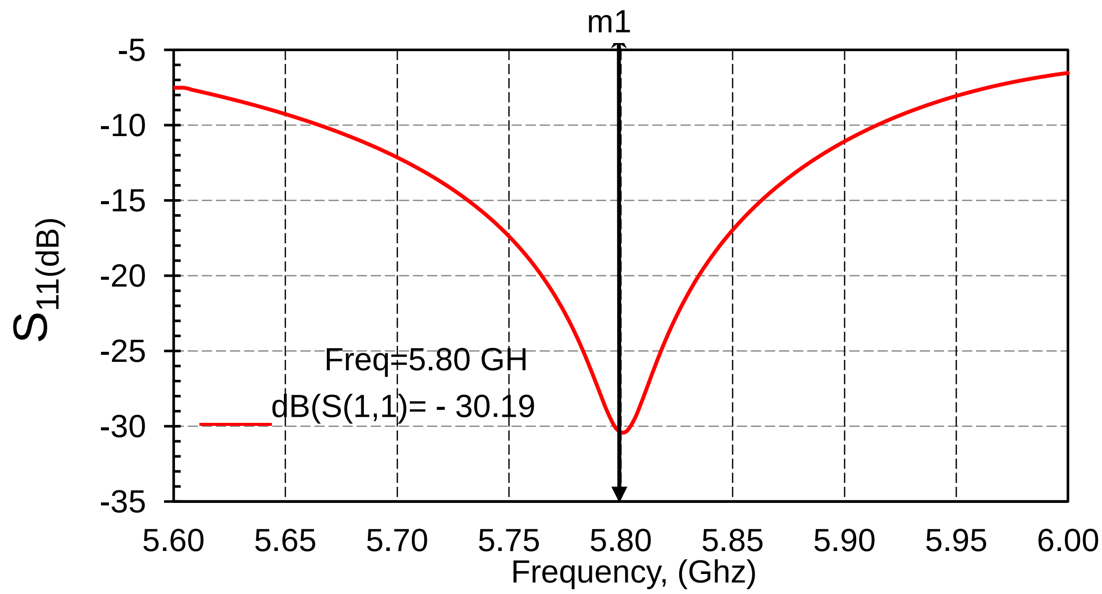

Figure 5.2.Simulated S_{11}(dB) of patch antenna.

Figure 5.3 shows the layout of the microstrip antenna having the size of 25.6 mm X 13.1 mm.

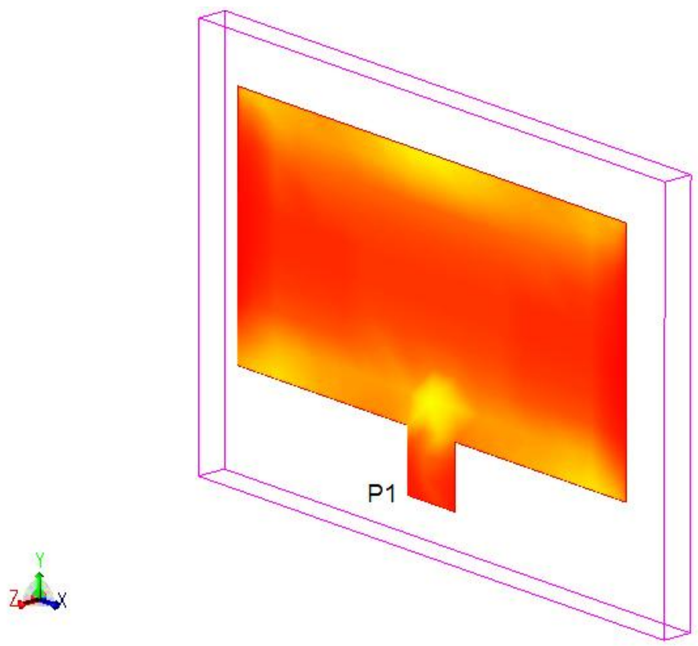

Figure 5.3. Layout of patch antenna.

The 3D antenna radiation pattern is plotted in Figure 5.4.

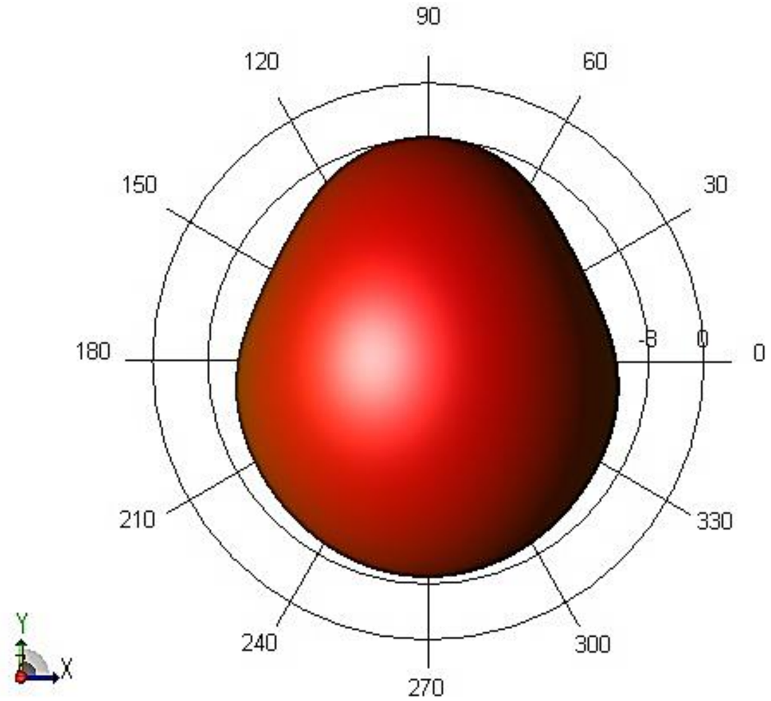

Figure 5.4. Three-dimensional radiation pattern of patch antenna.

Figure 5.5 shows the other simulation results of the patch antenna: maximum directivity 6.9 dBi and the gain 5.2 dB of the patch antenna.

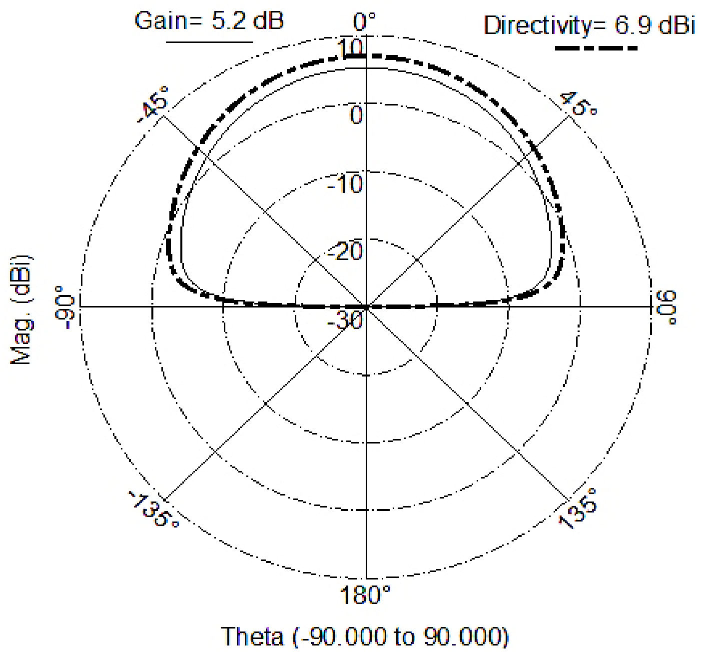

Figure 5.5. The directivity and gain of patch antennas.

5.3 Wilkinson power combiner design and simulation

The parameters of the substrate RO4350B used for PCB have been shown in Table 3.1. The variables and parameters are required for design are displayed in Table 3.2.

Figure 5.6 shows the schematic of the Wilkinson power combiner coupler. It is a robust power combiner, with all its ports matched. This coupler has a wideband performance. The transmission lines are microstrip types to integrate all components onto the same substrate.

ADS Linecalc tool calculates the dimensions of transmission lines on the substrate, for each requested characteristic impedance and phase shift. In equation (5.6) the TLs characteristic impedances are calculated:

Z_0 = 50 Ω and $(\sqrt{2} \cdot Z_0)$ = 70.7 Ω. (5.6)

The steps for the design of the Wilkinson power combiner coupler are as follows.

(A): Three ports are configured as transmission lines (TL), which have a width (W), and length (L). The characteristic impedance Z_o = 50 Ω, the effective electrical length of the line (EL) = 90º, the top cladding metal thickness (T) = 17.5 μm, and the loss tangent=0.004 mm. The substrate parameters and variables design are presented in Tables 3.1, and 3.2.

(B): Two curves of transmission lines are arranged to connect the ports, each curve has a characteristic impedance $(\sqrt{2} \cdot Z_0)$ is 70.7Ω, a length (L) of transmission line (TL) =λ/4, width (W) of the TL is less than the three TLs of the ports.

(C): Port 2 is connected with port 3 by resistor shows in equation (5.7) for high isolation, and lossless, due to the ports are matched and identical.

$$R = 2 \cdot Z_o = 100\ \Omega \tag{5.7}$$

The radius of the Wilkinson coupler is calculated after its characteristic impedance is set Z0 = 70.7 Ω in equation (5.8), then the W, and L are calculated.

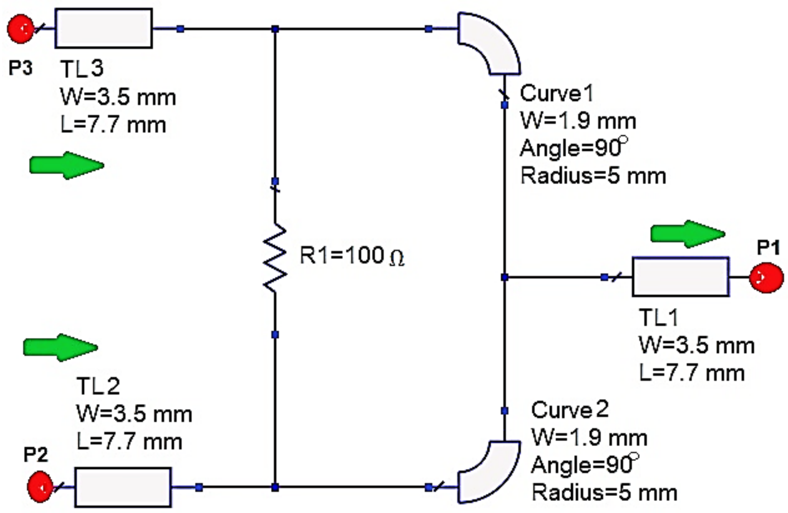

Figure 5.6. Schematic of Wilkinson power combiner coupler.

$$\text{Radius} \ = L/2 \cdot \pi. \tag{5.8}$$

Figure 5.7 shows the layout of the Wilkinson coupler. All ports are matched to 50 Ω. The resistance between the input ports is 100 Ω. This resistance has a crucial role in the return loss at ports 2 and 3 and in isolation between these two ports. Each curve of the Wilkinson coupler is around a quarter wavelength at the central frequency, and has the characteristic impedance equal to 70.7 Ω.

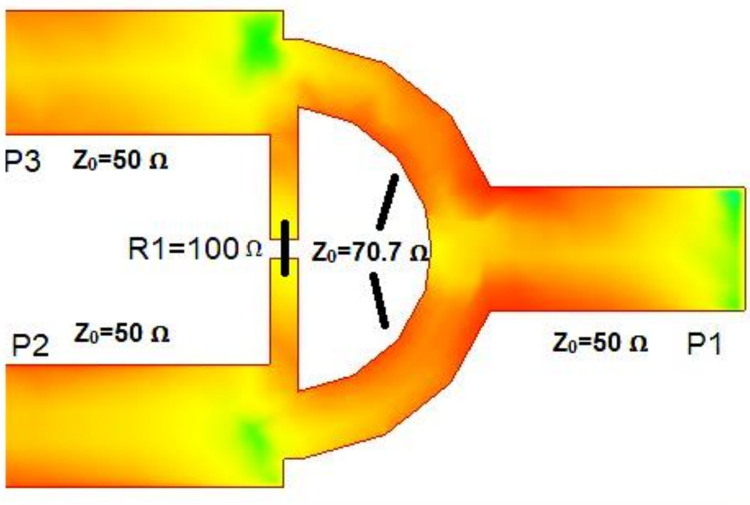

Figure 5. 7. Layout of Wilkinson power combiner coupler.

The optimized S-parameters of the Wilkinson power combiner coupler are shown in Figure 5.8. The transmission magnitudes of S_{12}, S_{13} are mostly -3 dB, and the S_{11} is lower than -10 dB from 1.7 GHz to 9.7 GHz, which corresponds to a bandwidth of 8 GHz. The S_{11} at the central frequency of 5.8 GHz is around -41 dB. Also, a high isolation S_{23} is obtained: - 46 dB at 5.8 GHz. This isolation is under – 10 dB in a band ranging from 2.5 GHz to 9 GHz.

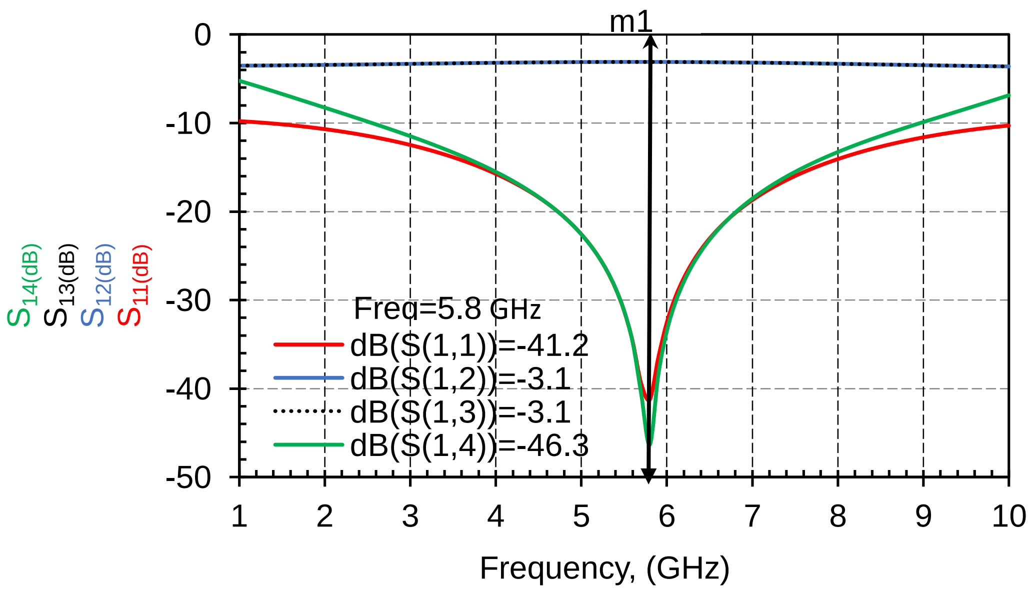

Figure 5.8. S-parameters of Wilkinson power combiner coupler.

The Wilkinson coupler is a symmetric circuit, and the phase balance is perfect, as seen in Figure 5.9. We estimate an improved gain. Therefore, the antenna pattern of the combined two patch antennas will have the maximum in the same direction as the single patch antenna.

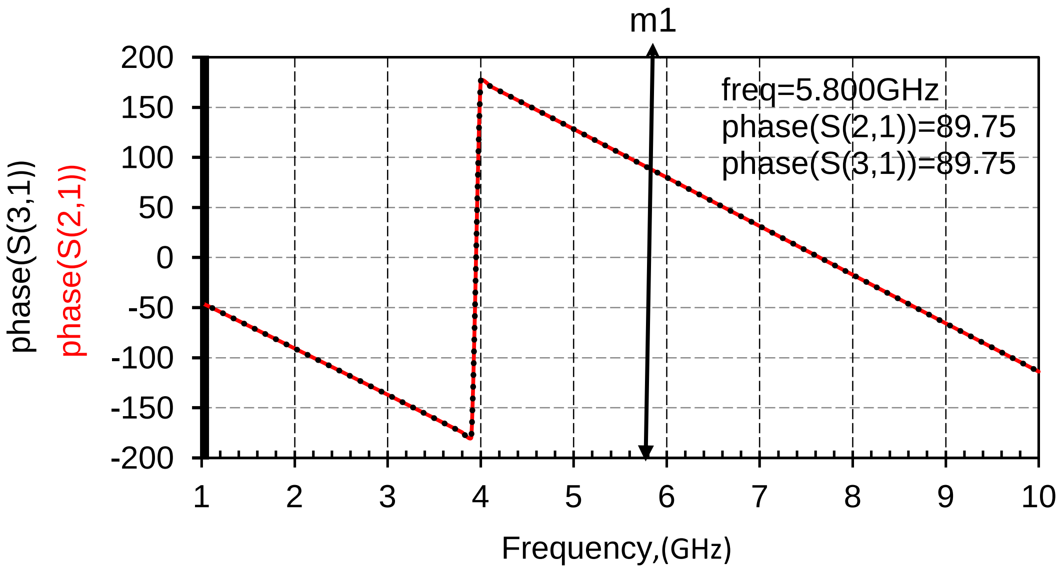

Figure 5.9. Simulated phase shift of the Wilkinson power combiner coupler.

Two elements of micro-strip antennas are integrated with the Wilkinson inputs by impedance transformers for matching purposes. The tuning technique has been conducted to improve the simulation of parameters S_{11}, gain, and directivity. There is also a space of around λ/2 between the centers of two antennas, to avoid coupling.

Two patch antennas are widely used parasitic for receiving signals in RF and microwave applications. It is the preferred option for obtaining high directivity and gain. The Wilkinson power combiner is integrated with patch antennas to make a dual antenna for enhancing the gain. It is designed by calculating the dimensions (length, width, and height). The TLs method is designed by virtue of mathematical calculations of dimensions of the Wilkinson coupler. In ADS the software results of directivity, gain, and efficiency are obtained by a Momentum EM simulator for accuracy. Figure 5.10 shows the layout of two patch antennas combined into the Wilkinson power combiner. It is designed into one layer, and the dimensions are shown in this Figure.

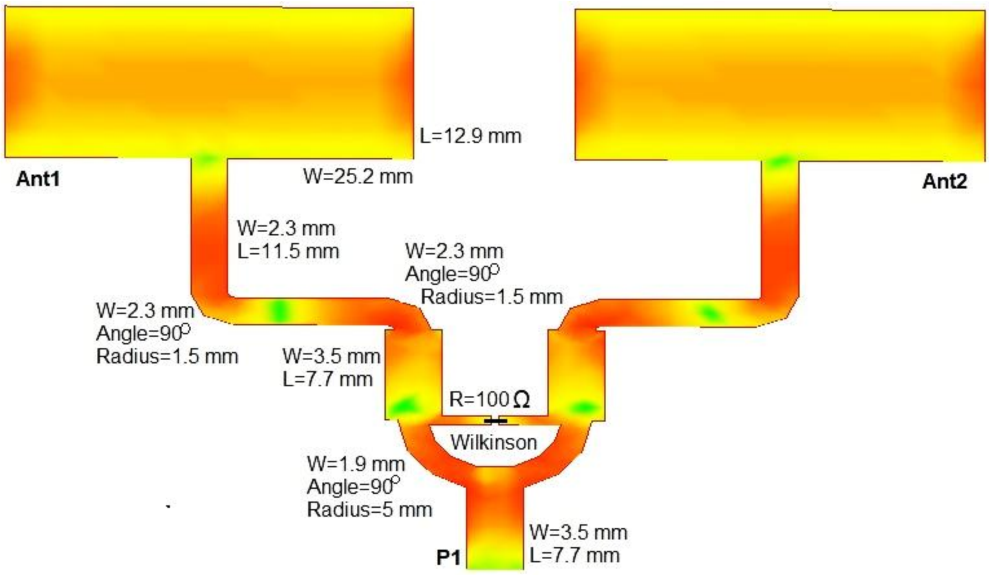

Figure 5.10. Layout in Momentum of the Wilkinson power combiner coupler, which is integrated with two rectangular patch antennas.

The simulation results of the S_{11} are shown in Figure 5.11. It is observed that the Wilkinson power combiner has (S_{11}) around -29.44 dB at frequency 5.79 GHz, which represented a very good performance.

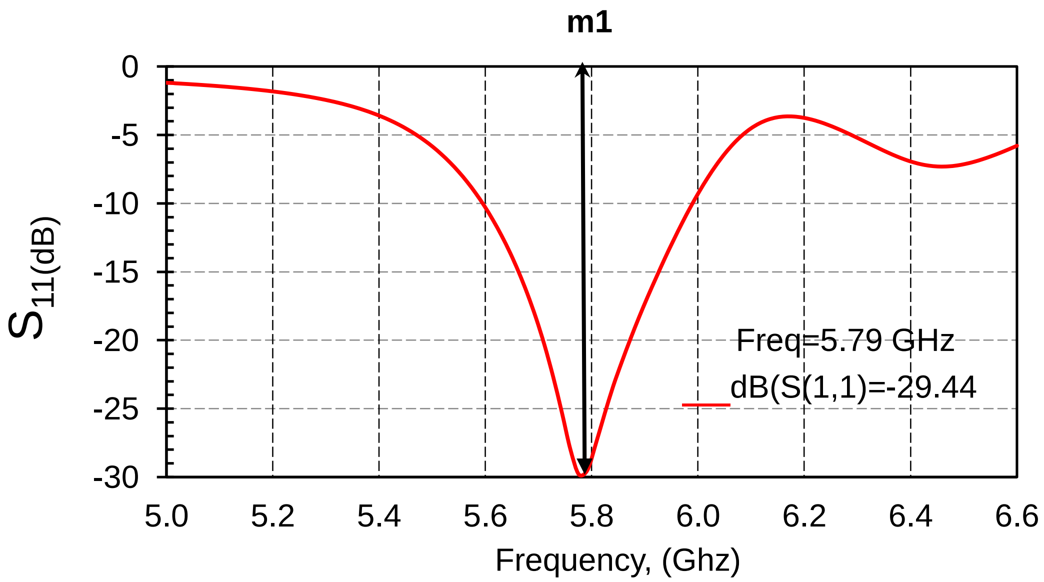

Figure 5.11. Shows S_{11} parameter of dual patch antenna integrated with the Wilkinson.

Figure 5.12 shows the directivity, and the gain of the antenna system. They are around 9.6, and 7.7 dBi, respectively.

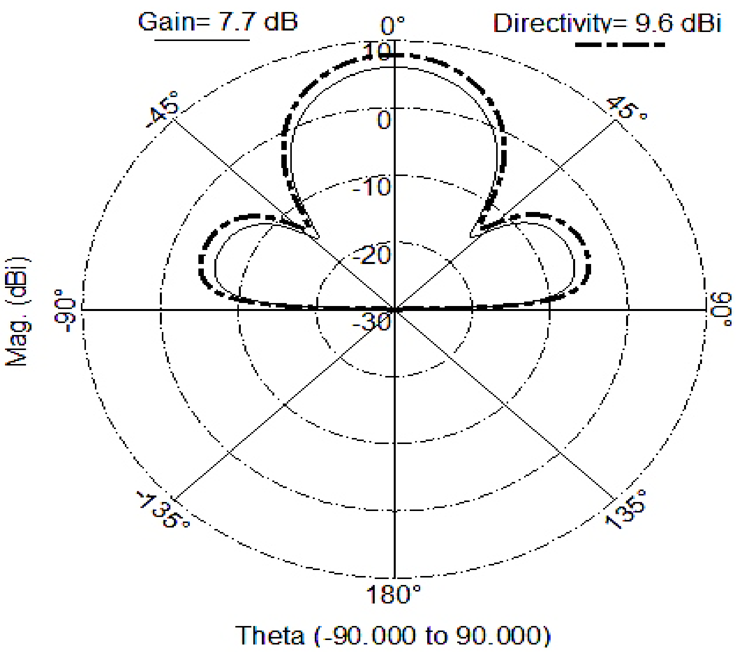

Figure 5.12. The directivity and gain of Figure 5.10, the layout of the Wilkinson power combiner coupler patch antennas.

The 3-D radiation pattern of the rectangular dual patch antenna system, excited at port 1, is plotted in Figure 5.13. It shows the 3-D radiation at 5.8 GHz. The main lobe shape confirms that the antenna system works properly.

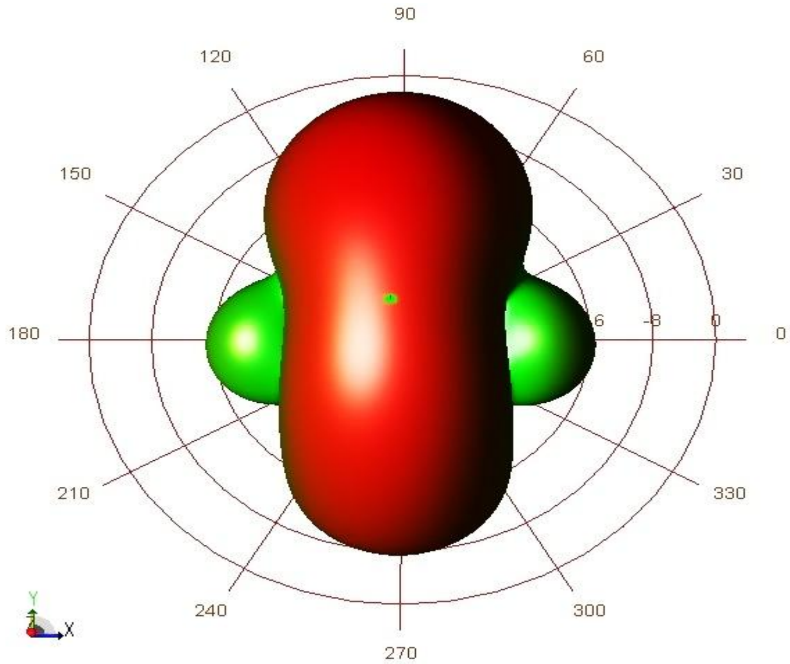

Figure 5.13. Three-dimensional radiation of the layout of the Wilkinson power combiner coupler patch antennas.

The setting up of the EM Momentum in ADS has simulated the maximum efficiency of around 65.80% at 5.79 GHz. From 5 GHz to 6 GHz the efficiency is greater than 50 %, as shown in Figure 5.14.

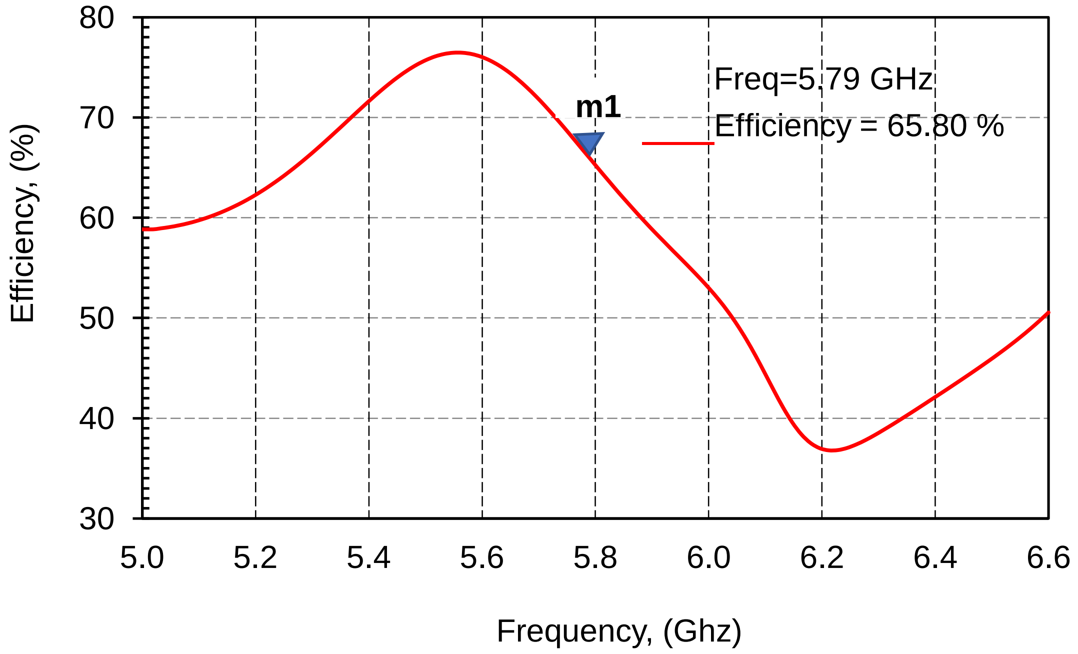

Figure 5.14. **The EM Momentum simulation of efficiency (%) versus the frequency (GHz) of the layout of the Wilkinson power combiner coupler patch antennas.**

5.4 Rectifier

The rectifier stage uses a voltage doubler topology. It is suitable for integration with the Wilkinson coupler. This topology has been mentioned in section 4.3. Schottky diode SMS7630_006LF is mounted in this stage. The diode model is based on its Spice model from the datasheet in [58].

5.5 Matching network

The matched circuit network is used in this circuit to transfer maximum power. Equations (5.9), and (5.10) calculate the B_1, and X_1 for the capacitor (C) and inductor (L). Thereby, the values of these elements are optimized and tuned for ideal results. The L-type matching network includes two inductors and one capacitor.

$$B_1 = \frac{6.247 \cdot 0.619 + \sqrt{6.247 \cdot 30.923 \cdot (30.923^2 + 0.619^2 - 6.247 \cdot 30.923)}}{6.247 \cdot (30.923^2 + 0.619^2)}$$

$$= 0.064$$

$$X_1 = \frac{6.247 \cdot (0.619) - 30.923 \cdot (-50.338)}{30.923} + \frac{30.923 - 6.247}{0.064 \cdot 30.923} = 62.75$$

$$\mathrm{C} = \frac{B_1}{2 \cdot \pi \cdot f} = 1.757 \text{ pF} \tag{5.9}$$

$$L = \frac{X_1}{2 \cdot \pi \cdot f} = 1.722 \text{ nH} \tag{5.10}$$

5.6 Simulation of rectenna

Figure 5.15 shows the schematic of four integrated components. These components are the Wilkinson, L-type matching circuit, voltage doubler, and load stage. Two inputs (Vin1, and Vin2) combine the power into a single port and transfer it to the matching circuit. The duty of the matching circuit is to maximize the output power. After that, it is integrated with the rectifier stage to obtain DC output voltage in the load stage. In the rectifier stage, a voltage doubler is mounted, which is an electronic circuit that charges C1. Therefore, the input voltage is converted into DC with twice the voltage at the output as it was initially present.

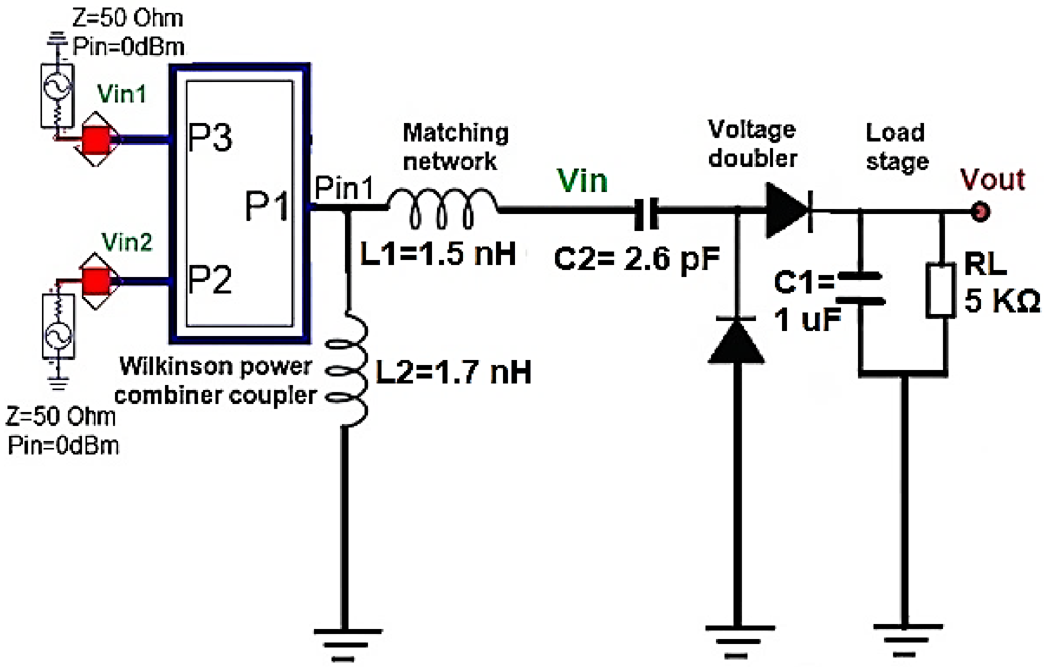

Figure 5.15. Schematic of the Wilkinson power combiner coupler with an L-matching network and a voltage doubler rectifier.

Figure 5.16 shows the simulation of the schematic of the Wilkinson power combiner coupler with an L-matching network and a voltage doubler rectifier. It is apparent that S_{22}, and S_{33} observed in Figure 5.16 are under -10 dB. The 10 dB bandwidths are from 1.6 to 2.0 GHz, 4.1 to 4.6 GHz, and 5.6 to 5.9 GHz.

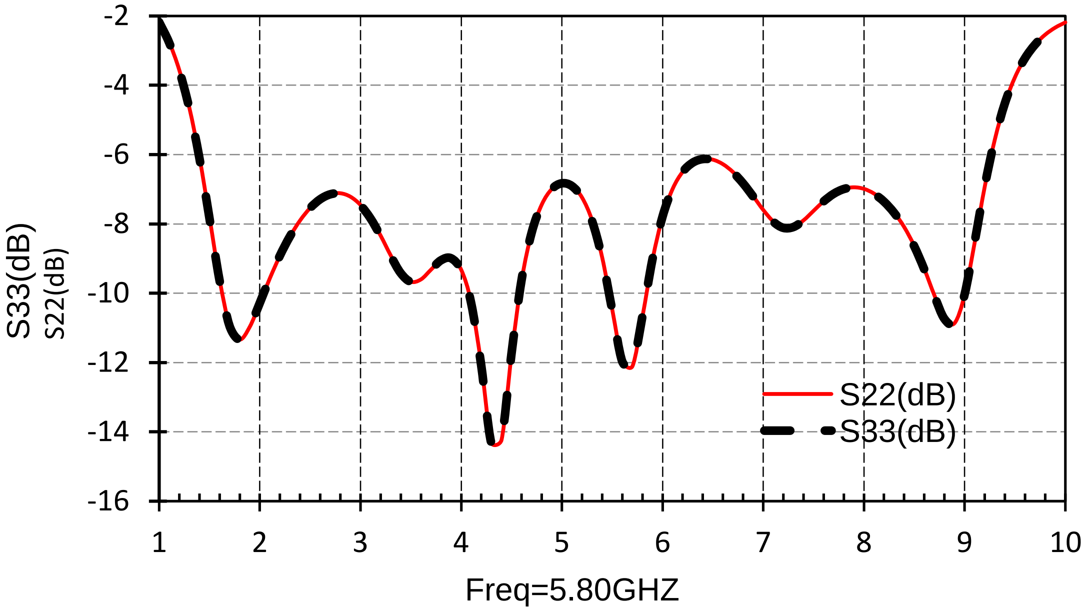

Figure 5.16. Simulation (S_{22}, and S_{33}) of the schematic of the Wilkinson power combiner coupler with an L-matching network and a voltage doubler rectifier.

The output power is calculated in equation (5.11). The rectifier stage shows the DC output power of the circuit that uses only one constant polarity. Figure 5.17 displays a -2.6 dBm output power at a 0 dBm input power level at each generator (P_2 and P_3) in (Figure 5.15) with zero-frequency. There are no RF components at the output rectifier stage. In power harvesting, parallel sources of RF design enhance the gain.

$$Pdc\_Watt = real\ (Vout\ [0] \cdot I_{load}[0]) \tag{5.11}$$

The efficiency circuit in Figure 5.5 is given by equation (5.12).

$$The\ efficiency\ (\eta) = \left(\frac{Pdc\_Watt}{\text{Input power 1+Input power 2}}\right) \cdot 100\% \tag{5.12}$$

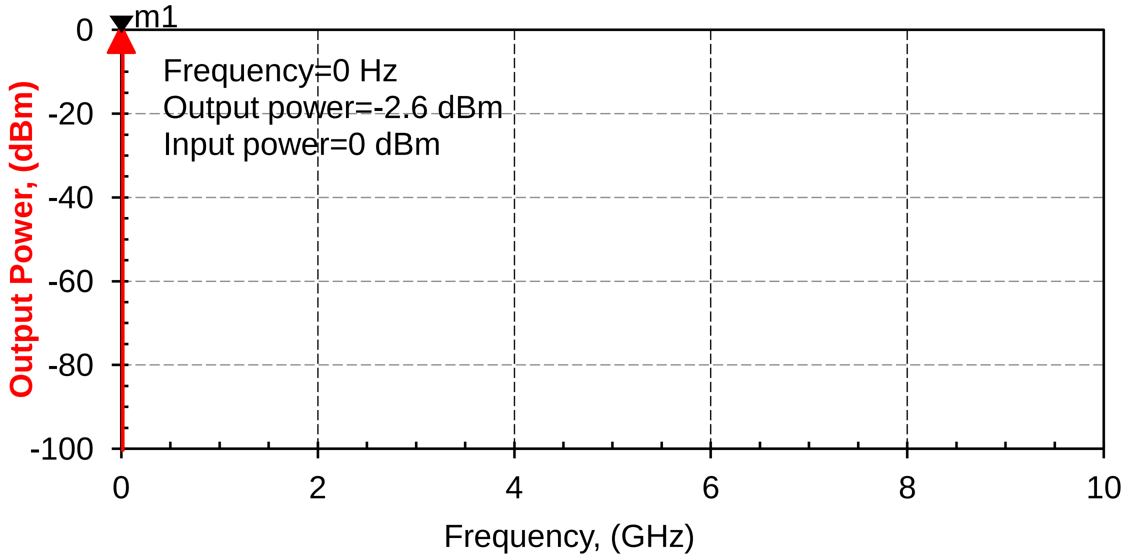

Figure 5.17. Output power (dBm) versus the frequency of the Wilkinson two patch antennas rectifier circuit.

Figure 5.18 shows that an efficiency of 51.86% is reached at an input power level of 0 dBm through two input terminals. The sensitivity metric is known as the lowest amount of power necessary to power an integrated circuit. Through the simulation, we can see that it begins around 2.72% with an input power of -25 dBm.

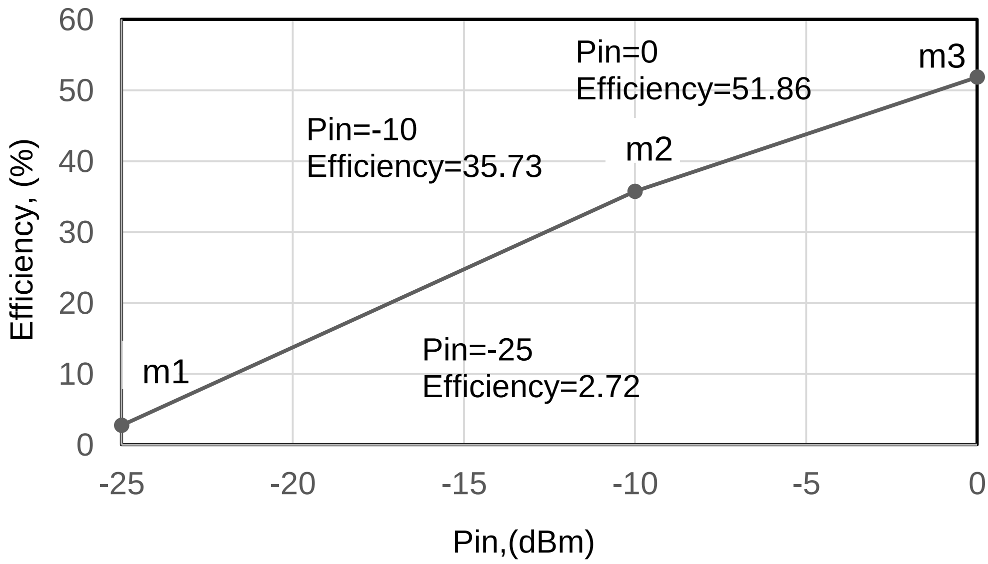

Figure 5.18. The simulation of efficiency versus input power P_{in} (dBm) of schematic in Figure 2.15.

V_{in} is feeding the voltage doubler which consists of C_2, a pair of diodes (SMS7630-006LF) and is connected with the element C_1 which has a capacitance of 1 μF, to eliminate the ripples. Rectified output voltages (V_{out}) of 0.08, 0.56, and 2.36 V are obtained for an input power of -20, -10 dBm, and 0 dBm at each part (P_2 and P_3), respectively. The Vout result is displayed as a straight red line in Figure 5.19.

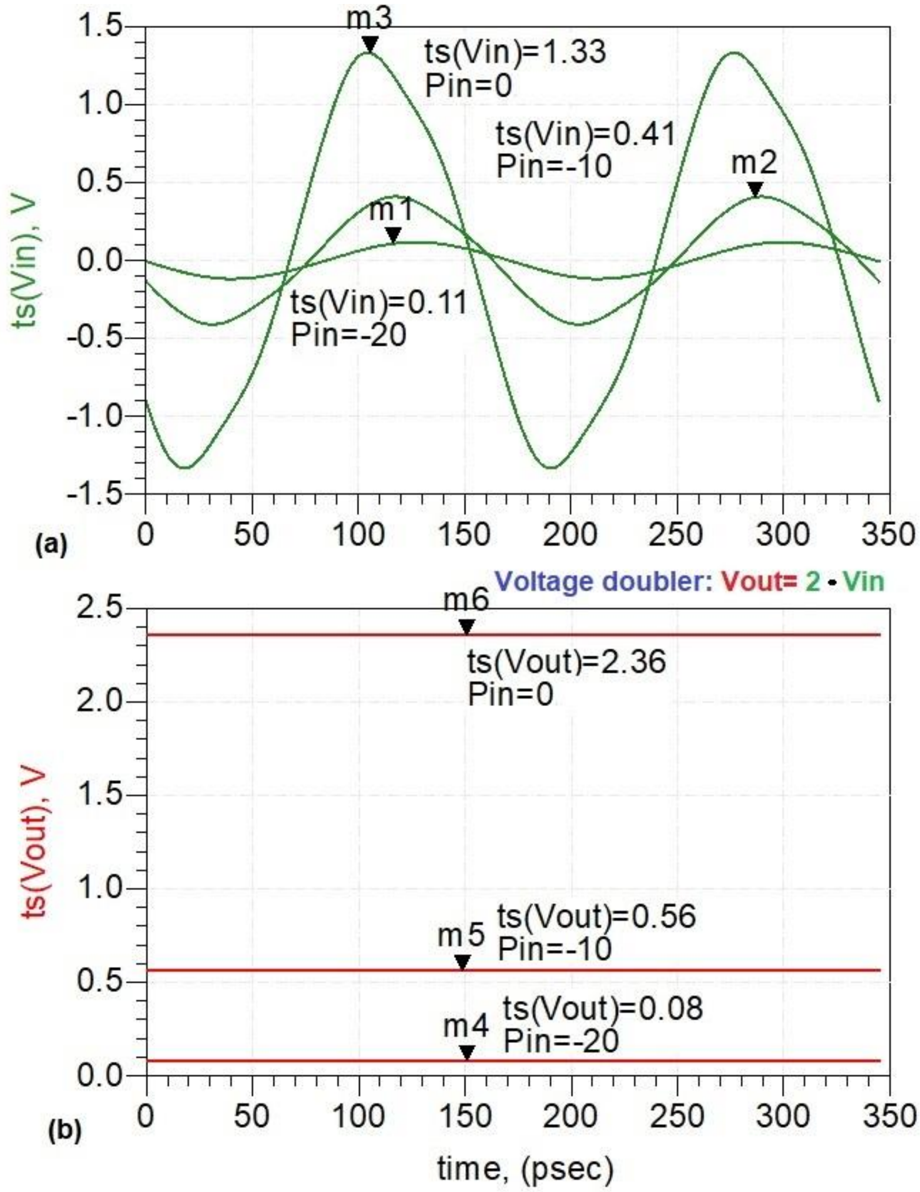

Figure 5.19. Output Vout in (V) versus time in (psec) of Wilkinson power combiner coupler.

Table 5.2 provides the output voltage (V_{out}) at different input powers. As obvious from Table 5.2, we can observe that increasing the input power P_{in} (dBm) increases the output voltage V_{out}.

Table 5.2. DC output voltage versus RF input power P_{in} (dBm).

P_{in} (dBm)	V_{out} (V)
- 20	0.08
- 10	0.56
0	2.36

5.7 Fabrication

The circuit is fabricated with the Wilkinson power combiner with an L-matching network and a voltage doubler rectifier on the same substrate. Figure 5.20 illustrates the photo of the circuit (7.5 x 7.5 cm) which resembles with a Printed Circuit Board (PCB). Also, the items are easily available and inexpensive, and the Rogers company provides the substrate.

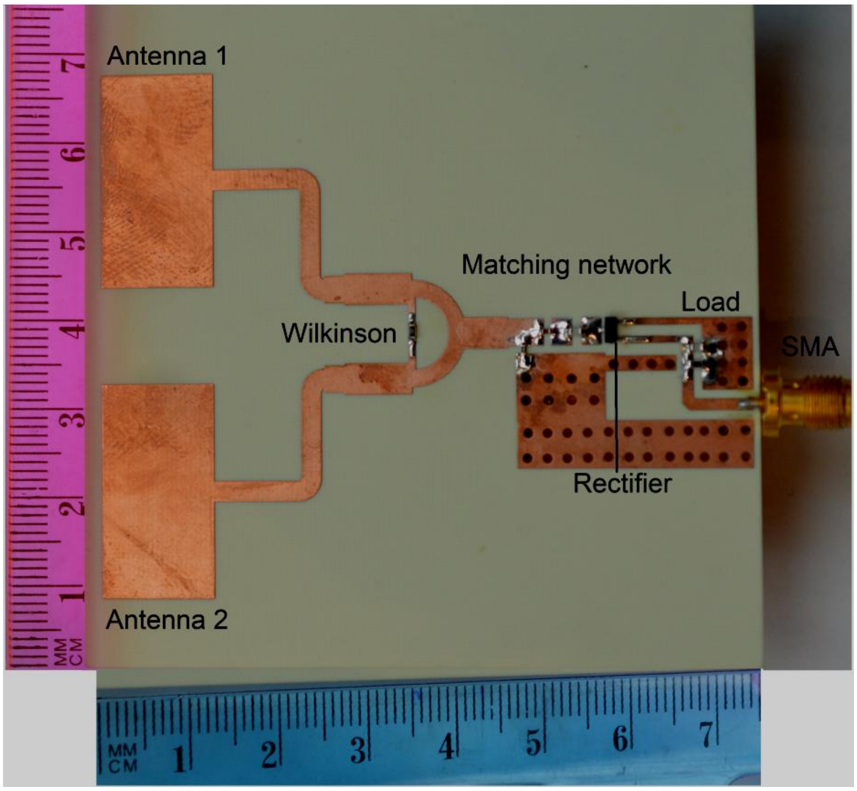

Figure 5.20. Photo of the fabrication circuit rectifiers.

5.8 Measurement

The measurement set-up is presented in Figure 2.22. The output power result is presented in Table 5.3. A transmitter power = 7 dBm is set up at the microwave generator output. There is an approximate agreement of results related to the simulation, Friis equation, and measurement setup process.

The Friis equation (5.13) is used to estimate the receiver power (P_{rx}) at the input of the detector circuit. The representative setup of the near field and far-field of WPT classification is based on Table 4.2.

By applying the values of the power transmitter (P_{tx}) of 7 dBm, the gain of the transmitter antenna (G_{tx} = 7 dBi), the receiver gain antenna (G_{rx} = 8 dBi), for a distance between transmitter and receiver 50 cm, a received power of -19.70 dBm is obtained at frequency 5.8 GHz.

$$Prx = Ptx + Gtx + Grx + 20 \cdot log10 \cdot \left(\frac{\lambda}{4 \cdot \pi \cdot \mathrm{d}}\right) = -19.7 \text{ dBm}. \qquad (5.13)$$

Equation (5.14) is used to find an estimation of the free space path loss at frequency 5.8 GHz, $Gtx = 7\ dB, Grx = 8\ dB, and\ d = 0.50\ meter$:

$$Path\ loss = Gtx + Grx + 20\ log10\ \left(\frac{\lambda}{4 \cdot \pi \cdot \mathrm{d}}\right) = -26.7 \text{ dBm}. \qquad (5.14)$$

Table 5 3. The measured results of Wilkinson output DC power rectifier.

D (cm) / (MHz)	100	75	50	25
	Output power (dBm) at 7 dBm input power level			
1760 to 1930	-32	-26	-22	-18
3020 to 3160	-34	-19	-17	-15
5320 to 5700	-35	-27	-21	-17
6000 to 6060	-36	-34	-24	-19

5.9 Conclusion

This work presents a prototype implemented with a Wilkinson combiner which is designed to collect more energy, from two integrated patch antennas. In addition, it delivers twice the magnitude of the RF voltage at the combined output due to the voltage doubler topology. It boosts the DC voltage, efficiency, and sensitivity by employing the full-wave topology rectifier. The efficiency of the rectifier circuit is 51.86% at 0 dBm for the R_L = 5 KΩ, and the sensitivity 2.7% at two terminals input power -25 dBm.

In measurement, a 7 dBm input power provides the output power with a wideband frequency. The output power is shown in Table 5.3. Accordingly, the power harvesting circuit could be used for 3G and also 5G that was launched in 2020 over L and C bands frequencies. Consequently, the voltage crop of the circuit proposed.

The future work will be expanded to combine RF in rectenna to accumulate more RF. Also, it might concentrate on some aspects that contribute to improving the result.

Chapter 6 – Integrated Rectifier using a Dual T-junction Power Combiner Coupler

6.1 Introduction

The approaches presented previously addressed some issues of converting RF to DC for EH. However, there are several challenges involved in increasing the DC output power. RF energy combined from several antennas and the distance between the transmitter and receiver are the issues. These challenges impact the high-power conversion efficiency (PCE).

This prototype was fabricated in two circuits for combining RF signals from 4 antennas. Voltage doublers are mounted in each rectifier stage to combine their DC energy to a single output port. The L-type matching network is integrated between each T-junction and the rectifier stage to maximize the output voltage. This circuit was called a multi-input, single output (MISO) in [59]. Since January 2007, Canada has stopped issuing licenses to Innovation, Science and Economic Development for new TV transmitters broadcasting in analogue [60]. Therefore, the use of such prototypes in a high-power transmitter environment in UHF or VHF is no longer possible. The purpose of this design is to increase the efficiency of RF to DC conversion and to protect the components in a compact box.

6.2 Design and simulation of T-junction power combiner coupler

The design parameters of the RO4350B laminate are mentioned in chapter 3, Tables 3.1, and 3.2. This substrate ordered from Rogers Company was chosen due to its low loss, availability, and low cost.

The Advanced Design System (ADS) software tool choice from Keysight Technologies was used to design the circuit, and to analyze its efficiency through Harmonic Balance (HB) simulations.

The physical dimensions of the T-junction are shown in Figure 6.1. This scheme is implemented using transmission lines (TL). The characteristic impedance Z_0 is 50 Ω for TL_1, TL_6, and TL_7, while it is $Z_0 \cdot \sqrt{2}$ = 70.7 Ω for TL_2, TL_3, TL_4, and TL_5 with the same width of the curve's sections.

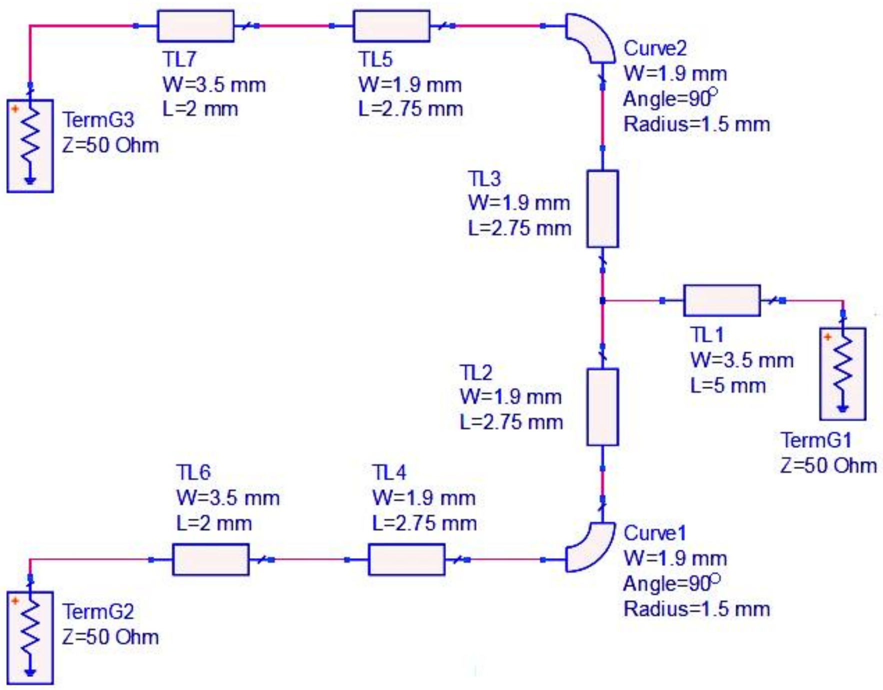

Figure 6.1. Generic schematic for the T-junction power combiner divider coupler.

6.3 Rectifier components

- **Voltage Doubler Topology**

Figure 6.2 shows a full-wave voltage doubler topology. This schematic illustrates a pair of voltage doublers combined with each other and connected to the load stage. The purpose is to combine DC output voltage for enhancing the efficiency.

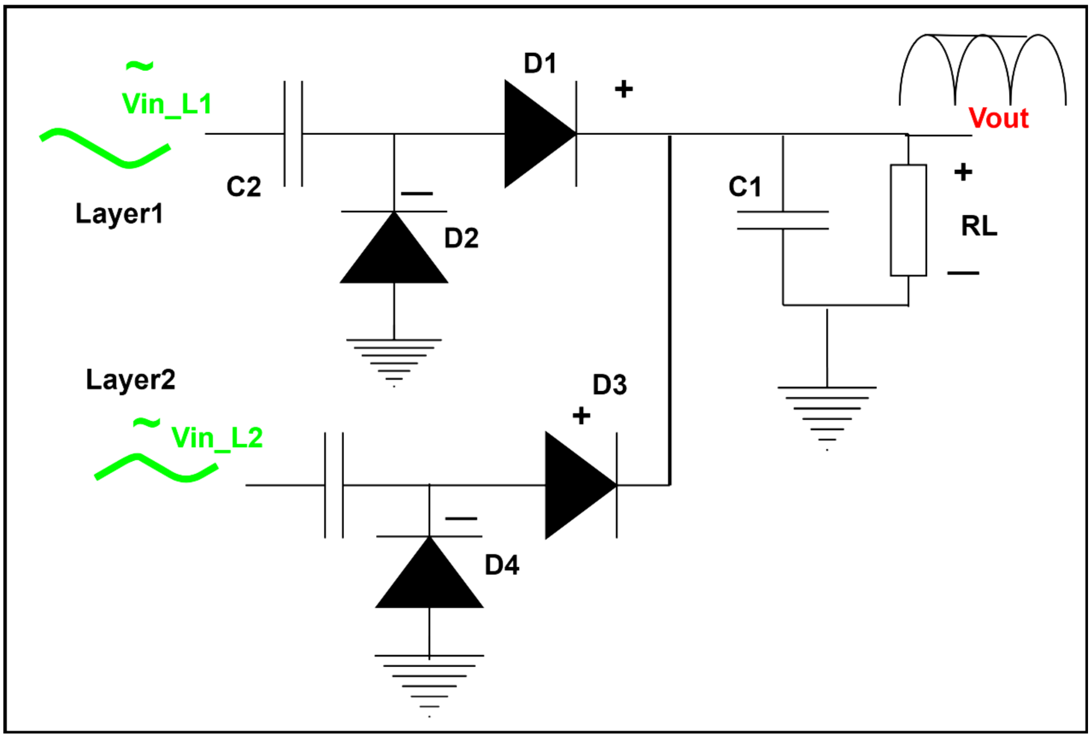

Figure 6.2. Full wave voltage doubler topology.

- **Practical implementation**

In Figure 4.6 of chapter 4, two pairs of SMS7630_006LF described in [58] were combined. Figure 6.3 shows the dual model of SMS7630_006LF. Each diode pair is mounted in the rectifier stage. The two inputs of the rectifier are receiving signals from the two outputs of the T-junctions. The rectifier converts the AC input to the DC output. The output positive DC signals are combined and delivered to the load.

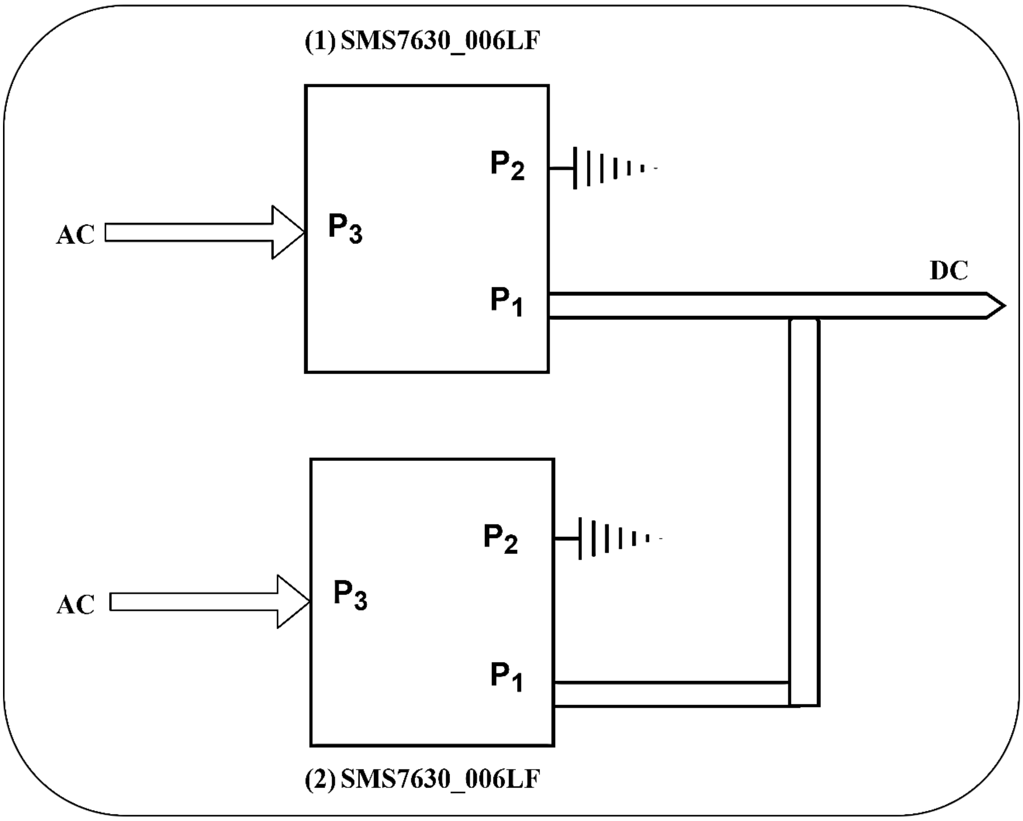

Figure 6.3. Dual model of SMS7630_006LF diode.

6.4 Matching circuit

The matching circuit is mounted between the source and the load stages. The source impedance is implemented with two layers of T-junction, and the load impedance is a dual voltage doubler diode rectifier with the load resistance. This circuit uses L-section network series matching. Parameters B_4 and X_4 are calculated initially to find the values of the capacitor (C) and inductor (L). Equations (6.1) and (6.2) are used for finding the values of the elements C and L.

B_4

$$= \frac{49.630 \cdot (-50.338) - \sqrt{6.247 \cdot 49.630 \cdot (6.247^2 + (-50.338)^2 - 6.247 \cdot 49.630)}}{49.630 \cdot (6.247^2 + (-50.338)^2)}$$

$$= -0.026$$

$$X_4 = \frac{49.630 \cdot (-50.338) - 6.247 \cdot (-0.762)}{6.247} + \frac{6.247 - 49.630}{-0.026 \cdot 6.247} = -133.319$$

$$C = -\frac{1}{2 \cdot \pi \cdot f \cdot X_4} = 2.059\, pF \qquad (6.1)$$

$$L = -\frac{1}{2 \cdot \pi \cdot f \cdot B_4} = 1.055 \text{ nH} \qquad (6.2)$$

6.5 Schematic of the rectifier integrated with T-junction power combiner coupler

The dimensions of T-junction TLs are shown in Figure 6.1. The element values are shown in Figure 6.4. Two diodes (SMS7630-006LF) are mounted in the rectifier stage to implement the dual voltage doubler. The load stage includes a capacitor in order to eliminate the ripples. It is connected with the resistor load (R_L) in parallel.

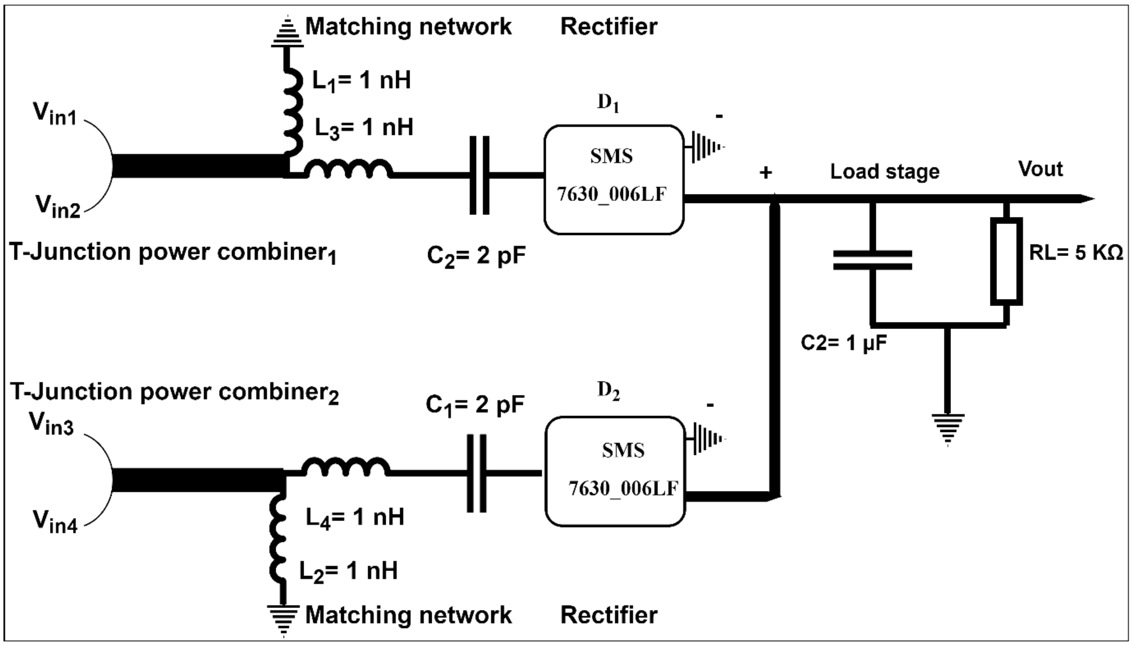

Figure 6.4 Schematic of a two-layer T-Junction power combiner coupler with an integrated dual voltage doubler.

Figure 6.5 plots the simulated DC output power (dBm). According to Figure 6.4, four V_{in} input generators are used to connect the receiver circuit to the combined DC output. The DC component shows an output power value of −1.77 dBm when the input power is 0 dBm (equal to 1 mW, combined from all the four generators, where each generator produces 0.25 mW). For the integrated T-junction rectifiers, the efficiency was improved compared to the single T-junction rectifier. This may be attributed to the reception of the more electromagnetic waves due to four inputs of the antennas in the case of the integrated T-junction rectifier. Similarly, there are two rectifiers in the integrated T-Junction system, therefore, the efficiency is further improved. These results were calculated using equation (6.3) which expresses the output power as follows:

$$Pdc\_Watt = real\ (Vout\ [0] \cdot I_{load}[0]) \tag{6.3}$$

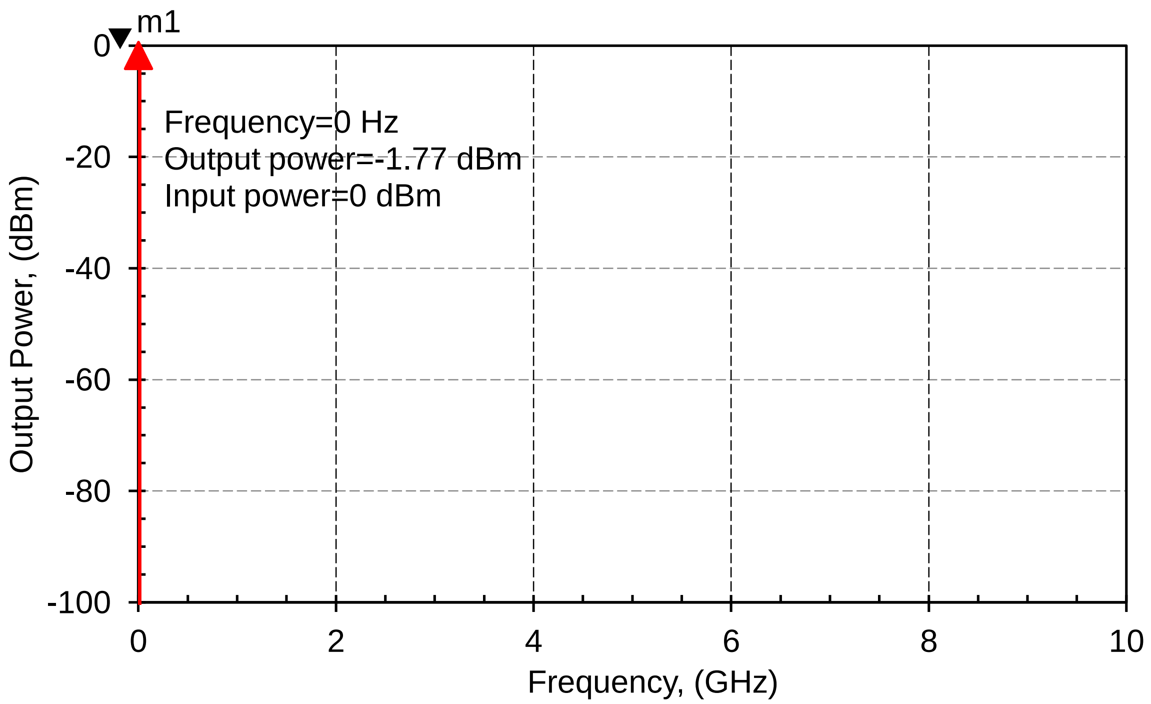

Figure 6.5. DC output power (dBm) at 0 GHz of the two-layer T-junction power combiner coupler with an integrated dual voltage doubler.

Equation (6.4) is used to calculate the efficiency:

$$Efficiency(\eta)$$

$$= \left(\frac{Pdc\_Watt}{\text{Input power 1}+\text{Input power 2} + Inputpower3 + Inputpower4}\right) \cdot 100\ \% \qquad (6.4)$$

Figure 6.6 shows the circuit's efficiency as a function of the total input power. Four RF generators (V_{in1}, V_{in2}, V_{in3}, and V_{in4}) are connected via the dual T-junctions in multi-input/single V_{out} configuration (MISO). The diagram shows efficiency of 2.86%, 14.27%, 38.80, and 75.10% at four input power terminals of -30, −20, -10, and 0 dBm, respectively.

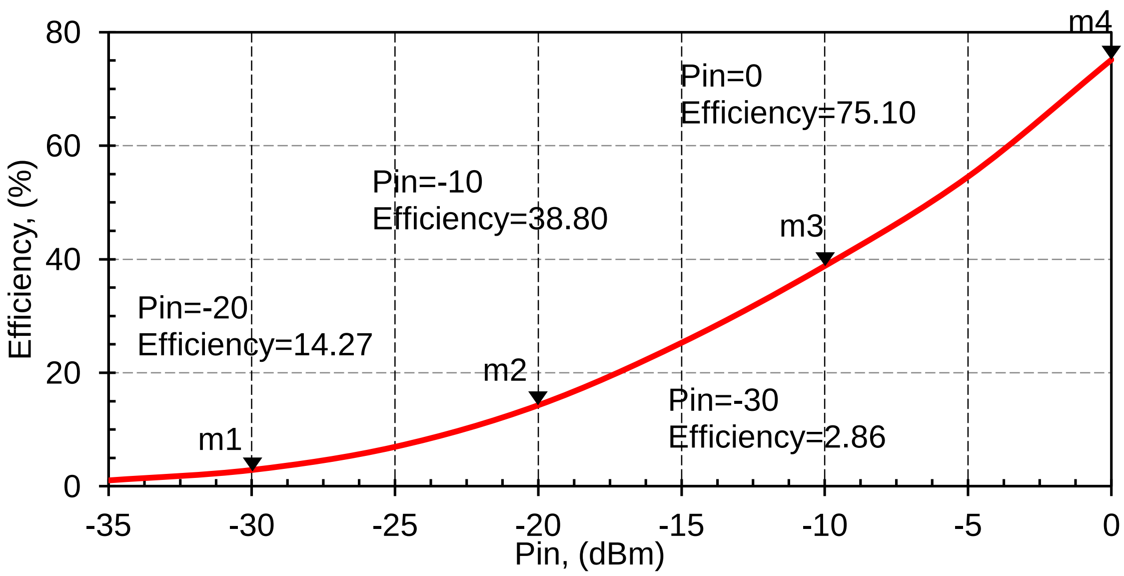

Figure 6.6. The simulation efficiency of the system: a two-layer T-junction power combiner coupler with an integrated dual voltage doubler.

Figure 6.7 illustrates that the input power levels of -20, -10, and 0 dBm give outputs of 0.13, 0.65, and 2.15 V, respectively. As for all prototypes, the function of the requested voltage to power a specific device, the minimal input power can be estimated.

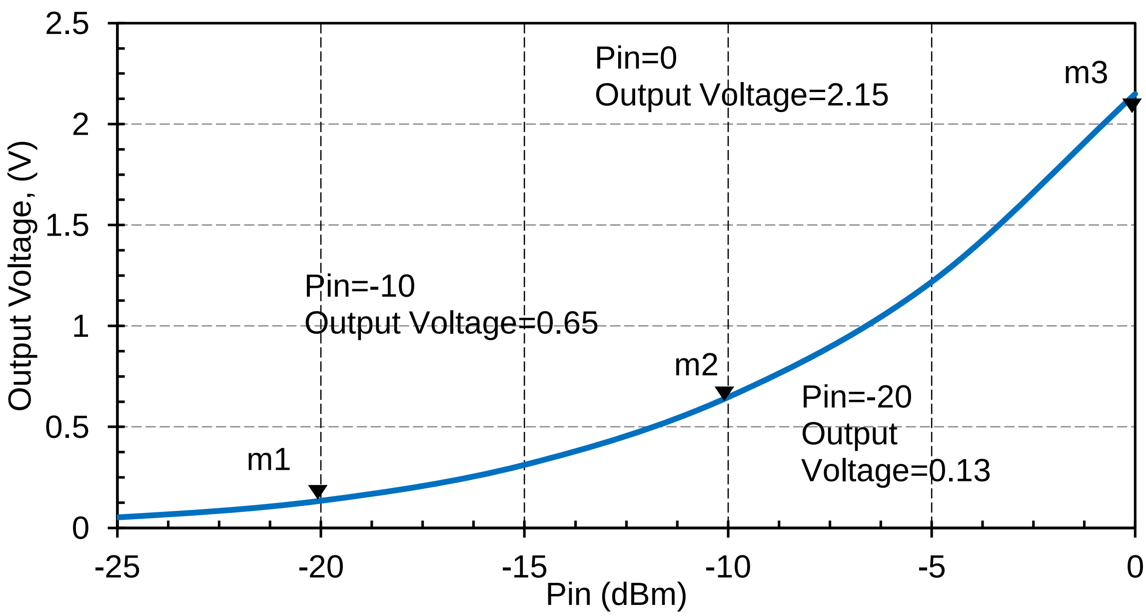

Figure 6.7. Shows the output voltage V_{out} in (V) of different input power in (dBm) of the two-layer T-junction power combiner coupler integrated with dual voltage doubler.

6.6 Fabrication

The proposed circuit, a dual T-junction power combiner coupler with parallel voltage doubler rectifier, is shown in Figure 6.8.

The photo of the fabricated prototype has dimensions of 4 cm x 3 cm x 1 cm, plus the size of the SMA in length.

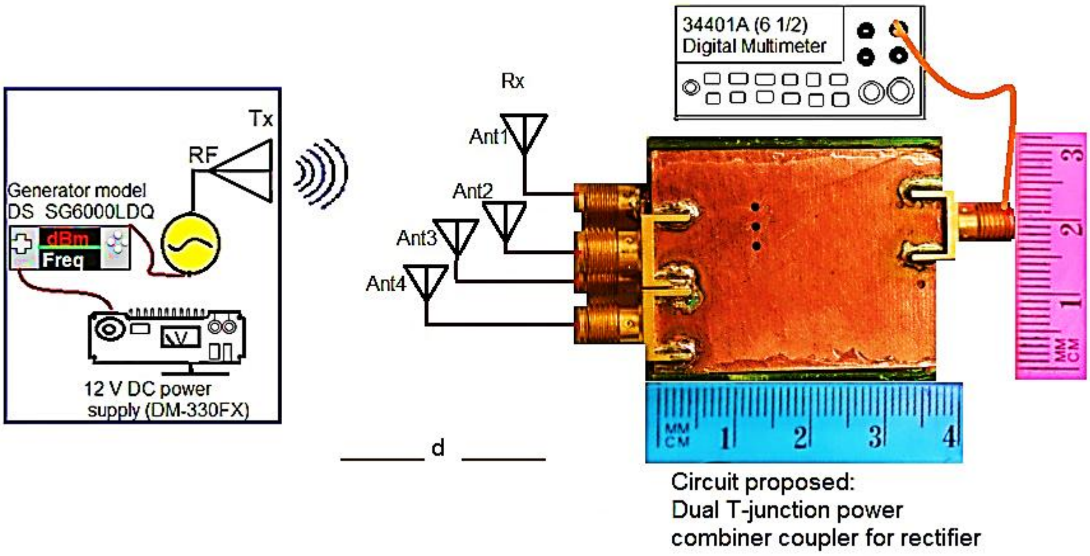

Figure 6.8. Photo of the fabricated circuit (dual T-junction power combiner coupler rectifier).

6.7 Measurement

Figure 6.8 shows the measured setup. It is apparent that a transmitter antenna is connected to the generator and four receiving antennas are connected to our fabricated prototype. The digital Multimeter is connected to the output of the prototype to measure the available power at the output.

Equations (6.5) and (6.6) are used to calculate the Far-field distance (d) at 2, and 6 GHz.

$$d \geqq \frac{2\,D^2}{\lambda} = \frac{2 \cdot 12^2}{15} = 19.2 \text{ cm} \qquad (6.5)$$

For a Far-field of 6 GHz:

$$d \geqq \frac{2\,D^2}{\lambda} = \frac{2 \cdot 12^2}{5} = 57.6\ cm \tag{6.6}$$

Friis equation (6.7) estimates of the received power.

$$Prx = Ptx + Gtx + Grx + 20 \cdot log10 \cdot \left(\frac{\lambda}{4 \cdot \pi \cdot d}\right) \tag{6.7}$$

For frequency = 2 GHz (λ = 15 cm), and substituting P_{tx}, G_{tx}, and G_{rx}, we have,

= −5 + 6 + 12 + (−38.46) = −25.46 dBm.

For frequency = 6 GHz (λ = 5 cm),

= −5 + 6 + 12 + (−48) = −35 dBm.

In the indoor measurements in the lab, the transmitter power was set at Ptx = - 5 dBm and the distance between the transmitter and the prototype was 1 m. The output power measured was – 20 dBm at (1650-1950 MHz), -14 dBm at (2000-2050 MHz), and -20 dBm at (6550- 7000 MHz).

The Friis equation in (6.8) – (6.9) is applied to find the output power of the fabricated receiver circuit, in the case of a transmitted power of 100 W (50 dBm). In this case, we take λ = 0.15 m and use a distance d = 500 m:

P_{rx} = 50 + 15 + 6 + (−92.4) = −21.4 dBm. (6.8)

If the distance d is reduced to 250 m with the same λ = 0.15 m, the received power is

P_{rx} = 50 + 15 + 6 + (−86.4) = −15.4 dBm. (6.9)

6.8 Conclusion

In this work, two T-Junction rectifiers were combined to enhance the performance of the individual T-Junction rectifier. It combined four RF signals to feed the rectifier stage. The rectifier was verified to cover most ISM frequency bands, especially for WPT. The efficiency achieved is 75% at 0 dBm input power level from four generators with low loss of in the DC output power, which is essential to self-power wireless electronic devices.

Moreover, the design's effectiveness makes it a prospective candidate for facilitating self-powering in communication systems. Furthermore, the circuit offers protection to the components from environmental impacts, and is low-cost, lightweight, and small in size. Future work will focus on improving multi-rectifier combinations to increase the efficiency and output power.

Chapter 7 – Conclusion and Future work

Five prototypes were proposed in this thesis, all based on combining and rectifying RF signals using a dual-voltage doubler or a bridge diode. Several couplers, from broadband couplers to simple T-junctions, were used as combining elements. Simulation and measurement results confirmed both the power efficiency and the DC output voltage of the proposed circuits. A comparison between this work and several previous studies is presented in Table 7.1.

Table 7.1. Comparison between the proposed circuits and other reported work.

Ref	Freq (GHz)	Circuit topology	Input power (dBm)	Efficiency (%)	Output (mV)	Load (Ω)
[13]	5.8	Single diode (HSMS-2860)	12.30	54.8	2600	600
[14]	5.8	Dickson Charge Pump (HSMS-2862)	30	63	2000	525
[15]	5.8	Shunt diode (HSMS-286B)	9, 6,	60.6 56.3	1500 1710	1300
[16]	5.2	Dickson charge pump (HSMS2862)	24	64.1	5100	1150
[17]	5.8	Class-F Load (HSMS2860)	30	71	5000	1300
[18]	2.4, 5.4	Series diode, (HSMS2860)	10	66.8 51.5	2600 2300	1050
[19]	5.8	Two different diodes (HSMS2860 and HSMS2850)	17, 9.5, and 2.5	50 to 70	2800, 1100, 450	220
[20]	1.2 to 5	differential rectifier Schottky diode (SMS7630)	9	30	-	1000
This work: 90º hybrid coupler rectenna	5.8	Bridge diode HSMS286K	- 5 0	39 43	1080 2290	5 k
This work 180º hybrid coupler rectifier	5.8	Bridge diode (HSMS286K)	0 5	50 54	4320 2360	5 K
This work: T-junction rectifier	5.8	Voltage doubler (SMS7630-006LF)	0, -10 -20	43.60 30.50 11.52	2160 570 80	5 K
This work: Wilkinson rectenna	5.8	Voltage doubler (SMS7630-006LF)	0, -10 -25	51.86, 35.73 2.72	2360 560 80	5 K
This work: Dual T-junction rectifiers	1.650-2.100 & 6.550 - 7	Voltage doubler SMS7630-006LF	0 -10 -20 -30	75,10 38.80 14.27 2.86	2150 650 130	5 K

7.1 Conclusions

The conclusions of this doctoral work are summarized below.

- WPT and PH can be useful when a BS radiates energy under specific conditions:
  - These technologies work best at short range to power sensors, WLAN, RFID, and Wi-Fi.
  - The use of the proposed devices depends on the T_x power level and distance, as will be discussed further.
  - WPT can be used to power implants at a few meters or other ISM applications.
- All of the experiments and fabrication prototypes reveal this limitation:
  - EH is limited to the range around a BS.
  - All five prototypes use various power combiners (90^{O} hybrid coupler, 180^{O} hybrid coupler, T-junction, Wilkinson), integrated patch, or external Omni-directional antennas.
  - Different rectifying techniques are applied (voltage doubler, bridge diode) to boost the output DC voltage.
  - As expected, the efficiency is better when RF input is increased. For example, as discussed in Chapter 6, efficiency can rise up to 75%.

Using the well-known Friis equation and the designed prototype specifications presented in this thesis, we can provide more details about their potential use.

The free-space attenuation is calculated in Equation (7.1) at a frequency of 6 GHz ($\lambda = 0.05\ m$). Figure 7.1 shows the distance (d) in meters (m) and the attenuation (Att) in (dB).

$$Att = 20 \cdot log10 \cdot (\frac{\lambda}{4 \cdot \pi \cdot d}) \quad (7.1)$$

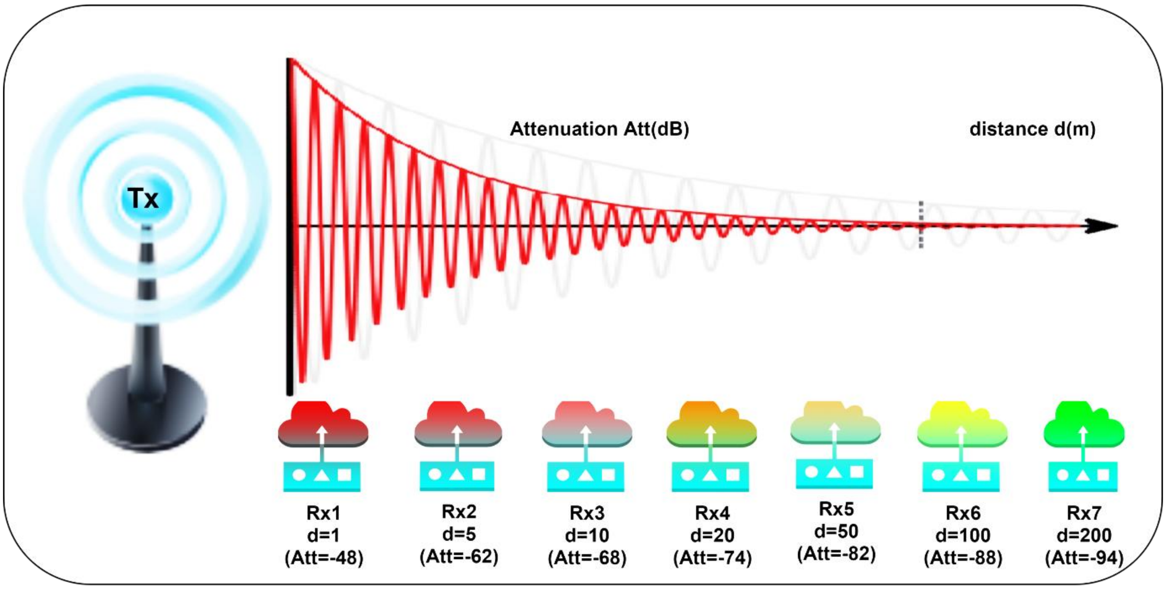

Figure 7.1. Illustration showing attenuation vs distance.

Base stations in urban and suburban areas transmit around 100 W (50 dBm) radiation (ERP) for wireless electronic devices [55], [56]. Equation (7.2) calculates the power receiver (P_{rx}) in the omnidirectional T_x (0 dB), at a max gain (6 dBi) of R_x. Table 7.2 shows the results of the power received, which decreases when the distance increases.

$$Prx = Ptx + Gtx + Grx + (\mathrm{Att}) \quad (7.2)$$

Table 7.2. Distance (d) and power receiver (Prx) of power harvesting (PH).

T_x (dBm)	50						
G_{rx} (dBi)	6						
d (m)	1	5	10	20	50	100	200
P_{rx} (dBm)	8	- 6	- 12	- 18	- 26	- 32	- 38

Table 7.3 Received power in WPT scenario function of distance.

Table 7.3. Distance (d) and power receiver (P_{rx}) of WPT.

T_x (dBm)	30						
G_{rx} (dBi)	6						
d (m)	1	5	10	20	50	100	200
P_{rx} (dBm)	- 12	- 26	- 32	- 38	- 46	- 52	- 58

With current levels of power, PH is only useful when the BS is in close vicinity, even at power levels in the order of hundreds of W. In the past, for powerful analog TV stations (MW of T_x power at the tower level) operating in VHF and UHF, PH was possible. However, this type of harvesting came at the cost of huge antennas and restrictions on the RF levels. Depending on the distance between the tower (transmitter) and receiver, the received energy could vary.

WPT can be also performed at short range for specific ISM applications, such as charging a medical implant. However, a decent power level is only achieved for a short time. If power density is limited due to FCC safety policies, a higher gain antenna can be used, but at the cost of larger dimensions and reduced directivity. Moreover, the antennas must always be oriented to the source of the energy. It is worth noting that the use of PH or WPT should be deeply analyzed in the context of each specific application.

7.2 Future work

Radio frequency source power is tightly controlled by governmental and safety restrictions. However, effective WPT and PH depend on the T_x power and distance, as discussed earlier. Therefore, government restrictions may prevent some of this emerging technology from commercially being adopted.

IoT applications are potential major users of WPT and PH technologies. When developing technology for IoT, some aspects must be considered, such as the antenna gain and dimensions, the required DC output voltage, and the operational efficiency of IoT devices when using PH and WPT. The main considerations are listed below.

- Antenna arrays have use limitations regarding input power, mutual coupling, and size, but they can be utilized for increasing the gain. Although the size and mutual coupling are usually considered challenges in array antennas, they could also be viewed as beneficial. For instance, size could assist in aspects of permittivity and wavelength, and mutual coupling could be reduced using techniques such as antenna element isolation and orientation.

- Novel diode multiplier topologies could be further studied to increase the output DC voltage at the required levels for specific devices. Diodes designed for low power levels are recommended. They are sensitive and have a low threshold, making them practical for PH in low RF density environments.
- Smart city systems are continuously evolving, and PH and WPT technology can be part of this evolution. Many IoT devices need self-powering. Some devices can integrate antenna arrays, especially at higher microwave frequencies, but increased free-space attenuation must also be considered.

To conclude, the actual and future designs of WPT and PH are challenging, and the use of such devices must be properly justified. It is not an option simply to increase the T_x power in order to have sufficient energy to wirelessly power a device. This approach may be acceptable for a short time and/or for specific applications. However, with respect to safety, this is not a viable source of green energy, as some researchers claim in their papers.

The work in this thesis proves that despite results in design and prototyping, WPT and PH concepts still show clear limitations for commercial applications.

7.3 References

[1] Nikola Tesla, “The Transmission of Electrical Energy Without Wires as a Means for Furthering Peace,” Electrical World and Engineer., p. 21, Jan. 1905.

[2] Brown, W.C, “The History of the Development of the Rectenna” Proc. Of SPS microwave systems workshop, p. 271-280, Jan. 1980.

[3] Xiao, L., Wang, P., Niyato, D., et al. "Wireless networks with RF energy harvesting: A contemporary survey", IEEE Commun. Surv. Tutor., 17, p. 757–789, 2015.

[4] L. Xie, Y. Shi, Y. T. Hou and A. Lou, "Wireless power transfer and applications to sensor networks," in *IEEE Wireless Communications*, vol. 20, no. 4, p. 140-145, doi: 10.1109/MWC.2013.6590061, August. 2013.

[5] Boutayeb, H., T. A. Denidni, and M. Nedil, “Bandwidth widening techniques for directive antennas based on partially reflecting surfaces,” Progress in Electromagnetics Research, PIER 74, 407–419, 2007.

[6] Barakat, R., Nerguizian, V., Hammou, D. & Tatu, S.O. Modified Ring Power Divider Using Stepped-Impedance Resonator. J. Microwaves, Optoelectron. Electromagn. Appl. 19, 26-38, 2020.

[7] Vullers, R., et al., *Micropower energy harvesting.* Solid-state Electronics, Vol. 53, no. 7, p. 684-693, 2009.

[8] Fiorini, P., et al. *Micropower energy scavenging*. In *ESSCIRC 2008-34th European Solid-State Circuits Conference*, IEEE, vol. 978-1-4244-2362-0, no. 08, p. 4-9, 2008.

[9] University of Ottawa. Wireless Communications and Health. Available online: http://www.rfcom.ca/faq/answers.shtml#q3.

[10] Luo, Y., et al., “RF Energy Harvesting Wireless Communications: RF Environment, Device Hardware and Practical Issues,” Sensors, vol. 19, no. 13, p. 1-28, 2019.

[11] Tran, L.-G., H.-K. Cha, and W.-T. Park, RF power harvesting: a review on designing methodologies and applications. Micro and Nano Systems Letters, vol. 5, no. 1, p. 14, 2017.

[12] W. Zahra and T. Djerafi, "Ambient RF Energy Harvesting for Dual-Band frequencies below 6 GHz, "*2018 IEEE Wireless Power Transfer Conference (WPTC)*, Montreal, QC, Canada, p. 1-2, doi: 10.1109/WPT.2018.8639488, 2018.

[13] K. Bhatt, S. Kumar, P. Kumar, and C. C. Tripathi, "Highly Efficient 2.4 and 5.8 GHz Dual-Band Rectenna for Energy Harvesting Applications," in *IEEE Antennas*

and Wireless Propagation Letters, vol. 18, no. 12, pp. 2637-2641, doi: 10.1109/LAWP.2019.2946911, Dec. 2019.

[14] H. Lee, "5.8 GHz ISM band energy harvester utilizing Dickson charge pump," *2016 17th International Symposium on Antenna Technology and Applied Electromagnetics (ANTEM)*, Montreal, QC, p. 1-2, doi: 10.1109/ANTEM.2016.7550144, 2016.

[15] Lee H, Lee J-C. Optimization of a 5.8-GHz rectifier considering ripple amplitude and DC-voltage pattern. Wireless Power Transfer Conference (WPTC). IEEE; 212-215, 2014.

[16] Bae J, Koo H, Lee H, et al. "High-efficiency rectifier (5.2 GHz) using a Class-F Dickson charge pump.", MicrowOpt Technol Lett; 59:3018–3023, https://doi.org/10.1002/mop.30862, 2017.

[17] C. Wang, N. Shinohara and T. Mitani, "Study on 5.8-GHz Single-Stage Charge Pump Rectifier for Internal Wireless System of Satellite," in *IEEE Transactions on Microwave Theory and Techniques*, vol. 65, no. 4, p. 1058-1065, doi: 10.1109/TMTT.2017.2672552, April. 2017.

[18] Wang D, Negra R. Design of a dual-band rectifier for wireless power transmission. Wireless Power Transfer (WPT). IEEE; 127-130, 2013.

[19] P. Lu, C. Song and K. M. Huang, "A Compact Rectenna Design with Wide Input Power Range for Wireless Power Transfer," in IEEE Transactions on Power Electronics, vol. 35, no. 7, p. 6705-6710, doi: 10.1109/TPEL.2019.2963422, July. 2020.

[20] Mansour M, Le Polozec X, Kanaya H. Enhanced Broadband RF Differential Rectifier Integrated with Archimedean Spiral Antenna for Wireless Energy Harvesting Applications. Sensors (Basel). 5;19(3):655, doi:10.3390/s19030655. PMID: 30764579; PMCID: PMC6386849, Feb. 2019.

[21] Dehghani S, Mirabbasi S, Johnson T. A 5.8-GHz bidirectional and reconfigurable RF energy harvesting circuit with rectifier and oscillator modes. IEEE Solid-State Circuits Lett (3): 66-69, 2018.

[22] Partal HP, Partal SZ, Belen MA. Design and implementation of a RF energy harvesting module with DC power control. 22nd International Microwave and Radar Conference (MIKON). IEEE; 33-36, 2018.

[23] Unich G, Olukoya O, Budimir D. Rectifiers based on quadrature hybrid coupler with improved performance for energy harvesting. IEEE Wireless Power Transfer Conference (WPTC). IEEE;1-5, 2018.

[24] El Badawe M, Ramahi OM. Efficient meta surface rectenna for electromagnetic wireless power transfer and energy harvesting. Progress Electromag Res;161(1070):35-40, 2018.

[25] Belo D, Georgiadis A, Carvalho NB. Increasing wireless powered systems efficiency by combining wpt and electromagnetic energy harvesting. Wireless Power Transfer Conference (WPTC). IEEE; 1-3, 2016.

[26] Khansalee E, Zhao Y, Leelarasmee E, Nuanyai K. A dual-band rectifier for RF energy harvesting systems. 11th. International Conference on Electrical Engineering/Electronics, Computer, Telecommunications and Information Technology (ECTI-CON). IEEE; 1-3, 2014.

[27] Gozel MA, Kahriman M, Kasar O. Design of an efficiency enhanced Greinacher rectifier operating in the GSM 1800 band by using rat-race coupler for RF energy harvesting applications. Int J RF Microwave Comput-Aided Eng; 29(1):1-8, 2019.

[28] Niotaki K, Kim S, Jeong S, Collado A, Georgiadis A, Tentzeris MM. A compact dual-band rectenna using slot loaded dual band folded dipole antenna. IEEE Antennas Wireless Propagation Lett; 12: 1634-1637, 2013.

[29] Mekid S, Qureshi A, Baroudi U. Energy harvesting from ambient radio frequency: is it worth it? Arab J Sci Eng; 42(7): 2673-2683, 2017.

[30] Kasar O, Kahriman M, Gozel MA. Application of ultra wideband RF energy harvesting by using multisection Wilkinson power combiner. Int J RF Microwave Comput-Aided Eng; 29(1):1-8, 2019.

[31] Mousa Ali E, Yahaya NZ, Nallagownden P, Zakariya MA. A novel rectifying circuit for microwave power harvesting system. Int J RF Microwave Comput-Aided Eng; 27(4):1-11, 2017.

[32] Shen S, Chiu C-Y, Murch RD. A dual-port triple-band Lprobe microstrip patch rectenna for ambient RF energy harvesting. IEEE Antennas Wireless Propagation Lett; 16:3071-3074, 2017.

[33] Shen S, Chiu C-Y, Murch RD. Multiport pixel rectenna for ambient RF energy harvesting. IEEE Trans Antennas Propagation; 66(2):644-656, 2017.

[34] Kim S, Vyas R, Bito J, et al. Ambient RF energy harvesting technologies for self-sustainable standalone wireless sensor platforms, Proc IEEE;102(11):1649-1666, 2014.

[35] Kaymaksut, E., Y. Gürbüz, and I. Tekin, *Impedance matching Wilkinson power dividers in 0.35 μm SiGe BiCMOS technology.* Microwave and Optical Technology Letters, vol. 51, no. 3, pp. 681-685, 2009.

[36] Wang, T.H. and J.H. Chen. *Power recycling using Wilkinson power combiner with pulse width modulation*. In *2017 IEEE International Symposium on Radio-Frequency Integration Technology (RFIT),* IEEE, vol. 978-1-5090-4036-, no. 7, pp. 223-225, 2017.

[37] Soyata, T., L. Copeland, and W. Heinzelman, “RF energy harvesting for embedded systems: A survey of tradeoffs and methodology,” IEEE Circuits and Systems Magazine, vol. 16, no. 1, pp. 22-57, 2016.

[38] Kitazawa, S., H. Ban, and K. Kobayashi, “Energy harvesting from ambient RF sources,” IEEE MTT-S International Microwave Workshop Series on Innovative Wireless Power Transmission: Technologies, Systems, and Applications, vol. 978, no. 12, pp. 39-42, 2012.

[39] Rajabi, M., et al., “Modulation techniques for simultaneous wireless information and power transfer with an integrated rectifier–receiver,” IEEE Transactions on Microwave Theory and Techniques, vol. 66, no. 5, pp. 2373-2385, 2018.

[40] Lu, J.-J., et al., “A four-band rectifier with adaptive power for electromagnetic energy harvesting,” IEEE Microwave and Wireless Components Letters, vol. 26, no. 10, p. 819-821, 2016.

[41] J. A. Hangerty, F.B. Helmberecht., W. H. Mccalpin, R. Zane, Z. B. Popovic, Recycling ambient microwave energy with broad-band rectenna arrays, Vol. 52, No. 3, p. 1014-1024, DOI: 10.1109/TMTT.2004.823585, 2004.

[42] Scheeler, R., Korhummel, S., Popovic, Z. A dual-frequency ultralow-power efficient 0.5-g rectenna, *IEEE Microwave Magazine*, vol. 15, no. 1, p. 109-114, DOI: 0.1109/MMM.2013.2288836, 2014.

[43] M. Abdallah, J. Costantine, A. H. Ramadan and Y. Tawk, "A Rectenna System with Power Combining Topology for Improved Power Handling Capabilities," *in IEEE Sensors Letters*, vol. 2, no. 4, pp. 1-4, Art no. 1501304, doi: 10.1109/LSENS.2018.2868825, Dec. 2018.

[44] K. Niotaki, A. Georgiadis, A. Collado and J. S. Vardakas, "Dual-Band Resistance Compression Networks for Improved Rectifier Performance," in *IEEE Transactions on Microwave Theory and Techniques*, vol. 62, no. 12, pp. 3512-3521, doi: 10.1109/TMTT.2014.2364830, Dec. 2014.

[45] Li Zhao, Xiaolu Jiao, Tong Zhu, and Feng Zhang, Anti-noise Algorithm Based on Time Domain Superposition in G3-PLC System, *International Journal of Circuits, Systems and Signal Processing*, pp. 328-335, volume 13, 2019.

[46] M.S. Kusuma, S. Shanthala, Cyril Prasanna Raj P., Design of 3.1-10.6 GHz CMOS UWB LNA Using Current Reuse Technique, *International Journal of Circuits, Systems and Signal Processing*, pp. 472-476, volume 13, 2019.

[47] Y. Peng, Z. Li, W. Zhang and D. Qiao, "Prolonging Sensor Network Lifetime Through Wireless Charging," *2010 31st IEEE Real-Time Systems Symposium*, San Diego, CA, pp. 129-139, 2010, doi: 10.1109/RTSS.35, 2010.

[48] H. Sun, Y. Guo, M. He and Z. Zhong, "A Dual-Band Rectenna Using Broadband Yagi Antenna Array for Ambient RF Power Harvesting*," in* IEEE Antennas and

Wireless Propagation Letters, vol. 12, pp. 918-921, doi: 10.1109/LAWP.2013.2272873, 2013.

[49] Norashidah Md. Din, Chandan Kumar Chakrabarty, Aima Bin Ismail, Kavuri Kasi Annapurna Devi, and Wan-Yu Chen, "Design of RF Energy Harvesting System for Energizing Low Power Devices," Progress in Electromagnetics Research, Vol. 132, p. 49-69, doi:10.2528, http://www.jpier.org/PIER/pier.php?paper=12072002, 2012.

[50] Rogers Corporation, Printed in U.S. ARO3000® Series Circuit Materials RO3010™High Frequency Laminates, Datasheet, www.rogerscorp.com, 2019.

[51] Balanis, C.A., "Antenna theory: analysis and design." *John Wiley & sons*, vol. 0-471, no. 66782, p. 811-826, 2016.

[52] Pozar, D.M., "Microwave Engineering." *4th Edition, Wiley*, vol. 978-0-470, no. 63155(3), pp. 343-345, p. 664-666, 2011.

[53] Data Sheet, Avago Technologies, AV02-1388EN, http://datasheet.elcodis.com/pdf/27/30/273075/hsms-2860-blkg.pdf, August 26, 2009.

[54] Behagi, Ali A. RF and Microwave Circuit Design: a Design Approach Using (ADS). Techno Search ser. 978-0-9964466-8-6, 2018.

[55] Mordachev, V. and A. Svistunov, "Reduction of the radiated power of cellular base stations on urban area at high intra system EMC requirements," IEEE International Symposium on Electromagnetic Compatibility (EMC), vol. 10, no. 1109, p. 1-6, 2015.

[56] Human Exposure to Radio Frequency Fields: Guidelines for Cellular Antenna Sites. https://www.fcc.gov/consumers/guides/human-exposure-radio-frequency-fields-guidelines-cellular-andpcs-sites. Accessed December 11, 2019.

[57] Rogers Corporation, Circuit Materials, RO4350B, Printed in U.S.A, www.rogerscorp.com, 2018.

[58] Data Sheet, Surface-Mount Mixer, and Detector Schottky Diodes, *Skyworks Solutions, Inc*, https://id.ic-components.com/files/1e/SMS7621-005LF.pdf, June 1, 2018.

[59] S. Ma, T. Zhang, S. Lu, H. Li, Z. Wu and S. Li, "Energy Efficiency of SISO and MISO in Visible Light Communication Systems," in *Journal of Light wave Technology*, vol. 36, no. 12, p. 2499-2509, doi: 10.1109/JLT.2018.2812831, June 15, 2018.

[60] Innovation, Science and Economic Development Canada Advisory Letter — The Use of Unplanned Over-the-Air (OTA) Broadcasting Television Spectrum and the Manufacturing and Importation for the Sale of Digital Capable Television Receiving Apparatus, 2007.